DOCTOR OF PHILOSOPHY

Thermally stimulated current and electrokinetic investigations of HV cable models

Hobdell, Stephen Barry

Award date:
1999

Awarding institution:
Bangor University

Thermally Stimulated Current and Electrokinetic Investigations of HV Cable Models

Stephen Barry Hobdell

Thesis submitted to the University of Wales
in candidature for the degree of Doctor of Philosophy
September 1999

School of Electronic Engineering and Computer Systems
University of Wales Bangor

Summary

Space charge in extruded model polymeric high voltage cable samples has been assessed under various conditions using the thermally stimulated current (TSC) technique. All of the cable samples under investigation consisted of a stranded aluminium core, covered by three concentric layers of polymer: (1) an inner semiconducting carbon-loaded polymer screen electrode; (2) an XLPE insulation layer, and (3) an outer semicon screen electrode. Effects on the TSC due to the composition of the materials used in both the XLPE insulation and the semiconducting screens have been studied. The semicon-insulation combination was also seen to have an important influence on the TSC.

Thermal cycling affected the TSC, and is conclusively attributed to morpological changes in some of the samples. The TSC measurements of other samples could not be interpreted so definitely, however, as a consequence of their complicated TSC curves, which arose from the novel composition of the cable materials.

TSC curves at different poling voltages were interpreted as appearing due to the relaxation of different poled mechanisms. The TSC was measured in the 27°C to 107°Ctemperature range. Poling voltages of upto 45kV in magnitude and of either a positive or a negative polarity were used to pole each sample at temperatures between room temperature and 107°C. The maximum poling voltage magnitude of 45kV corresponds to a geometric electric field at the inner semicon-insulation interface of $\sim$ 14kV.mm^{-1} and a field at the outer interface of $\sim$ 7.4kV.mm^{-1}. Typically, low poling voltages produced TSC peaks which were correlated with the work of other authors, and which showed these TSC to be attributable to charge accumulation at crystalline-amorphous boundaries. Space charge injection appeared to be promoted when higher voltages (and hence, fields) were employed. The voltage threshold above which space charge injection occurred was influenced by the different magnitudes of electrical field at the two different interfaces.

A novel method of investigation, called the Electro-Kinetic (EK) measurement technique, was also used to measure electrically-induced displacements at the surface of the cable samples to further characterise the electrical response of the model cables. A correlation was seen between the EK measurements, made at room temperature and with an a.c. stimulating voltage of upto 10kV$_{rms}$, and the total space charge derived by integrating the TSC with respect to time.

Acknowledgments

I would like to thank BICC Cables Limited (now BICCGeneral) and the EPSRC for funding this work through a Co-operative Award in Science and Engineering (CASE) studentship. As a consequence, I have had the honour of working with Professor T.J. Lewis and Doctor J.P. Llewellyn, both of whom have been helpful and encouraging and have engaged me in many hours of stimulating and thought-provoking discussions. I wish to thank Dr. S.M. Moody and Dr. R.N. Hampton of BICC for revealing the realities of corporate research to me.

I dedicate this thesis to the following people:

To my parents (Chris and Barbara Hobdell) who have encouraged and congratulated me in everything I have achieved and supported me through the low points, and my brother, Richard, for the telephone guitar jamming sessions and refreshing tales of drunken debauchery;

Dave, Emma, Henri and Molly Williams for being my surrogate family;

Dr. Steven Betteridge and Mr. Paul Sayers, for friendship and time shared in the lab;

Pete Hobley for companionship through the quiet summer months and the infrequent — but intense — social evenings;

Finally, to Kate German for consistent reality checks and for standing by me through my grumpiest of moments.

Without the support of all of these people, this thesis would never have been completed. I extend my sincerest thanks to everyone.

Contents

List of Figures

List of Tables

Chapter 1

Introduction

The primary objective of this thesis was to investigate whether the TSC method can be used to distinguish various cable model samples subjected to high-voltage DC poling. Consequently, the effect of factors such as voltage magnitude, voltage polarity, temperature, semicon or insulation type on the space charge and polarisation produced in the cable model samples has been determined.

Chapter 2 introduces some important aspects of the morphology of the materials associated with the cable models investigated in this work. The insulation is typically semi-crystalline crosslinked polyethylene (XLPE) with layers of carbon-loaded polymer ("semicon") separating the insulation and the metal conducting electrodes. The interface between the XLPE and semicon is believed to play an important role in determining the space charge concentration within the XLPE.

Chapter 3 describes the poling stage. It details the ways in which the internal polarisation of the cable models become so distorted under the influence of high electrical fields. The mechanisms involved include dipolar polarisation, internal interfacial polarisation, space charge migration within the bulk of the insulation,

and electrode effects (electronic injection and electrostatic double layers) which contribute to the polarisation of the sample. A model for quasi-continuous electronic charge transport through a semi-crystalline polymeric material is presented which has special relevance to the cable models investigated later.

Chapter 4 details the thermally activated relaxation processes that dominate after removal of the poling electric field. The popular models of dipolar and space charge relaxation are described; these have been used with limited success historically to describe ideal dipolar and polarised charge systems. Analysis methods for ideal thermally stimulated relaxation curves are also described. However, the difficulty in introducing these ideal models to the complicated, non-ideal, real system of a cable model is emphasized, with reference being made to recent works concerning Thermally Stimulated Current (TSC) analysis techniques.

Chapter 5 contains a specific literature review of XLPE and LDPE samples. The number of cited articles has been carefully limited to particularly relevant works. The reviewed articles discuss TSC measurements of plaque and cable samples, which have been investigated been performed under similar conditions to the present work. Extraordinary papers have also been included which have special relevance to the later discussion.

Chapter 6 describes the TSC measurement Procedures I and II that have been used in this investigation. Sample preparation is first described, followed by a full description of the heating, poling, cooling, removal of poling voltage and the subsequent isothermal and thermally stimulated current measurement cycle.

Chapter 7 describes the results obtained using the TSC procedures. The

primary cable types investigated are 1Aa, 1Ab and 1Ba, which all have the same insulation, but have different semicon compositions. Measurements were made on these samples using Procedure I with negative and positive poling voltages. The negative Procedure I measurements performed and then repeated on fresh samples of these types show incremental changes but general repeatability due to the temperature and voltage cycling. Procedure II measurements are also reported for these cables. Less comprehensive measurements on samples of cables 2Ba and 3Ab are also reported in this chapter,which serve to illustrate some effects of different semicon types and of different XLPE composition. These measurements are utilised in the discussion.

Chapter 8 gives some results of novel measurements of the electrokinetic (EK) effect and presents the associated theory. The results of measurements performed on the primary cable types 1Aa, 1Ab and 1Ba are reported here.

Chapter 9 contains the discussion, and brings together all of the main points which arose from the TSC and EK measurements. The effects of the semicon base resin, semicon carbon and insulation on the measurements are discussed, as are the effects of thermal and voltage cycling. The thesis as a whole is summarised in the conclusions at the end of this chapter.

Chapter 2

Energy Cable Materials

This chapter describes the physical characteristics of the polymers used in the energy distribution cables studied. In particular, the chemical composition and morphology of the insulation and semiconducting screens are discussed. An understanding of these are required before the 'polarisation' processes of the material, discussed in chapter 3, can be considered.

The main insulating material in HV energy cables is cross-linked low-density polyethylene (XLPE), which has almost entirely replaced oil-filled paper insulation over the last 20 years. The XLPE is located between inner and outer semiconducting polymer ('semicon') screens (figure 2.1) which are incorporated into the cable geometry to reduce local field enhancement at the conductor core and to eliminate electrical treeing from asperities on the surface of the metal conductors [17]. An additive package containing a cross-linking agent, anti-oxidant, ultraviolet radiation damage inhibitor, treeing inhibitor and other such compounds is usually added to both the XLPE and semicon to protect the materials from thermal and electrical degradation. These additives may also modify the morphology of

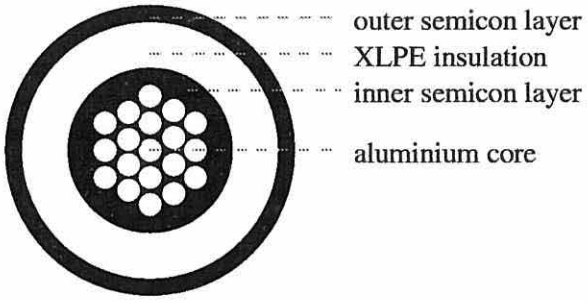

Figure 2.1. Schematic cross-section of a triple-extruded energy cable.

the materials [18].

2.1 Polyethylene

The polyethylene molecule consists of long covalently-bonded hydrocarbon chains (figure 2.2a) formed from approximately 1000 ethylene monomer units (figure 2.2b). Unfortunately, the polyethylene molecule is rarely so ideal, often forming branches (figure 2.3) which may be anything from a few repeat units long to the equivalent length of the parent chain. The chains may also have 'cross-links', molecular units of any size which join polymer chains as connecting branches [17]. Cross-links are encouraged in XLPE to improve the mechanical and dielectric properties of the polymer. Most notably, cross-linking restricts the flow of the polyethylene above the maximum LDPE cable operating temperature of $\approx 70°C$, so that the cable can continue in service at operating temperatures of 80-90°C without excessive softening becoming a problem. XLPE cables can also withstand brief short circuit operation at higher temperatures, up to 250°C, in comparison to LDPE cables which have a lower limit of 160°C. Cross-linking is achieved by

addition of dicumyl peroxide (DCP) to the polyethylene prior to manufacture of the cable. Figure 2.4 shows the chemistry of the cross-linking process, with step (3) showing the actual cross-link. The DCP reaction is thermally initiated during the extrusion of the cable by raising the polyethylene temperature to 180°C, well above its melting point. It should be noted that the DCP cross-linking reaction forms volatile by-products: methane, cumyl-alcohol, α-methyl styrene and acetophenone. These by-products are unwanted impurities, as are other methyl, ethyl and butyl residuals left after the cross-linking process, although acetophenone is known to improve the resistance of XLPE to water trees. Other chemical additives may also be considered as impurities. These impurities will later be shown to contribute to the polarisation stage in the TSC experiment (chapter 3).

2.2 The Polyethylene Solid

Polyethylene solid is semi-crystalline, consisting of crystalline regions of well ordered chains which are surrounded by disordered amorphous regions (figure 2.5). The crystalline regions form a folded lamella structure, while the amorphous regions contain tangled chains. Individual polymer chains may pass through both crystalline and amorphous regions, however. The two regions have different electrical and mechanical properties and can be considered to be different materials. Note that the amorphous phase has the lower density and has much higher free volume, so that impurities can more easily be accommodated there. The interfaces between the amorphous and crystalline phases are important because they are likely to be sites of charge trapping, as described in chapter 3. It is these

regions which will alter significantly when temperature-induced phase changes occur in the polymer.

2.3 Semicon

The semicon shields are usually formed from polyethylene or a copolymer of polyethylene with acetates or acrylates. Acrylates are more common in Europe because of the environmental aspect. Carbon is added to reduce the resistivity of the material to between 2–4 Ωcm. The semicon morphology is illustrated in figure 2.6. The carbon may be one of two types: 'super-smooth black' carbon is formed by the pyrolysis of acetylene to produce a clean, smooth carbon powder, while 'furnace black' carbon is literally scraped from the walls of a furnace to produce a rougher, less pure carbon. Furnace black is likely to contain other elements, for example sulphur. Geographical origin also has a bearing on the contamination factor: furnace black from the US contains almost ten times more sulphur (1700ppm) than European furnace black (200ppm). The super-smooth carbon particles are rounder and smooth, and are more regular in size and shape, while furnace black particles are rough and angular, with a wider distribution of particle sizes. Although much has been written about the macroscopic properties of semicon, there is little information about the size of the carbon particles. Okamoto *et al* [19] used transmission electron microscopy to show agglomerations of furnace and super-smooth carbon particles with diameters in the 100–300nm range. At a high carbon concentration of 41 vol% the particles agglomerate to form larger carbon regions, although the degree and distribution of agglomeration is ultimately

dependent on the semicon additives. Betteridge *et al* [20] found similar results determined from atomic force microscopy images. The furnace black particles in XLPE were twice the size of the super-smooth particles, which were approximately 100nm in diameter. By contrast, Nakamura *et al* [21] report much smaller particle sizes of between 30 – 90nm for three specific carbon black types.

The dependence of the resistivity of the semicon material as a function of the carbon content has been reported [21]. The resistivity of the semicon drops rapidly above a 'percolation threshold' for a carbon content of about 5 vol%. Although extensive empirical evidence exists, modelling work is continuing to investigate the exact nature of the percolation threshold conduction process [22]. The popular model describes conduction paths of almost-touching carbon particles through the material, with a tunnelling process providing conduction from one carbon particle to the next. A possible conduction path of this sort through the semicon is shown in figure 2.6.

The semicon in the samples studied contains approximately 40 vol% carbon, providing a high likelihood of direct conduction through the semicon, although tunnelling will be the main particle-particle conduction mechanism.

2.4 Semicon-XLPE Interface

The semicon-XLPE interface is a crucial region of the cable, affecting its overall electrical properties. The likely interfacial morphology is illustrated in figure 2.7. Ideally, the carbon particles would be coated with the semicon polymer so that the interface with the XLPE insulation would be a polymer-polymer interface, as

shown at A in figure 2.7. This situation has important consequences for charge storage at the interface, as discussed in chapter 3. However, it is also possible that a 'bare' carbon particle will extend across the interface as at B, creating a direct route for charge injection into the insulation (also discussed in chapter 3) and enhancing the probability of electrical failure there.

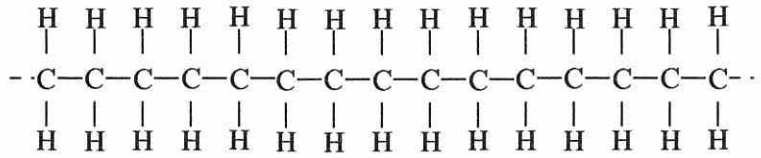

a) small portion of a polyethylene chain

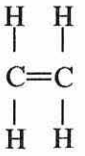

b) ethylene monomer unit

Figure 2.2. Chemical composition of polyethylene.

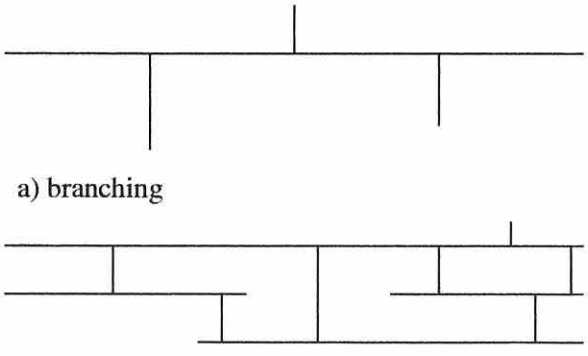

a) branching

b) crosslinking

Figure 2.3. Branching from and cross-linking between polyethylene chains

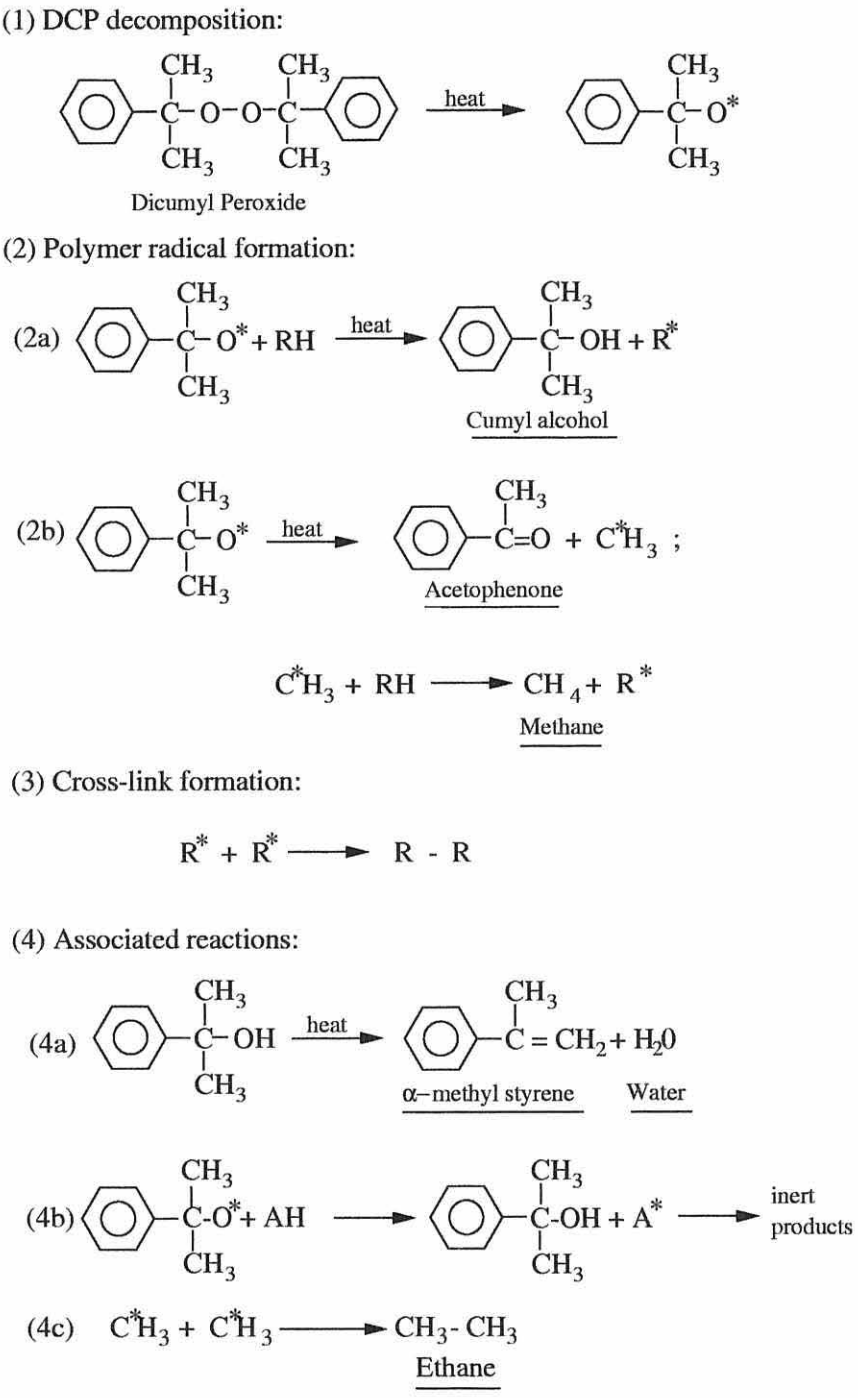

Figure 2.4. Chemistry of the cross-linking process, showing the unwanted by-products (underlined) of cumyl alcohol, acetophenone, α–methyl styrene, water and other inert products. R is the polymer chain and A is the anti-oxidant. (after [1].)

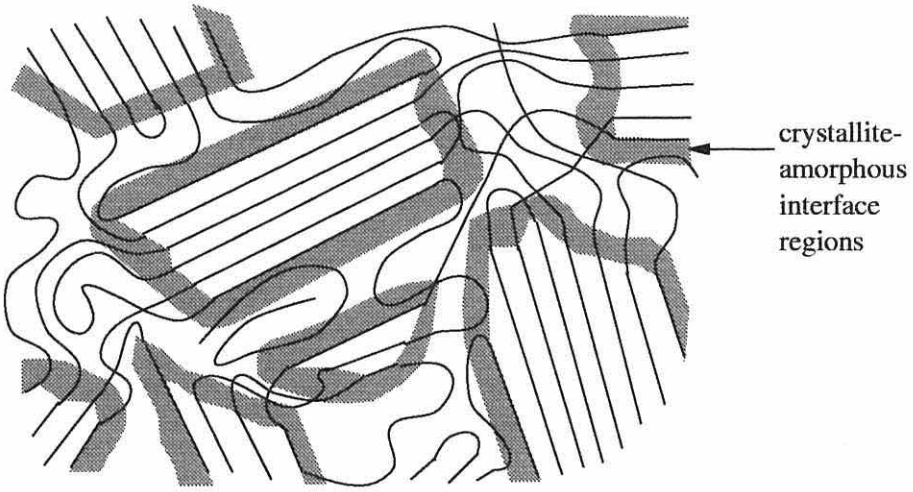

Figure 2.5. Crystalline-amorphous regions in polyethylene

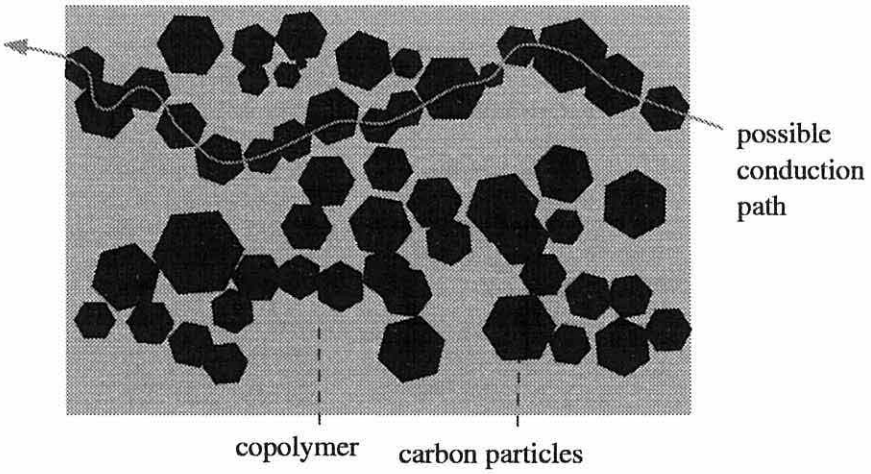

Figure 2.6. Schematic of semicon morphology

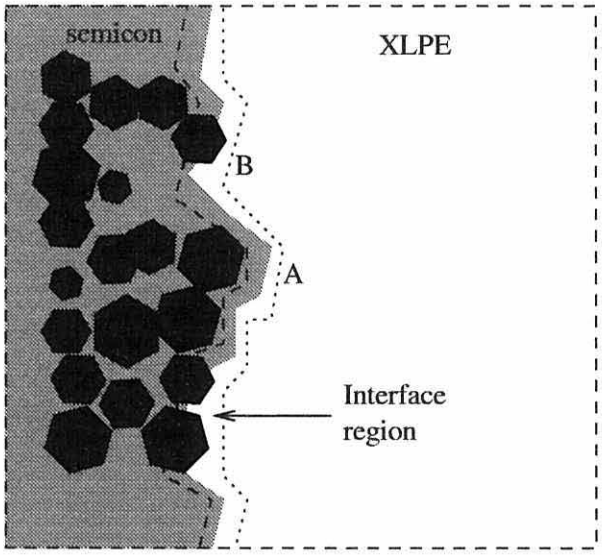

Figure 2.7. The interface between semicon and XLPE insulation

Chapter 3

The Poling Stage

An essential first step in the TSC procedure is to polarise the dielectric by applying a high field at elevated temperature and then to cool the sample whilst maintaining the field, so that the induced polarisation is frozen in. The processes that occur during this poling stage are described below.

3.1 Dipolar Polarisation

Although polyethylene molecules are highly non-polar, dipoles still exist in solid XLPE as molecular impurities. Some of the branches and end-groups on the polyethylene chains may also be dipolar (for example -CH_2COOH). These dipoles will experience an orienting torque that will rotate them in the direction of an applied electric field (figure 3.1). The degree of orientation is thermally and sterically limited. Lower temperatures and higher electric fields produce a correspondingly greater polarisation.

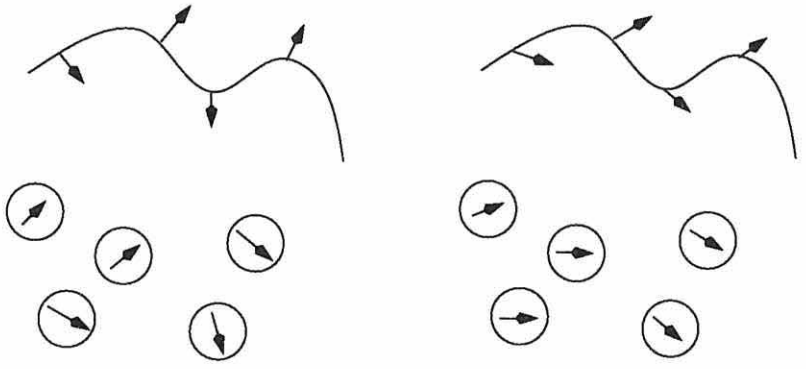

(a) No Field (b) Field F applied

Figure 3.1. Orientation of dipoles under an applied electric field.

3.1.1 Internal Interfacial Polarisation

It was noted in section 2.2 that the crystalline and amorphous regions in XLPE have different electrical properties. Applying an electric field F will cause a Maxwell-Wagner-like charge accumulation at the interfaces between these regions due to migration of the free space charges, as long as there is a difference in the conductivity between regions (figure 3.2). Charge accumulation in this way will create long-range dipoles within the material.

3.2 Space Charges

Two types of space charge may exist within XLPE: ionic and electronic.

Ionic space charge consists of the various free ionic species which may be present as impurities after cable manufacture, or may originate from reactions of these impurities with water and oxygen which diffuse into the cable during its service lifetime. Under the influence of an applied electric field the ionic species

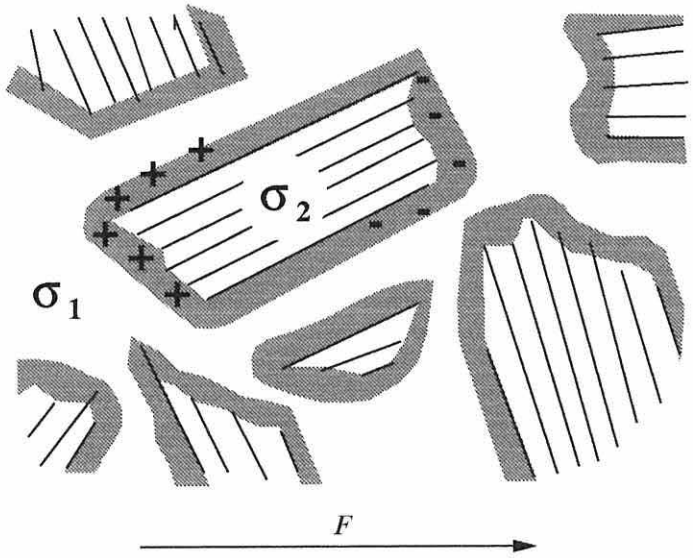

Figure 3.2. Interfacial polarisation of crystalline-amorphous interfaces due to the different electrical properties of the phases.

will drift through the free volume of the amorphous XLPE regions. Large ions are likely to become trapped within the bulk amorphous regions, while small ions will be able to pass through the free volume and although some may become trapped at the amorphous-crystallite interfaces (figure 3.2), others will drift through the polymer ultimately to accumulate at the electrode of opposite polarity to form a heterocharge. Some of this charge may be neutralised by a counter charge injected at the electrode (see section 3.3). Note that non-ionic dipolar molecules may also become ions by gaining or losing net charge at an electrode.

Electronic space charge (electrons or holes) in the material (as distinct from ionic space charge) will originate via transfer of electrons between an electrode and the polymer matrix. The injection/ejection process will be described later in section 3.3.

It is generally accepted that the electronic charge is accommodated within

crystalline materials in coherent extended electronic states which arise from long-range atomic or molecular ordering [23]. In order to accommodate injected charge, polyethylene must possess similar energy states. It has been noted however that XLPE is semi-crystalline (chapter 2). The crystalline regions will be characterised by these regular extended-state energy bands with edges E_v and E_c (figure 3.3a), which are separated by a band gap E_g. The electron affinity χ for polyethylene is negative, such that E_c falls *above* the vacuum energy level E_{vac}, making electron injection into the XLPE extremely difficult. However, the irregular spacing of the

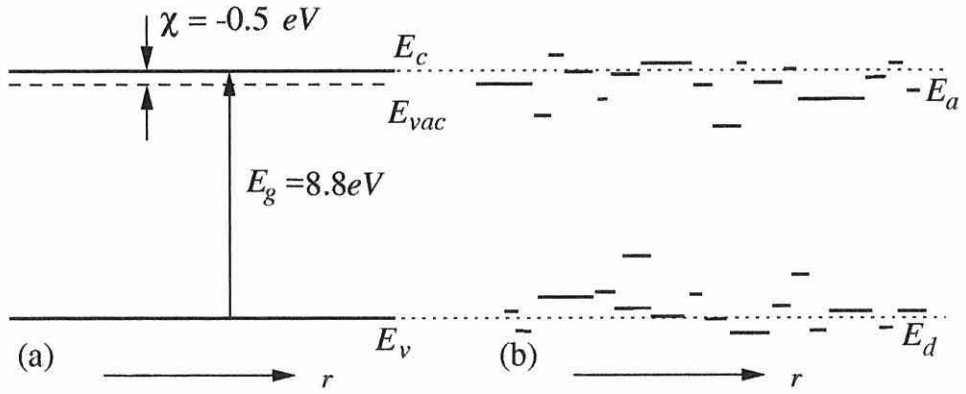

Figure 3.3. The energy band diagram for (a) extended electronic states in crystalline polyethylene and (b) localised electronic states E_a and E_d in amorphous polyethylene (after [2]).

molecules in amorphous XLPE gives rise to a localisation in space of the energy states within the energy band gap ($E_c - E_v$). It should be noted that this energy state localisation is also found in many other amorphous solids [24]. The localised donor or acceptor states, E_d or E_a, can be associated with the band edges E_v and E_c, respectively, of the crystalline polyethylene (figure 3.3b). Injected electronic charge can access these localised states more readily than the conduction band states above E_c. The extent of a state along a given coordinate direction r depends on the degree of localisation. In the amorphous regions, the states will be

highly localised since the periodicity of the polymer will be interrupted by kinks and folds in the chains . However, the high degree of ordering and periodicity of the polymer chains in crystalline regions will produce extended electronic states in the direction of r. Electronic charge transport through these extended energy states will be relatively easy when compared to transport through states in the amorphous regions [25] which will have to occur by a combination of thermal activation and quantum-mechanical tunnelling [26].

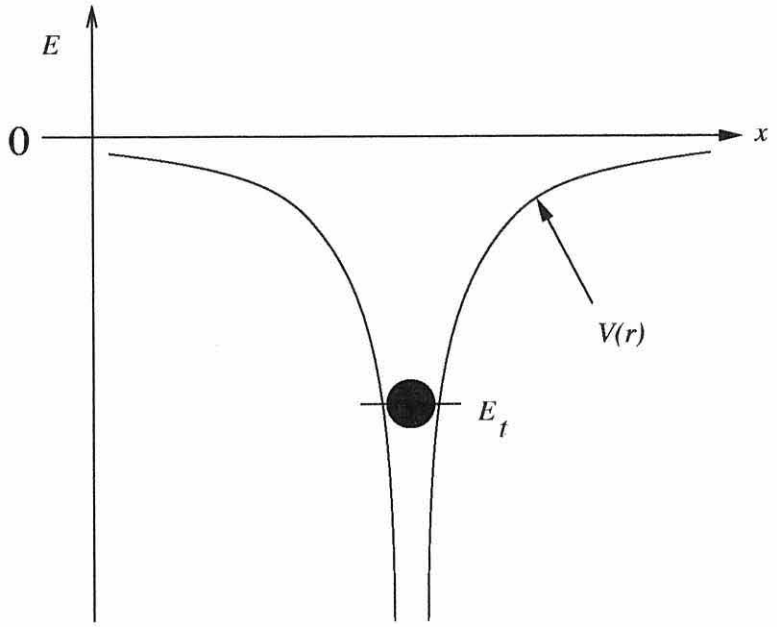

Figure 3.4. Energy diagram for a single 'trap' state.

If the localised electronic state, or 'trap', is an acceptor type E_a, it will be negatively charged when filled and electrically neutral when empty. A donor state E_d conversely will be neutral when filled, but positively charged when empty. Both types of trap can be represented by a coulombic potential well $V(r)$ as in figure 3.4. An electronic charge resident in the trap must gain sufficient energy E_t to escape from the trap if it is to become mobile and contribute to the conduction

	τ/s	
E/eV	(T=300K)	(T=400K)
0.6	1.20×10^{-5}	3.63×10^{-8}
0.8	2.75×10^{-2}	1.20×10^{-5}
1.0	6.31×10^{1}	3.98×10^{-3}
1.2	1.45×10^{5}	1.32
1.4	3.31×10^{8}	4.36×10^{2}
1.6	7.58×10^{11}	1.45×10^{5}

Table 3.1. Electronic charge residence times in traps of depth E.

and polarisation of the polyethylene. E_t will be equivalent to E_d or E_a, depending on the trap type. Detrapping is governed by thermal activation, such that the probability p_e of escaping from the trap is given by

$$p_e = \nu . \exp\left(-\frac{E_t}{kT}\right) \tag{3.1}$$

where the pre-exponential factor ν is usually taken to be the phonon frequency of $\sim 10^{15}$Hz, although it could be much less for polyethylene [27]. The time τ that the electron stays in the trap for any given E_t will be $1/p_e$ [28]. Trap energies which might be typical for polyethylene are listed together with values of τ in table 3.1, and illustrate how a small change in E can have a significant effect on τ. For example, charge trapped in a $1.4eV$ trap may be resident for an average time period of 10 years at room temperature! Elevating the trap temperature to 400K will reduce this time to less than 10 minutes. This sensitivity to temperature forms the basis of the TSC method as described in chapter 4. Applying an electric field F to the trap will reduce the height of the energy barrier as shown in figure 3.5, where E_t is reduced to E_t', making τ less and making charge migration, macroscopic conduction and polarisation more facile.

If an electronic charge comes to rest in a trap for a period of time which is

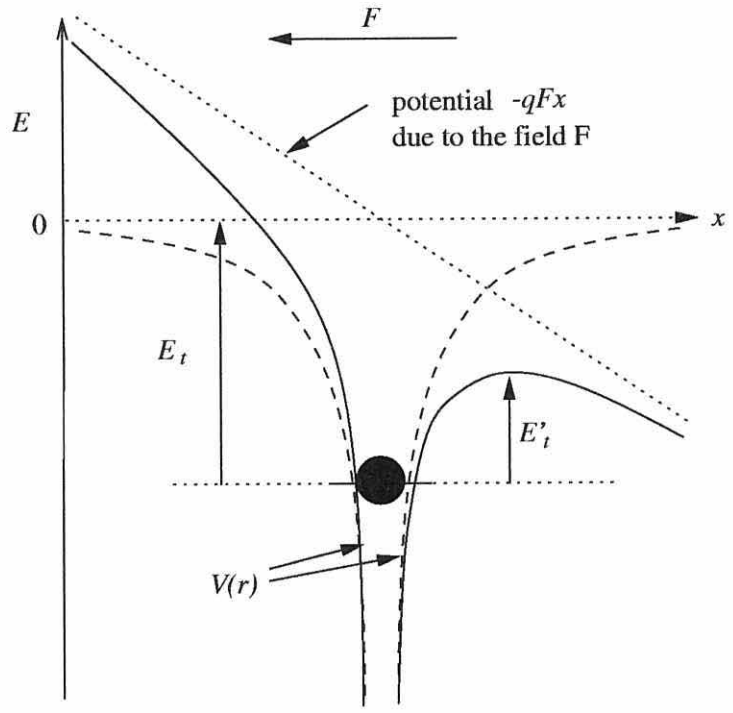

Figure 3.5. Reduction of the trap energy depth E_t to E'_t by modifying $V(r)$ with an electric field F.

comparable to the relaxation time of the dipoles surrounding the trap, then these dipoles will become polarised by the electric field of the charge. The trap energy will be significantly modified by the energy P of the induced polarisation, which can be as much as $2eV$ for polymers [29, 30]. Now it will be more difficult for the charge to be thermally activated from the energy state, as it will be deeply trapped within the polyethylene.

Charges trapped in localised states, whether negative (electrons) or positive (holes) constitutes a space charge in the polymer. If the traps are sufficiently deep, the charge may persist for very long times (table 3.1), but raising the temperature sufficiently will release the charge.

In general, charge will be transferred between two adjacent trap states i and j by a process of thermally-activated quantum-mechanical tunnelling (A-T,

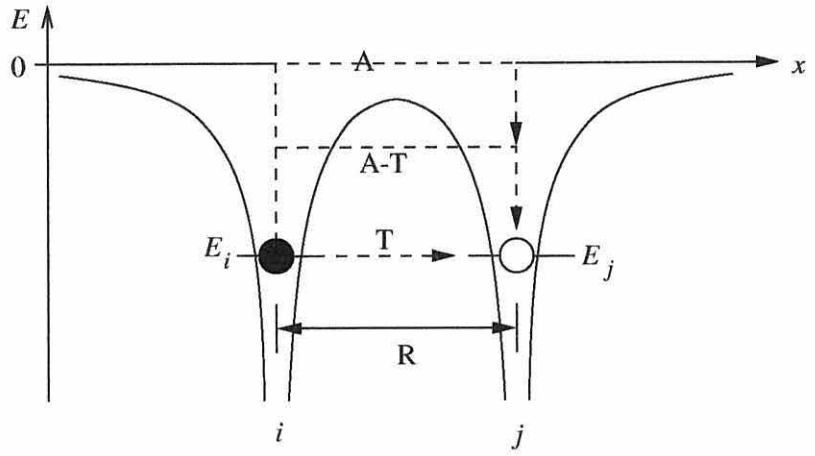

Figure 3.6. Transfer mechanisms between two trap states i and j.

figure 3.6) for which there are two limiting cases: simple thermal activation (A); and complete tunnelling (T). Charge transfer between a trap and crystallite band states, and between a trap and an electrode (section 3.3) can also occur by this process. Redi and Hopfield [26] give a simplified treatment of the situation (see figure 3.6), such that the rate of transfer p_t from a filled trap state i to an empty state j is

$$p_t = \nu_{ij} \exp(-2\alpha_{ij} R) \exp\left(-\frac{W_{ij}}{kT}\right) \tag{3.2}$$

where ν_{ij}, α_{ij} and W_{ij} are complex functions of the trap energies E_i and E_j, the polarisation energies P_i and P_j and the physical width of the trap states [2]. Note that equation 3.2 corresponds to that for hopping transport in amorphous solids [31].

Ultimately, the mobile space charges may arrive at the opposite electrode, where they will either form a heterocharge, be ejected from the material or neutralise charges of opposite polarity. This is described further in the next section.

3.3 Electrode Effects

Most of the theoretical treatments of the charge transfer processes at an interface describe metal-polymer contacts (for example, [27, 28, 32, 33]), while little has been written for the specific case of semicon-polymer contacts. The former case is first described, then assumptions later will be made concerning the nature of the latter.

3.3.1 Electronic Injection

The process of charge injection at a metal-polymer electrode is similar to that for hopping transfer, described in the previous section. At a cathode, electrons can be transferred by hopping from occupied states in the metal electrode into neutral acceptor states E_a in the polyethylene (figure 3.7a). Electrons injected from the metal may also neutralise ionised donor states E_d^+ in the polymer (figure 3.7b). Similarly at the anode, electrons can be ejected from neutral donor states E_d (equivalent to injection of holes) (figure 3.7c) or from ionised acceptor states E_a^- (figure 3.7d) in the polymer into free states in the metal. Application of an electric field will necessarily enhance the injection processes at the electrodes. An applied field lowers E_a and E_d^+ with respect to the cathodic E_f (figure 3.8a) and raises E_a^- and E_d with respect to the anodic E_f (figure 3.8b).

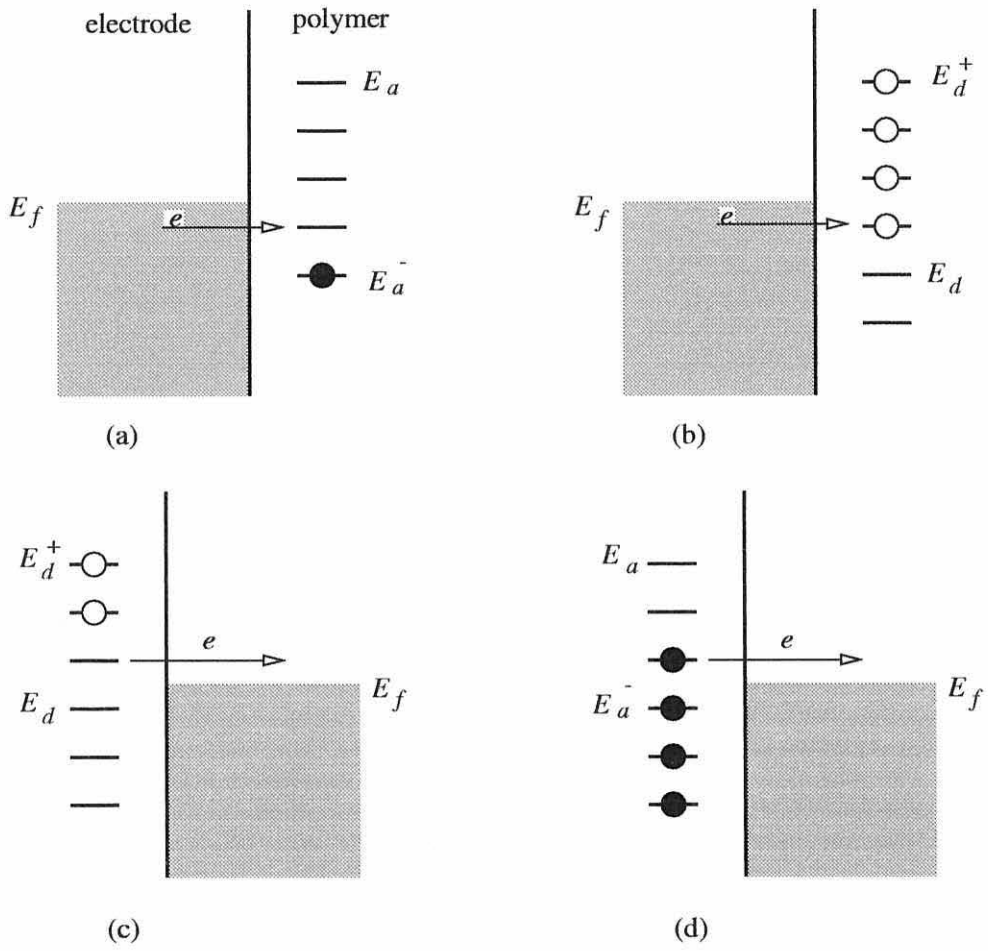

Figure 3.7. Injection/ejection processes at (a,b) the cathode and (c,d) the anode

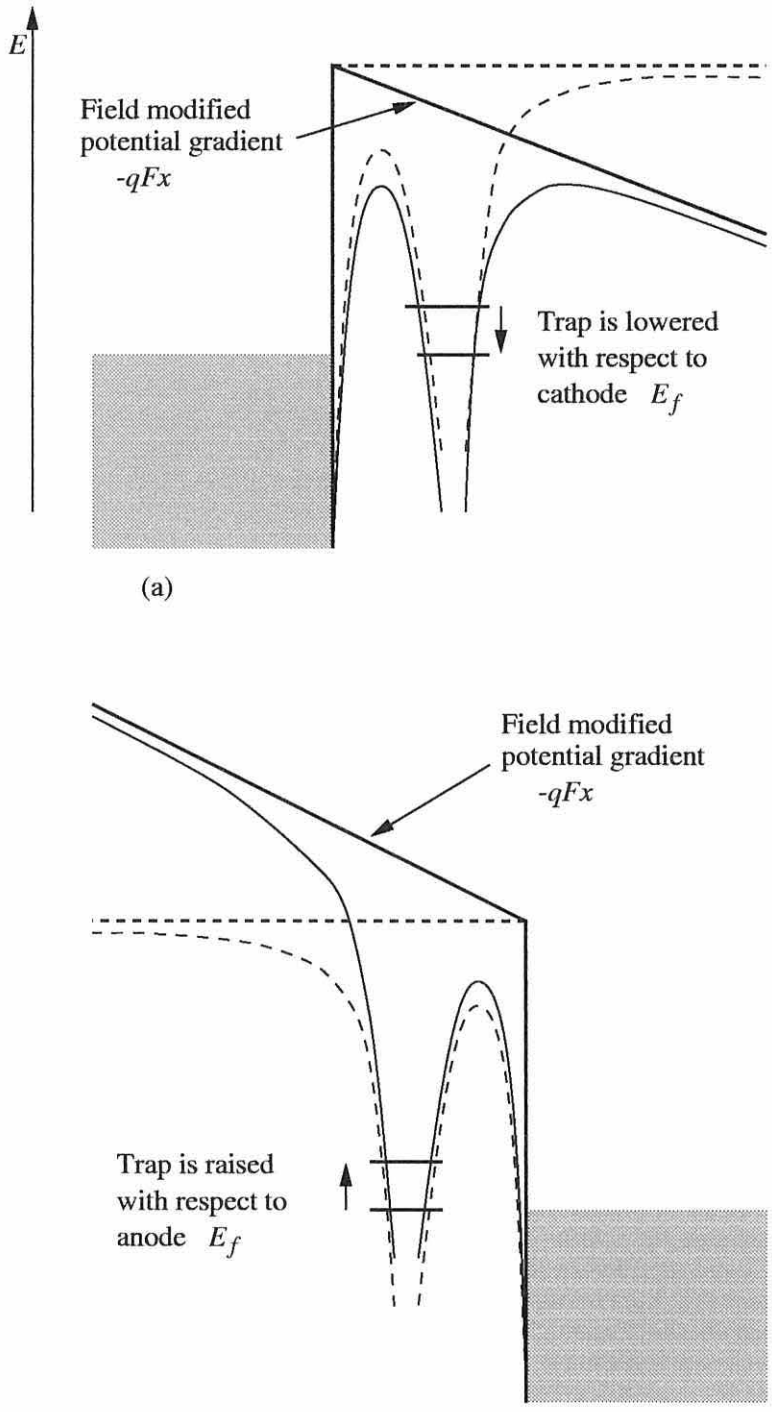

Figure 3.8. (a) lowering of traps at the cathode and (b) raising of traps at the anode, both as a result of an applied electric field F.

3.3.2 Double Layers

Now that charge injection is understood regarding the localised states E_a and E_d in the region of the electrode interface, the case for large separations in these levels can be considered. One of several processes may occur. At the cathode, if $E_f > E_a$ then a large number of electrons will be injected into the surface states of the polymer. Assuming that the rate of electrons hopping away from the cathode through E_a states is low, then the injected charge will accumulate to form a homocharge at the interface as shown in figure 3.9(a). This accumulation of negative charge will in turn induce a positive image charge in the electrode, creating an interfacial double layer. Conversely, if $E_f < E_d^+$ then the neutral donor states will become positively ionised as their electronic charge passes into the metal electrode. These states will accumulate at the interface, this time forming a heterocharge (figure 3.9(b)). A negative image charge will be induced, once more creating an interfacial double layer. A similar situation will also occur at the anode: a negative heterocharge accumulates when $E_a^- < E_f$ and a positive homocharge accumulates for $E_d > E_f$. If the charge hopping is slow, a double layer will be established.

The molecules that have energy states and that are located within 3Å of the interface can become strongly adsorbed to the metal, while molecules further away from the electrode will have energy levels more related to the bulk but modified by the presence of ionic space charge, for example [28]. The magnitude of the field in the region of the metal-polymer double layer may be as high as 10^9 V.m^{-1} and is largely independent of an applied field.

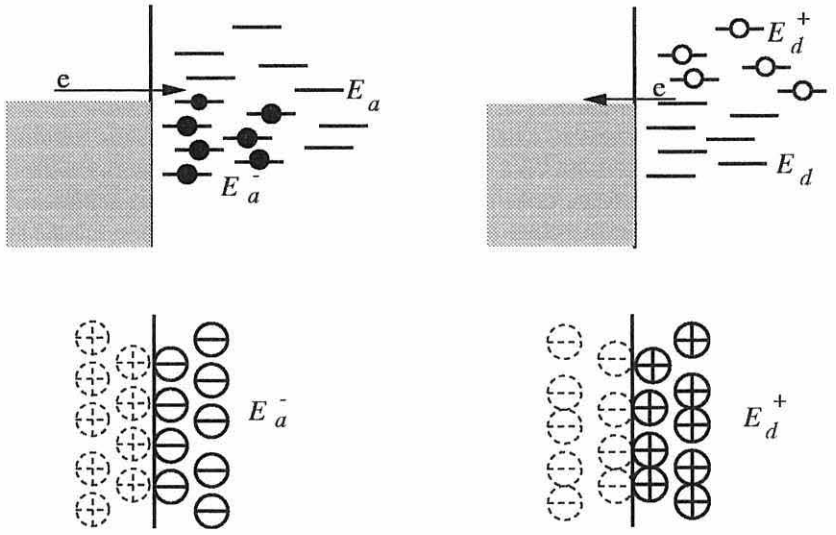

(a) negative homocharge (b) positive heterocharge

Figure 3.9. Double layers formed at the cathode.

In comparison to a typical metal-polymer interface, studies have shown that the interface between semicon and XLPE is confusingly different. Sigmond and Hegerberg [34] have reported that, while metallic or pure carbon electrodes only ever inject electrons, semiconducting electrodes can inject both electrons and holes equally well. They attribute this effect to the field intensification and current constriction near the tips of carbon grains bordering to the pure insulator, implying that no contribution is made to the injection process from the polymer-coated carbon particles described in figure 2.7. However, It is not certain which base polymer type was used in the semicon of Sigmund and Hegerberg's studies. If a different polymer base resin is used, then perhaps different effects would have been observed. Further discussion of this situation will appear in chapter 9.

Chapter 4

Thermally Stimulated Depoling Processes

Following the polarisation stage, the cable materials will be in a thermodynamic quasi-steady-state, ready to begin the TSC depoling process. Dipolar relaxation and space charge migration will occur as a result of the thermal energy made available and the influence of the electric field present in the cable sample at the instant that the polarising field is removed. The idealised models which describe these temperature dependent processes are generally based on planar geometries, and have been reviewed extensively by Chen and Kirsh [35] and Vanderschueren and Gasiot [36]. The models that are specifically relevant to Thermally Stimulated Current (TSC) measurements made on XLPE are summarised below.

The TSC method measures the current density $j(t)$ that flows through the polarised sample placed in a circuit as shown in figure 4.1. The current results from the depoling processes within the material, which can be expressed as

$$j(t) = \sigma(x,t).F(X,t) + \epsilon_\infty \frac{\partial F(x,t)}{\partial t} + \frac{\partial P(x,t)}{\partial t}. \tag{4.1}$$

where σ is the bulk conductivity, F is the electric field, ϵ_∞ is the optical permittivity and P is the sample polarisation. The charge density ρ within the sample

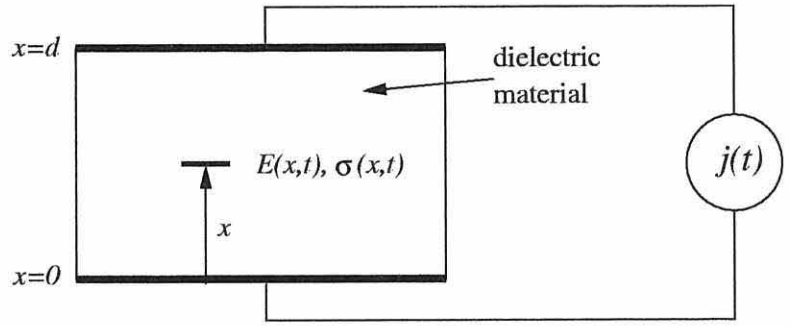

Figure 4.1. Current flow through an external circuit as a result of depoling of dipoles and space charge.

is

$$\rho(x,t) = \epsilon_\infty . \frac{\partial F(x,t)}{\partial x} + \frac{\partial P(x,t)}{\partial x} \tag{4.2}$$

which is Poisson's equation. ρ consists of mobile and trapped charge. The charge will in turn influence F and ρ, and thus will modify $j(t)$. After some simple algebraic manipulations, and assuming $\epsilon_\infty . F(0,t) + P(0,t) = 0$ [37] equation 4.1 can be rewritten as

$$j(t) = \sigma(0,t)F(0,t) + \frac{\partial \bar{P}}{\partial t} \tag{4.3}$$

where $\bar{P}$ is the mean polarisation within the sample, and consists of contributions from the dipole polarisation $\bar{P}_d$ and the space charge distribution $\bar{P}_q$, that is, $\bar{P} = \bar{P}_d + \bar{P}_q$. The contributions $\bar{P}_d$ and $\bar{P}_q$ can be modelled separately as described below.

4.1 Contribution from $\bar{P}_d$

In considering the dipolar contribution, the simplest approach is to adopt the model of Bucci and Fieschi [38]. They assumed a uniform polarisation $P_d(t)$, that

is, $\bar{P}_d(t) = P_d(t)$, which was generated by a set of non-interacting ideal dipoles which relaxed at a rate proportional to the existing polarisation. Hence,

$$\frac{dP_d}{dt} = -P_d \tag{4.4}$$

or

$$P_d(t) = P_d(0).e^{-t/\tau} \tag{4.5}$$

where $P_d(0)$ is the initial polarisation at $t = 0$ when the poling voltage V_p is removed, and τ is the relaxation time. It is assumed that τ is given by a simple temperature activated process, so that

$$\tau(T) = \tau_o . \exp\left(\frac{E}{kT}\right) \tag{4.6}$$

where τ_o is independent of temperature and E is an activation energy for dipole relaxation.

In a TSC experiment, the sample is heated at a constant heating rate β such that

$$T = T_0 + \beta t \tag{4.7}$$

where T_0 is the temperature at the start of heating (normally room temperature). Thus, using equations 4.1, 4.5 and 4.7, the current $j(t)$ arising from dipolar polarisation becomes

$$j(T) = A \exp\left(-\frac{E}{kT}\right) . \exp\left[\frac{B}{\beta}\int_{To}^{T} \exp\left(-\frac{E}{kT'}\right) dT'\right] \tag{4.8}$$

where

$$A = \frac{P_d(0)}{\tau_o} \quad \text{and} \quad B = \frac{1}{\tau_o}. \tag{4.9}$$

Equation 4.8 has the form shown in figure 4.2. When T is near to T_0, that

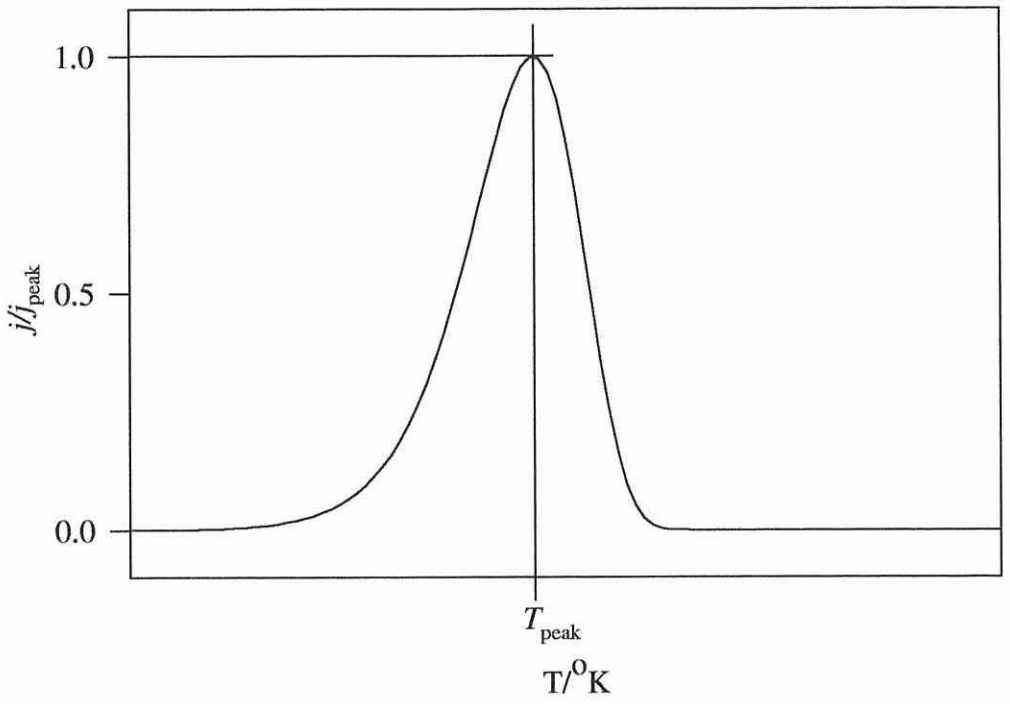

Figure 4.2. A normalised first order thermally stimulated relaxation curve.

is in the initial stage of temperature rise, the second exponential term in equation 4.8 will approximate to unity and the first exponential term alone will describe the rise in current with increasing temperature. As the temperature rises further, the second exponential term will become important and the current will then go through a maximum j_{peak} at temperature T_{peak} before rapidly decreasing, describing the progressive depletion in the number of dipoles available to contribute to $j(t)$.

4.2 Contribution from $\bar{P}_q$

There are two approaches to the modelling of the relaxation of the induced polarisation P_q from space charge. The first approach, taken by Kunze and Müller was

to make assumptions as to the state of the electric field F between the electrodes and leads to a model based on macroscopic parameters. The second approach requires detailed algebra to derive P_q from the thermally activated processes of conduction, retrapping and recombination of individual electrons, and uses localised parameters.

4.2.1 Kunze and Müller's Model

The model of Kunze and Müller [39] assumes that a non-uniform charge distribution within a material can be represented by a surface charge density Q on the electrodes which generates a uniform field F between these electrodes such that

$$F(t) = \frac{Q(t)}{\epsilon} \tag{4.10}$$

where ϵ is the permittivity of the material. The current density j will be

$$j(t) = -\frac{dQ(t)}{dt}. \tag{4.11}$$

which can be related to the bulk conductivity $\sigma(t)$ as

$$j(t) = \sigma(t).F(t). \tag{4.12}$$

Assuming that the conductivity $\sigma(t)$ arises from a single type of defect within the material corresponding to a trapping state with a single energy level E, then the temperature-dependent conductivity can be expressed approximately [35] as

$$\sigma(T) = \sigma_\circ . \exp\left(-\frac{E}{kT}\right), \tag{4.13}$$

so that the depolarisation current

$$j(t) = -\frac{dQ(t)}{dt} = \frac{\sigma_\circ}{\epsilon}.Q(t). \exp\left(-\frac{E}{kT}\right). \tag{4.14}$$

Integration of equation 4.14 and using $dT/dt = \beta$ gives an equation of the same form as equation 4.8, but now

$$A = \frac{\sigma_o}{\epsilon}.Q(0) \text{ and } B = \frac{\sigma_o}{\epsilon}. \tag{4.15}$$

Although Kunze and Müller's model gives an expression for $j(t)$ of similar form to that for dipole relaxation, the model is based on dubious assumptions, particularly as it is unlikely that the field F is uniform throughout the dielectric. A treatment which considers the localisation of the space charge in the bulk is more appropriate.

4.2.2 A Model Based on Localised Charge

The localisation of energy levels in materials such as XLPE (section 3.2) and the transfer of charge between these local states by thermally-stimulated quantum-mechanical tunnelling (also section 3.2) suggests that the TSC current $j(t)$ arises from these charge transfer processes.

Assuming electrons to be the dominant mobile species, figure 4.3 show the various processes that may occur. An electron in a trap state (a) may be thermally activated into a conduction state (b) where it will contribute to a conduction current in a field $F(x,t)$. The initial activation of this electron will occur with a probability per unit time r_r. Once in the conduction state, the electron may then become retrapped (c), or may recombine with a corresponding counter charge in a valence state (d). Retrapping and recombination will occur with a probability per unit time r_t and r_n, respectively. A trapped electron may also recombine with

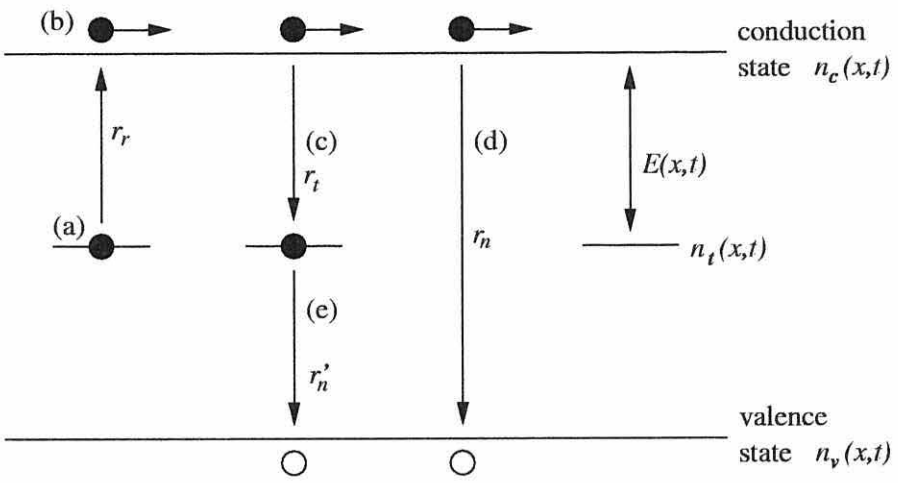

Figure 4.3. Mechanisms contributing to the thermally stimulated depoling of space charge.

a counter charge in a valence state (e) with a probability per unit time r_n'.

The charge density within the sample can be shown to be [37]

$$\rho(x,t) = q[n_c(x,0) + n_t(x,0)] \exp\left(-\int_0^t R^{-1}.dt\right) \tag{4.16}$$

where

$$R = \frac{r_t + r_n}{r_r.r_n + (r_t + r_n).r_n'}, \tag{4.17}$$

q is the elementary charge (1.6×10^{-19}C), n_c is the concentration of mobile electrons in the conduction state and n_t is the concentration of trapped electrons. The expression for R may be simplified for certain ideal cases. Hence, for fast retrapping, i.e., $r_t \gg r_n$:

$$R = \frac{r_t}{r_r.r_n + r_t.r_n'} \tag{4.18}$$

while for slow retrapping ($r_t \ll r_n$),

$$R = \frac{1}{r_r + r_n'}. \tag{4.19}$$

The effective mobility μ' of charge undergoing trapping and release will be

less than the mobility μ of mobile charge in the conduction state. Lewis *et al* [37] show that

$$\mu' = \frac{r_r}{r_r + r_t + r_n}.\mu. \tag{4.20}$$

For isothermal conduction, the current density is

$$j(t) = -\frac{d\bar{P}_q(t)}{dt} = -\frac{\mu' Q_o^2}{2d\epsilon_\infty} \exp\left[-2\int_0^t R^{-1}dt\right] \tag{4.21}$$

where Q_o is the initial total charge in the sample. solving equation 4.21 for a linear heating rate β with appropriate expressions for R (equations 4.18 and 4.19) and μ' (equation 4.20) will result in an expression for the time-dependent charge relaxation of the standard form (equation 4.8). The parameters A and B will be dependent on the retrapping rate as given below:

	A	B
slow retrapping	$-\frac{\mu Q^2 \nu}{2d\epsilon_\infty r_n}$	$2.\nu$
fast retrapping	$-\frac{\mu Q^2 N_c}{2d\epsilon_\infty N_t}$	$\frac{2r_n N_c}{N_t}$

(4.22)

where ν is the pre-exponential trap-escape probability defined in section 3.2, N_c is the density of conduction states and N_t is the density of trap states within the sample.

4.3 Analysis of Thermally Stimulated Curves

The ideal method of analysis would be to fit the mathematical model to the real data. The early curve fitting technique for simple TSC curves with single peaks was that of Cowell and Woods [40]. This technique was used with limited success by Creswell and Perlman [41] to fit data from the complex TSC of corona-charged

polyethylene terephthalate. There have been several papers on the subject of curve fitting since (for example, [42, 43]) although only the peak *shape* and not the precise physical parameters have been determined. Obtaining these exact parameters is not a straightforward task, as Henn *et al* have recently shown [44]. They indicate that the TSC peak analysis methods traditionally used, based on a distribution of relaxation times or of pre-exponential factors, are extremely unreliable, mathematically demonstrating the doubts raised by Halpern [45] concerning these traditional methods.

Several effects may contribute to the formation of a non-ideal $j(t)$ characteristic. For example, dipole-dipole interactions during dipolar relaxation or a different retrapping rate during space charge relaxation may alter the symmetry of the curves as detailed below in section 4.3.1.

Specifically for trapped charge, Chen and Kirsh ([35], p88) reported that in thermoluminescent (TL) experiments, a quasi-continuous distribution of activation energies is quite common in amorphous samples, which was originally suggested by Randall and Wilkins [46]. For a semi-amorphous material such as XLPE, the amorphous regions will create a broader, asymmetric charge relaxation TSC peak with an apparently lower activation energy, while crystalline regions are likely to produce a peak of the standard form. However, overlapping of the two peak types on the temperature scale will make one indistinguishable from the other.

For dipolar relaxation peaks, although the Bucci-Fieschi model assumes a single Debye relaxation where τ_o is independent of temperature, relaxation pro-

cesses with a distribution of τ_o have been found (see [35]) although not specifically in polymers. A distribution in the activation energies E *is* common in polymers, however. For example, Fischer and Röhl [47] determined the TSC spectrum of polyethylene in the range 80–320K to consist of three peaks centered near 140K, 205K and 245K, each of which resulted from a Gaussian distribution of activation energies.

4.3.1 Kinetic Order

Although Bucci and Fieschi derived the standard mathematical function for thermally stimulated depolarisation of dipoles (equation 4.8), Randall and Wilkins had earlier derived a function of an almost identical form for thermoluminescent (TL) emission as a result of localised trapped electronic charge recombination [46]. Because the form of the equation is identical, analytical methods for determining the parameters for one type of curve (TL, TSD, TSC) can be used for another type ([35], p11).

Randall and Wilkins' theory for TL relaxation was described by a 'first order kinetic' equation for the recombination of charge in alkali halide phosphors. Assuming the retrapping to be insignificant, the TL intensity for the first order kinetics was given as

$$I = \frac{-dn(t)}{dt} = n(t).s \exp\left(-\frac{E}{kT}\right) \tag{4.23}$$

where n was the number of electrons in traps of a single depth E, and $s \approx 10^{8\pm1}\mathrm{s}^{-1}$ for most phosphors. Solving for a linear temperature rise β (equation

4.7), the first order kinetic equation 4.23 became

$$I = A.\exp\left(-\frac{E}{kT}\right).\exp\left[-\frac{B}{\beta}.\int_{T_0}^{T}\exp\left(-\frac{E}{kT}\right)dT\right] \tag{4.24}$$

where

$$A = n(0).s \quad \text{and} \quad B = s. \tag{4.25}$$

Garlick and Gibson extended Randall and Wilkins' theory [48] to include the case of strong electronic retrapping. They assumed that the probability of an electron recombining with a vacant luminescence centre was equal to the electron retrapping probability, as evidenced in Randall and Wilkins' work ([46], p405).

If a phosphor contains N traps of which n are filled, then there will be $(N-n)$ empty traps and n empty luminescence centres previously vacated by the trapped electrons. The probability p_c that an electron will recombine and *not* become retrapped will be

$$p_c = \frac{n}{(N-n)+n} = \frac{n}{N} \tag{4.26}$$

and the TL intensity I will now be described by a second order kinetic equation such that

$$I = -\frac{dn}{dt} = \frac{n^2}{N}.s\exp\left(-\frac{E}{kT}\right) \tag{4.27}$$

which, when solved for a linear temperature rise β becomes

$$I = \frac{n(0)^2}{N}.s\exp\left(-\frac{E}{kT}\right).\left[1+\frac{n(0)}{N}.\frac{s}{\beta}\int_{T_0}^{T}\exp\left(-\frac{E}{kT}\right)dT\right]^{-2}. \tag{4.28}$$

The shapes of first and second order TL relaxation peaks given by equations 4.24 and 4.27 are compared in figure 4.4. The second order peak is more symmetrical than a first order peak. This symmetry is discussed further below.

Second order TSC peaks may describe, for example, dipole-dipole interactions during the relaxation of dipoles. However, the ideal cases of first and second order peaks are unlikely. Halperin and Braner [49] formulated the empirical 'general order kinetic' model for their TSC charge peaks, such that, using the same notation as for equation 4.8,

$$j(t) = A.\exp\left(-\frac{E}{kT}\right).\left[1+\frac{B}{\beta}\int_{T_0}^{T}\exp\left(-\frac{E}{kT}\right)dT\right]^{-\frac{b}{b-1}} \tag{4.29}$$

where b is the kinetic order. Equation 4.29 includes the second order case and, although not valid for the first order case, it reduces to the standard first order TSC equation (equation 4.8) as b tends to 1 ([35],p10).

The simplest method for determining the kinetic order for a TSC peak is by measuring its symmetry factor μ_g [49], such that

$$\mu_g = \frac{T_2 - T_{\text{peak}}}{T_2 - T_1} \tag{4.30}$$

where T_1, T_2 and T_{peak} are defined in figure 4.4. $\mu_g = 0.42$ is the characteristic symmetry factor for a first order TSC peak, while $\mu_g = 0.52$ for a second order peak. Fractional kinetic orders of $1 < b < 2$ have been observed experimentally by Halperin and Braner, and are more likely than the ideal first and second order cases.

4.3.2 Initial Rise Method for Determining E

The activation energy E of a TSC process can be derived simply using the initial rise method of Garlick and Gibson [48]. For temperatures T close to the initial temperature T_0, the second exponential term in equation 4.8 will approximate to

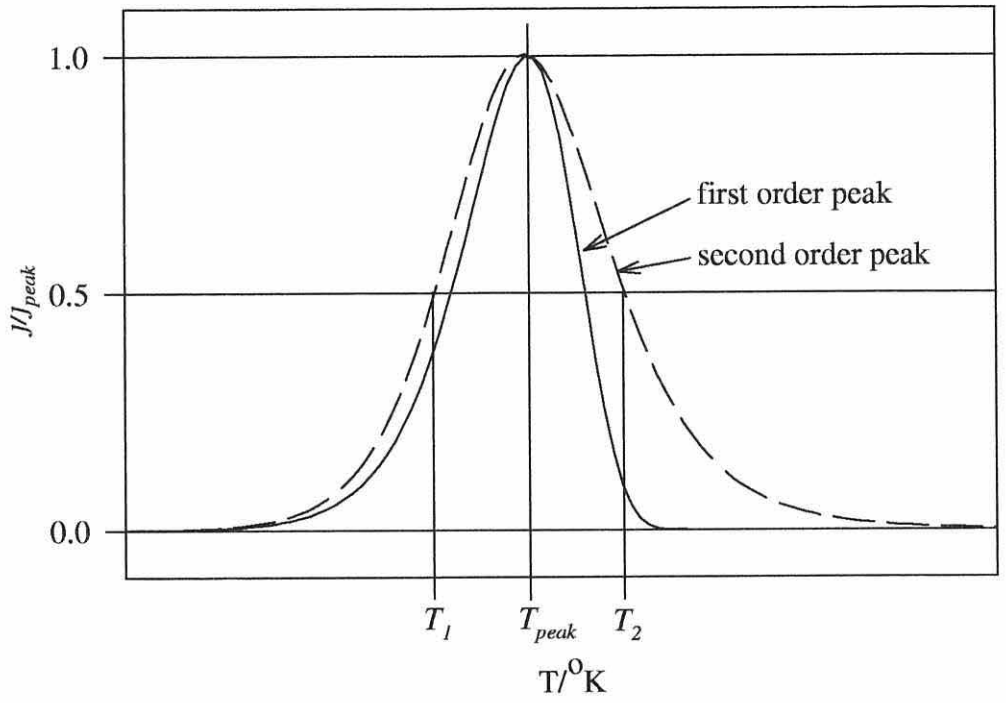

Figure 4.4. Comparison of first and second order TSC peaks.

unity. In this initial phase of temperature rise, the current will be given by

$$j(T) = A.\exp\left(-\frac{E}{kT}\right). \tag{4.31}$$

A plot of $\ln j(T)$ versus $1/T$ yields a linear curve of gradient $-E/k$, where k is Boltzmann's constant, equal to 8.6175×10^{-5}eV/K. As k is known, the activation energy E of the process may be found. The initial rise method is also valid for the second order and general order kinetic cases, as the arguments regarding the smallness of the second exponential term still hold in these instances.

It should be noted, however, that application of the initial rise method to the analysis of a peak originating from a distribution of the relaxation times (Bucci-Fieschi model, section 4.1)

$$\tau(T) = \sum_{i=1}^{n} . \sum_{j=1}^{m} \tau_i \exp\left(\frac{E_j}{kT}\right) \tag{4.32}$$

or a distribution of conductivities (Kunze-Müller model, section 4.2.1)

$$\sigma(T) = \sum_{i=1}^{n} . \sum_{j=1}^{m} \sigma_i \exp\left(-\frac{E_j}{kT}\right) \tag{4.33}$$

will result in inaccurate values of E.

For the case of a distribution only in pre-exponential factors τ_i or σ_i such that E is a single, constant value, the initial rise method invariably yields a value of E that is too low due to overestimation of the role of the slowest relaxation times ([36], section 4.6.4). For a symmetrical distribution in pre-exponential factors, van Turnhout [50] has shown via model calculation that equation 4.31 becomes

$$j(T) = A. \exp\left(-\frac{\omega E}{kT}\right) \tag{4.34}$$

where ω depends on the distribution type of the pre-exponential factors.

Note that a similar, simple relation cannot be derived for a distribution in E.

Chapter 5

Review of the Literature on TSC in LDPE and XLPE

The preceding chapters have laid the theoretical foundations. This chapter provides a review of the published works that are most relevant to the experimental work discussed in chapter 9.

Comprehensive reviews of TSC literature have recently been published. Lavergne and Lacabanne [51] cover a variety of materials, while Suh *et al* [52] targets polyolefins and particularly polyethylene. For this reason, the number of works reviewed here have been limited. Since the cable samples under investigation are cross-linked low-density polyethylene (LDPE), TSC studies of HDPE and LLDPE samples have largely been omitted. Papers in which corona charging and irradiation was used to polarize and inject charge into the samples have also been largely omitted, since these experimental conditions are very different from those adopted here. Finally, papers which investigate TSC in a temperature range well below that employed here have also been omitted, since the processes relating

to that temperature range will have become fully relaxed during the isothermal conditioning stage and thus will not make a contribution to the TSC at higher temperatures.

Literature that reports TSC measurements made specifically on plaque and film samples will be discussed first, followed by work that reports TSC on triple-extruded cable samples or on the polymer material from such cable samples.

5.1 TSC in Plaque Samples

The work of Fleming and Balbachus [3] presents an interesting and simple introduction to TSC measurements performed on plaque samples. The samples employed were plaques of XLPE, each of which had one aluminium and one copper evaporated electrode to reproduce the conditions of a cable with inner aluminium and outer copper electrodes. The sample had been crosslinked with dicumyl peroxide which was added to the polyethylene in a weight ratio of 100:2, a similar ratio to that used in commercial HV cable. The 100μm thick samples were polarized with a voltage $V_p = \pm 1\text{kV}$ (ie, $F_p = 10\text{kV/mm}$) which was applied to the aluminium electrode, while the copper electrode was grounded. The TSC spectrum for this arrangement is shown in figure 5.1, where the temperature T_{peak} at which the current reached its maximum current value is 50°C. Fleming and Balbachas assumed that the current originated from movement of space charge in the material. They also found that repetition of the polarization/depolarization cycle at the same polarity yielded similar TSC peaks and magnitudes, indicating that the space charge that remained in the sample after depoling did not disturb

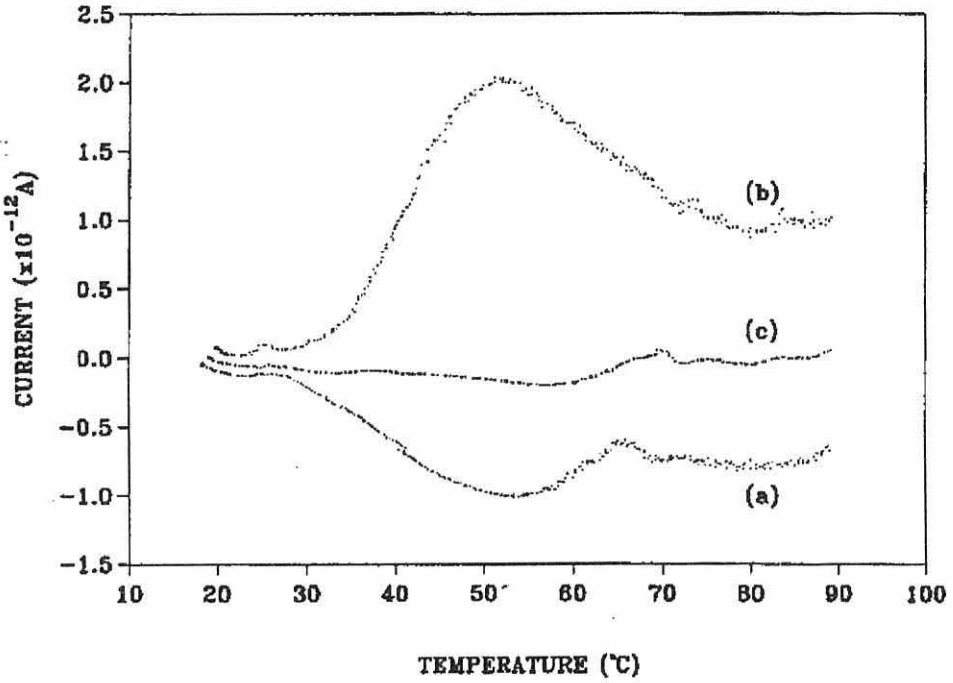

Figure 5.1. TSC spectra for (a)$V_p = +1$kV, (b) $V_p = -1$kV and (c) $V_p = 0$kV (from [3]).

the electric field and charge profile during the next polarization cycle. This result will be important for the discussion in chapter 9. However, it can be argued that the ability to repeat the results without change in the TSC spectra indicates that the samples had been well-conditioned, so that no morphological changes (for example, annealing or degassing) occur during subsequent repetitions of the TSC measurement cycle. Interestingly, figure 5.1 shows that positive poling produces a peak with double the magnitude compared with that for negative poling voltages. Fleming and Balbachas neither provide an explanation for, nor acknowledge, this difference, although there is evidence to suggest that the different electrode metals will permit different quantities of charge to be injected at the electrode-insulation interfaces [53].

Other authors have reported TSC spectra recorded in similar low-density polyethylene samples which are similar to the spectrum obtained by Fleming and Balbachus, although the temperature T_{peak} is found to vary slightly. This variation may be due to a number of factors which include different material specifications (e.g., manufacturer, additives, density) or different sample preparation conditions, although it is difficult to be more specific from the often inadequate information provided in the literature. An example of this variation in T_{peak} is provided by Oda *et al* [4], who performed TSC measurements on sheets of XLPE using both corona and contact charging. Their as-grown XLPE films, polarized at a voltage $V_p = -5\text{kV}$ at $T_p = 96°\text{C}$ for $t_p = 2\text{h}$, produced a T_{peak} at 60°C, a slightly higher temperature than Fleming and Balbachas' T_{peak} (figure 5.2a). Oda *et al*'s second XLPE film sample was annealed for 6 hours at 85°C and then poled at $T_p = 85°\text{C}$ for $t_p = 2$ hours with $V_p = -5\text{kV}$. They identified a positive polarity TSC peak observed during the heating of this second sample similar to the peak in their first sample (figure 5.2b). However, they fail to report that there appears to be a second peak superposed on the falling side of the first at about 80°C, similar to the peak observed by Gubanski *et al* [15] in an unaged, sand-blasted sample, which is discussed further below. The peak current I_{peak} is also slightly lower for the annealed sample, but this may be due to variations in the sample geometry or in the field F_p, since the film thicknesses are quoted as being between 150μm and 2mm. However, assuming the value of $F_p = 28\text{kV.mm}^{-1}$ reported for a later sample is the same in these first two samples, F_p is approximately twice as large as the highest fields employed in the present work. The poling field will be shown below to have an important influence on charge injection into polymeric

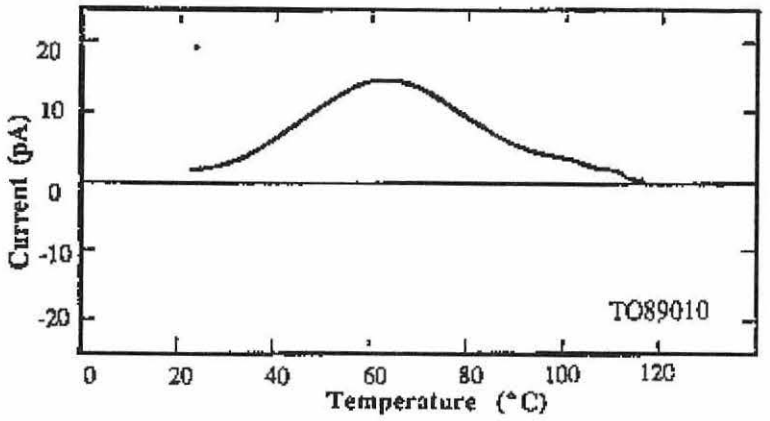

(a) as-grown XLPE film. -5kV, 96° C, 2hours

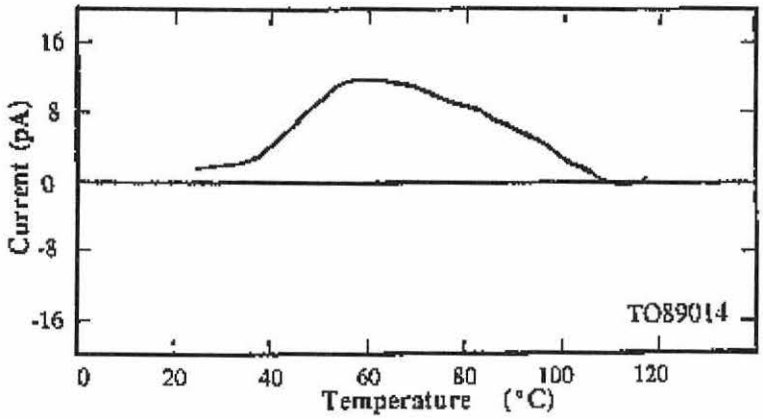

(b) 6-hour annealing at 85° C. -5kV, 85° C, 2hours

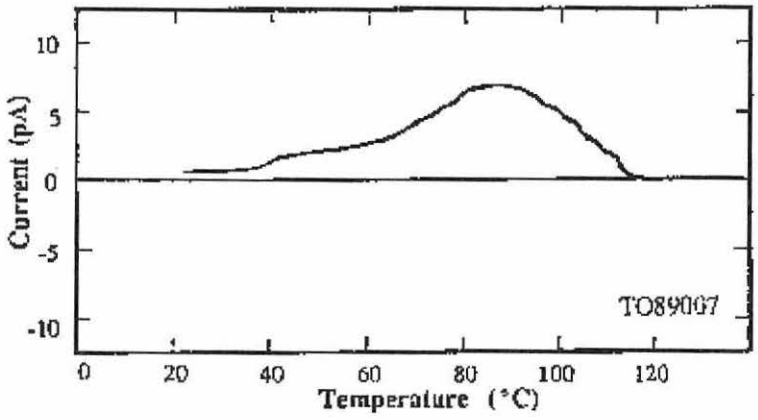

(c) AC stressing of 4.8kv for 9 hours at 85° C. -5kV, 85° C, 2hours

Figure 5.2. Oda's TSC Curves of XLPE with both sides metallised and DC poling (from [4], figure 8).

materials. Oda *et al* also studied a cable sample and slices from a cable; these will be discussed in section 5.3.

Dorlanne *et al* [5], using a.c. stressing and double needle electrodes in their investigations, produced an interesting TSC spectrum, similar to those of Oda *et al* and Fleming and Balbachas. Room temperature poling of blocks of high purity LDPE, into which pairs of 50μm steel needles had been molded at a point separation of 3mm, was employed. The spectrum, shown in figure 5.3, has two peaks: a smaller one at 65°C and a larger one centred at 85°C. Since a high field

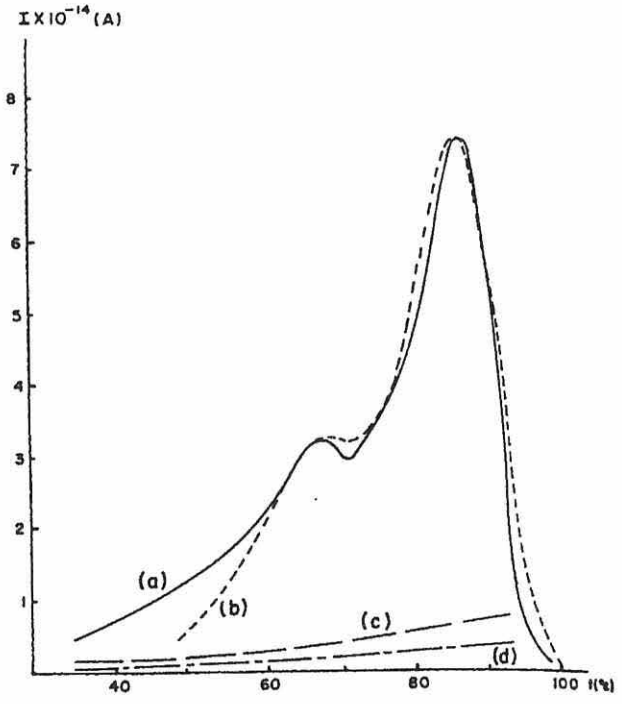

Figure 5.3. Dorlanne *et al*'s TSC curve from a double needle polyethylene sample using a.c. stress (from [5]).

(F_{max} = 120kV.mm^{-1} at the needle tips) was used, the 85°C peak may result from a massive charge injection, although it is possible to argue that the high

purity of the material may have had a more important influence on the shape of the spectrum, reducing the low temperature peak (which is believed to result from charge trapped at crystalline-amorphous interfaces) so that the 85°C peak became more dominant. Dorlanne *et al* concluded that the TSC measurements of space charge agreed well with the "conventional" TSC experiments of Fischer and Röhl [47]. This statement is incorrect, however, as Fisher and Röhl studied the *dipolar* relaxation of LDPE in the temperature range -197°C to 47°C, while Dorlanne *et al* had earlier stated that their TSC spectrum, in the higher 35°C to 100°C range was due to injected space charge. Dorlanne *et al* also found the space charge density to be $\sim 2.7 \times 10^{-3}\text{C.cm}^{-3}$ in agreement with other authors [54, 55], although the injection threshold field was an order of magnitude lower than other reported values.

It is useful to emphasize here that Dorlanne have used needle electrodes to verify that space charge injection can occur and give rise to a TSC. This is important for the interpretation of the experiments reported in the present work.

Sawa *et al* [6] had previously observed similar TSC spectra to those of Dorlanne *et al* while using plaques of Yukalan-LK50 LDPE with gold evaporated electrodes and a lower heating rate of $0.5°\text{C.min}^{-1}$. Peaks appear in Sawa *et al*'s spectra at 85°C and 50°C with $F_p = 100\text{kV.mm}^{-1}$ and $t_p = 1$ hour (figure 5.4). Li *et al* [7] have also studied treeing in LDPE and found similar two-peak TSC spectra in plaque samples polarized using a voltage applied to contact electrodes, although Li *et al* examined the effect of water treeing with ionic solutions, and not electrical trees, on the TSC. Their TSC peaks occur at lower temperatures

than either Dorlanne *et al*'s or Sawa *et al*'s peaks (figure 5.5).

Referring back to the work of Sawa *et al*, an interesting observation was that the charge decay time constant, estimated from the isothermal decay currents, was much longer that the time constant calculated from the TSC peak at 85°C. Consequently, Sawa *et al* suggested that the detrapping of charge by heating is enhanced by physical changes to a trap state itself, as well as from the increase in thermal energy of the carrier in this state. Such a comment is in agreement with Boustead and Charlesby's suggestion that the potential well of the trap might decay due to molecular motion as a result of heating [56]. Sawa *et al* reported that the magnitude of the 85°C peak depends on the crystallinity of the polyethylene, and suggested that a peak at this temperature may be associated with the crystalline phase. Sawa *et al* also stated that the difference in magnitude of the 85°C peak in the TSC spectra for the LDPE and HDPE materials was too great to depend solely on the bulk crystallinity of each material, and they suggested that the main TSC contribution to this peak was provided by traps at amorphous-crystalline interfaces, an idea that corresponds closely to those which are proposed in the present work and which shows some agreement with the thermo-mechanical relaxation work of Ward [57]. Sawa *et al* also emphasized the invalidity of standard analytical methods with respect to the analysis of the $T_{\text{peak}} = 85°\text{C}$ peak, due to the aforementioned molecular motion altering the trap state itself, a point which is similar to one made in chapter 4.

Finally, Gubanski *et al* [8] have performed TSC investigations on a number of LDPE and XLPE plaque samples. The samples, 0.8mm thick and 8mm in

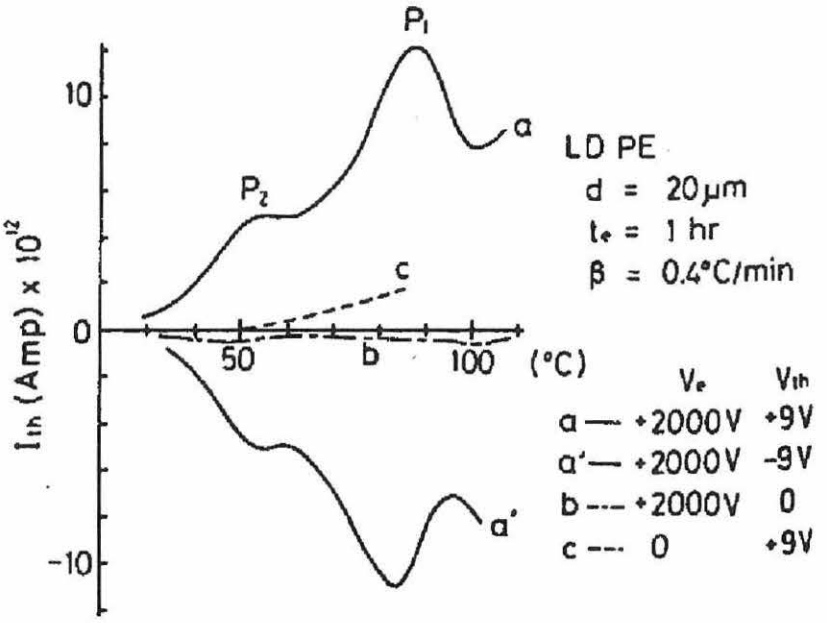

Figure 5.4. Sawa *et al*'s TSC curve observed from a Yukalan-LK50 LDPE plaque with gold evaporated electrodes after d.c. poling at 100kV.mm^{-1} for 1 hours(from [6]).

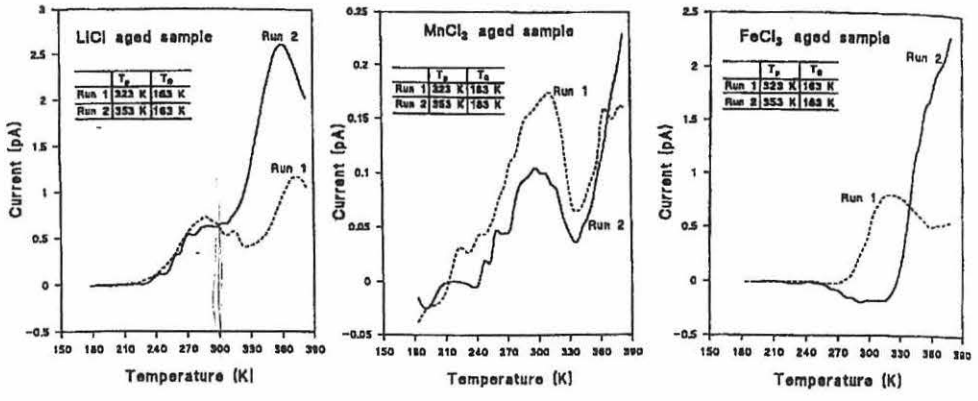

Figure 5.5. An example of Li *et al*'s two-peak TSC spectra (from [7]).

diameter, were fully degassed and had vacuum-evaporated gold electrodes. The mean poling field was only 3.5kV.mm^{-1}, which is very low in comparison to the fields employed in the other TSC experiments discussed above. This may explain why there is very little detail in the TSC spectra of the LDPE samples in the temperature range 25°C to 107°C (figure 5.6), of interest in the present work.

However, sharp TSC peaks observed by Gubanski *et al* above $T = 100°\text{C}$ were attributed to the melting of the samples, since they correlate well with the corresponding melt peaks determined by differential scanning calorimetry. Gubanski *et al* also examined the TSC spectra of DCP-crosslinked polyethylene homo- and copolymers. The TSC spectrum for the XLPE homopolymer (figure 5.7) will later be compared with the spectra for one of the cable samples investigated in the present work (chapter 7). The spectrum of this XLPE homopolymer exhibits three main peaks: a strong positive peak in the temperature range 50°C to 125°C; a second, negative polarity peak between 125°C and 175°C; and a sharp, positive melt peak, superposed over the first at $T = 100°\text{C}$.

In comparison to the homopolymer spectrum, the TSC of the XLPE copolymers (figure 5.8) shows much broader peaks between 50°C and 175°C, all with melt peaks above $T = 100°\text{C}$. In their conclusions, Gubanski *et al* noted that only the peroxide-crosslinked copolymers were without a negative component to the TSC spectrum and suggested that this may indicate that the copolymers possessed a stronger resistance to space charge accumulation. As a point of interest, it will be seen in the present work (chapter 7) that although the TSC spectra may be of a single polarity, it may also comprise peaks of opposite polarity which are not

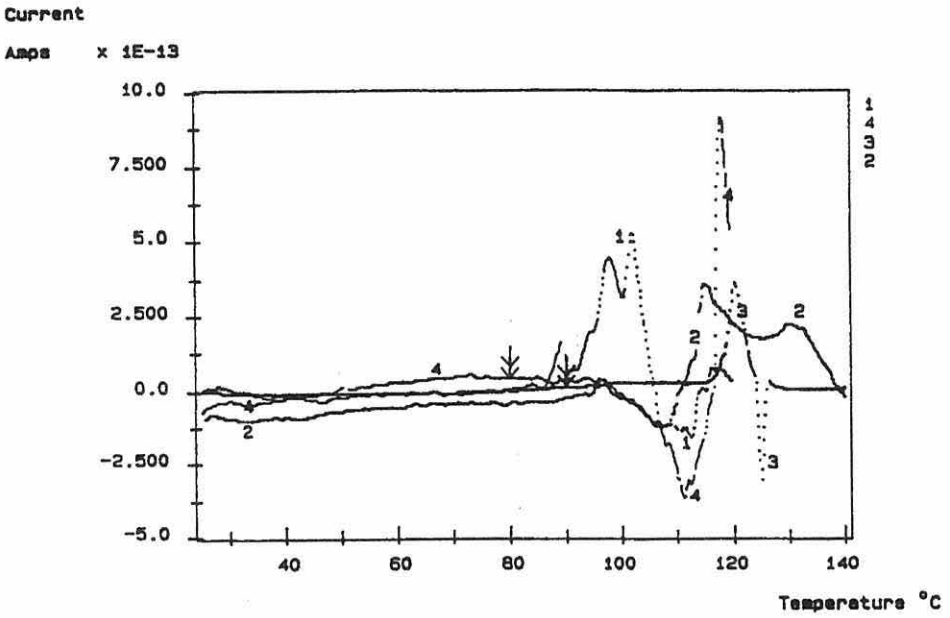

Figure 5.6. TSC spectra obtained from LDPE samples by Gubanski *et al* (from [8], figure 2).

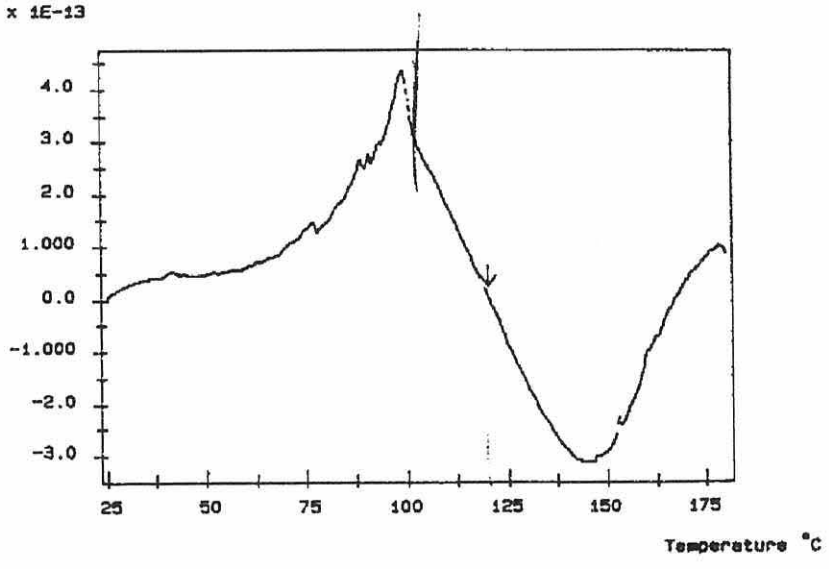

Figure 5.7. TSC spectrum obtained from XLPE (from [8], figure 3).

sufficiently large to change the polarity of the total TSC in its local range.

The number of different sample types and experimental conditions allows only vague speculative comparisons to be made between the works reviewed above. It is important to note that high fields will inject significantly more charge as shown by Dorlanne *et al.* Peaks at temperatures close to 55°C are usually present in both LDPE and XLPE samples, and probably result from charge accumulation at crystalline-amorphous interfaces. However, the crosslinking process can both broaden this peak, and introduce new peaks at higher temperatures. Repeated thermal cycling of polyethylene may alter the material morphology and consequently can cause physical changes to the trap states. These changes have an important effect on the resultant TSC spectra. A melt peak can be observed in different polyethylene materials in the temperature range 100 to 120°C which is influenced by the additives included in the material during manufacture.

5.2 TSC in Copolymers

As described in section 2, the semicon electrodes consist of carbon mixed into a base polymer of either polyethylene or a copolymer of polyethylene. Since it is possible that the copolymer used in the semicon electrodes may become polarized and thus contribute to the TSC spectra of the cable samples used here, it is useful to review the limited information available on the TSC of copolymers.

Chern *et al* investigated carboxylated polybutyl-acrylate (BA) with added acrylic acid (AA) or methacrylic acid (MAA) [9], which formed a latex material.

They used TSC to determine the glass transition temperatures T_g of the copolymers. The TSC polarization conditions were not reported. They also calculated T_g for a homogeneous BA/AA blend containing 90% BA and 10% AA to be -46°C and for a BA/MAA blend in similar proportions to be -43°C. However, the TSC spectra for BA/AA (figure 5.9a) and for BA/MAA (figure 5.9b) exhibited two separate peaks instead of the single peak expected for a well-blended homogeneous copolymer. Chern *et al* suggested that the peak separation was related to the heterogeneity of the copolymer mixes, such that the BA/AA TSC peaks indicated accumulation of the AA at interfaces, while the closer proximity of the BA/MAA TSC peaks indicated a better distribution of MAA within the latex. This peak separation will be important in the samples examined in the present work (chapter 9); the position of $T_{\text{peak}} \sim 32$°C for BA/AA must especially be born in mind.

Ibrahim *et al* [10] studied polyvinylalcohol- polyethylene copolymers and also observed two TSC peaks (figure 5.10), one at $T \sim 77$°C and a second at $T \sim 127$°C, after poling ($T_p = 75$°C, $t_p = 2$ hours) with various fields. However, I_{peak} and T_{peak} show no correlation with the poling field, an effect which was not satisfactorily explained by Ibrahim *et al.*

Thermally stimulated *polarization* (not depolarization) by Mizutani *et al* [11] of 30μm thick poly(ethylene-vinylacetate) films containing between 6 and 22 wt% of vinyl acetate revealed a current inversion peak at $T \approx 27$°C (figure 5.11). They derived the average effective dipole moment of the vinyl acetate branch unit from the peak to be 1.8 Debye, significantly smaller than the value of 4.8 Debye reported in the "Polymer Handbook" [58]. Mizutani *et al* also studied

LDPE films, but those samples which were not x-ray irradiated showed only an increasing current from T =57 to 107°C, and so will be excluded in this review.

It has been seen that there is very little work that examines the TSC of the semicon copolymers, implying that charge accumulation in these materials has, in general, been insufficiently considered. However, from the work above, inadequate blending of copolymers have been shown to introduce dipolar peaks into the TSC spectrum in the temperature range of interest in the present work. It has also be observed that parameters predicted from TSC spectra can be quite inaccurate.

5.3 TSC of Cable Models

Recently, the TSC technique has increasingly been used to determine the charge storage and polarization properties — and thus to diagnose the effect of ageing processes — within cable materials. Authors of earlier papers tended to study slices of material taken from cables, while more recently, TSC of whole cable sections or cable models have been used. It is important to note that the poling voltage was applied to the inner electrode for all of the concentric cable samples studied, while the outer electrode was grounded.

Braun *et al* [12] have investigated the effect of the roughness and cleanliness of the semicon screen/insulation interface in four different 15kV XLPE cables (designated A to D) using TSC. Their cable samples had the same geometry as those examined in the present work (chapter 6.1). The TSC parameters used were

$0\text{kV} < V_p < \pm 140\text{kV}$, $T_p = 22°\text{C}$ and $\beta = 3°\text{C}$. Cables A and B were nominally made of the same compounds, although cable B had been manufactured a year after cable A, and improvements in semicon quality over that time resulted in a smoother and cleaner semicon/insulation interface in cable B. The measurements were performed on as-received cable samples, i.e., they had not been either voltage or environmentally aged.

Only one TSC spectrum for cables A and B was illustrated (figure 5.12), but Braun *et al* reported that the resultant TSC spectra of cables A and B contained peaks of the same polarity as V_p increased. Consequently, the charge that was injected could be determined simply by integrating the thermally stimulated current-time curve (figure 5.13). Braun *et al* found that cable A released more charge during the TSC measurements than cable B, consistent with a rougher screen/insulation interface for cable A. A threshold field for charge injection was determined to be of the order of 12kV.mm^{-1}, but this field was lower for cable A than cable B, again reflecting the superior charge injection characteristics of the rougher, dirtier semicon in cable A.

It should be noted here that the field at the inner screen is approximately twice as large as at the outer screen (see section 7.2) by virtue of the concentric cable geometry. Although Braun *et al* expected a negative poling voltage to inject more charge than a positive one, the converse was found to be true, for which no firm explanation was given. They did suggest however that when a negative voltage is applied, negative charges accumulated and were trapped at the semicon-insulation interface, thus reducing the local field there and limiting the injection

of electrons. By comparison, if there was a lower trapping probability (higher mobility) for injected *positive* charges (holes) compared with electrons, they would not influence the local field at the interface to the same extent as negative charges. Therefore more holes could be generated in a larger volume at the interface. This is a very important point which will be discussed further in chapter 7.

Cables C and D had a different type of insulation to cables A and B, one which was specifically designed to resist electrical and water treeing. No comment is made by Braun *et al* as to the semicon type in comparison to cables A and B, but cable C was reported to have a conventional, furnace black screen while cable D had a supersmooth screen. The TSC spectra of samples C and D had both negative and positive peaks. It was therefore impossible to determine the total charge released from the TSC of these two cables using the same simple method of current integration used for cables A and B. At low V_p, cable C showed a conventional response (figure 5.12). As V_p increased, small side peaks appeared (figure 5.14) which were presumed to be evidence of a broad heterocharge peak that overlaid a narrower homocharge peak. Cable D exhibited almost exclusively a homocharge peak which moved from $T_{\text{peak}} = 85°\text{C}$ to $T_{\text{peak}} = 55°\text{C}$ as V_p increased from -50kV to -100kV. It will be seen that similar TSC spectra are observed for certain cable types investigated in the present work (chapter 7).

A similar TSC spectrum to that for cable C was observed by Doughty *et al* [13] after poling 100mm long 15kV XLPE cable samples in an oxygen atmosphere, of a similar cross-sectional geometry to the samples examined in the present work (section 6.1), with $V_p = 5\text{kV}_{a.c.}$. However, the spectrum changed

when a nitrogen atmosphere was used (figure 5.17). By poling similar samples at $T_p = 56°C$ with half-rectified a.c. voltages, Doughty *et al* also showed that a positive poling voltage injected more charge than a negative one (figure 5.16), in agreement with Braun *et al*'s findings. Note that the poling field ($F_p \sim$ 1kV.mm^{-1}) was significantly lower than Braun's 12kV.mm^{-1}, although T_p was higher. This suggests that injection of charge is likely to be enhanced at elevated temperatures, in agreement with the model described in section 3.2.

Doughty *et al* also studied d.c. poled cable samples, and found that the TSC spectrum from samples poled for $t_p = 1000$s at $T_p = 58°C$ with $V_p = +10$kV was an almost exact mirror image of identical sampled poled with the opposite polarity of V_p(figure 5.15). Doughty *et al* attribute this effect to the 'symmetry' of the system, although it is uncertain what was meant by this. However, as can be seen in figure 5.15, a large peak was observed at $T_{\text{peak}} = 65°C$. A similar peak was observed by Motori *et al* [14] (figure 5.18) in cable samples with XLPE insulation type 4201, aged for 800 hours at $T_p = 130°C$ according to the testing standard IEC 216. However, it is unlikely that Motori *et al* and Doughty *et al*'s peaks originate from the same physical conditions. Doughty *et al*'s peak was associated with charge injection, although interfacial polarization could also have occurred. However, Motori *et al* reported that their 55°C peak resulted from the relaxation motions of ionic charge carriers that were already present in the samples, and not from injected charge, a sensible assumption when one considers the low poling voltages involved (350V). Although there is little similarity between the origin of the two peaks, this example illustrates the difficulty of determining the location and origin of individual relaxation peaks, as mentioned in chapter 4.

It is interesting to note that Motori *et al* suggests that their TSC peak resulted from ionic charge motion, as this implies that the charge in the sample (and therefore the 55°C peak) appears as a result of the cable degradation, and not from injection of space charge. Motori *et al* emphasized the role of ions as part of this process. However, it could be argued that the low poling voltage is sufficient to inject charge at the semicon-insulation interface (described in chapter 3) if the semicon screen is sufficiently rough to cause localised field enhancement there.

Amyot and Pélissou [59] examined 200μm-thick ribbons of material, peeled from both unaged and service-aged 28kV power distribution cables which had the same XLPE insulation as the samples investigated by Motori *et al* — XLPE type 4201. The magnitude of a TSC peak at -25°C was seen to correlate with the cable age, and peaks were observed above 100°C which could be argued to be melt peaks as seen in Gubanski *et al*'s work described above in section 5.1. No peaks were observed at temperatures between 0°C and 100°C, which possibly explains the general lack of published information from TSC studies on ageing in this temperature region.

In addition to the work cited above on plaque samples, Oda *et al* [4] have also studied 0.35mm thick slices from 15kV cables polarized using a -5kV corona voltage. In contrast to Amyot and Pélissou, Oda *et al* found 3 peaks in the 20°C to 120°C temperature range: a small peak at 50°C; a large peak at 65°C; and a broad, medium sized peak at approximately 100°C (figure 5.19). Since corona charging allows all the traps on the surface to be filled, it can therefore be argued that this is analogous to an efficiently injecting semicon electrode. This will be

discussed further in chapter 9.

Oda *et al* also made measurements on 5m long 6.6kV cables. The TSC spectra (figure 5.20a+b) show similar spectra to that for Braun's cable D, indicating a heterocharge peak located at $T_{\text{peak}} = 70°\text{C}$, which had a threshold injection field of 7.4kV.mm^{-1} ($V_p = 20\text{kV}$) and a homocharge peak at $T_{\text{peak}} = 50°\text{C}$ with a higher injection threshold of 14.8kV.mm^{-1}.

Gubanski *et al* [15] studied TSC of 0.6mm thick films cut from 35kV cables with 4201 type XLPE insulation. The films were fully degassed and assumed to be free of volatile crosslinking by-products. The films were cut into 27mm diameter discs and an aluminium electrode was evaporated onto one side of the disc while the other side was lightly sand blasted, to provide water tree initiation sites. The initial TSC spectrum for a sandblasted sample before poling or ageing (figure 5.21) revealed a small peak at $\sim 75°\text{C}$. Ageing of the samples with a field $F_p = 6\text{kV.mm}^{-1}$ a.c. at 1kHz was thought to generate water trees in the insulation and produced a TSC peak at 50°C. This peak became larger as the ageing time increased. The authors noted that the TSC peaks shown in figure 5.21 disappear after the samples were dried, suggesting that the ionic species which are associated with water trees either are removed or become immobile after the removal of the water solvent.

After polarizing the samples using $F_p = 0.73\text{kV.mm}^{-1}$ and $T_p = 110°\text{C}$ for $t_p = 10$ minutes, and then cooling to 25°C, the subsequent TSC spectra shown in figure 5.22 were recorded. The peak magnitudes can be seen to have initially increased with ageing time, but then have subsequently decreased for an ageing

time of 500 hours. T_{peak} is also seen to decrease with ageing time. Gubanski *et al* reported that van Turnhout [60] observed similar changes in the TSC spectra of polymer electrets which were attributed to varying depth of charge penetration; an increase in charge penetration caused T_{peak} to shift towards lower temperatures.

In a later paper Gubanski *et al* [16] found that ageing created a peak at 75°C (figure 5.24). By using a fractional poling technique, similar to procedure II (section 6.2), on this single peak, a number of 'elementary' peaks were found and were deemed to be a result of ionic relaxations. However, Gubanski *et al* stated that the fractional poling peaks have a normal distribution similar to that of fractional poling peaks associated with the dipolar glass transition peak at $T = -25$°C, figure 5.23, implying that the 75°C peak may have originated from dipole relaxation. This point has important consequences for the analysis of the results obtained in the present work, as will be discussed further in chapter 9.

5.4 Summary

The papers reviewed above illustrate how the TSC spectra can vary significantly depending on the field, the poling conditions, the cable age and also the materials which are used in cable manufacture.

Plaques and cable slices sometimes produce similar TSC spectra to cable geometry samples, although the results of Oda *et al*, and perhaps also those of Braun *et al*, illustrate that this correlation between plaque and cable spectra is very dependent on the materials used. Peak temperatures are not strictly dependent on

the magnitude of the poling fields, but are more likely to be related to the morphological characteristics of the materials, especially to interfaces between dissimilar regions, for example semicon-insulation, electrode-insulation or crystalline-amorphous regions. Higher fields were seen to increase the total charge derived by integrating the thermally stimulated current-time curve. However, assuming the spectra of cable geometry samples to be solely due to space charge relaxation would be ill-advised, as the polarization of the copolymeric semicon material is likely to introduce dipolar relaxation peaks. Increasing the poling temperature generally increases the total polarization and thus the total depolarization current but, as shown in rare cases, not necessarily in a predictable manner.

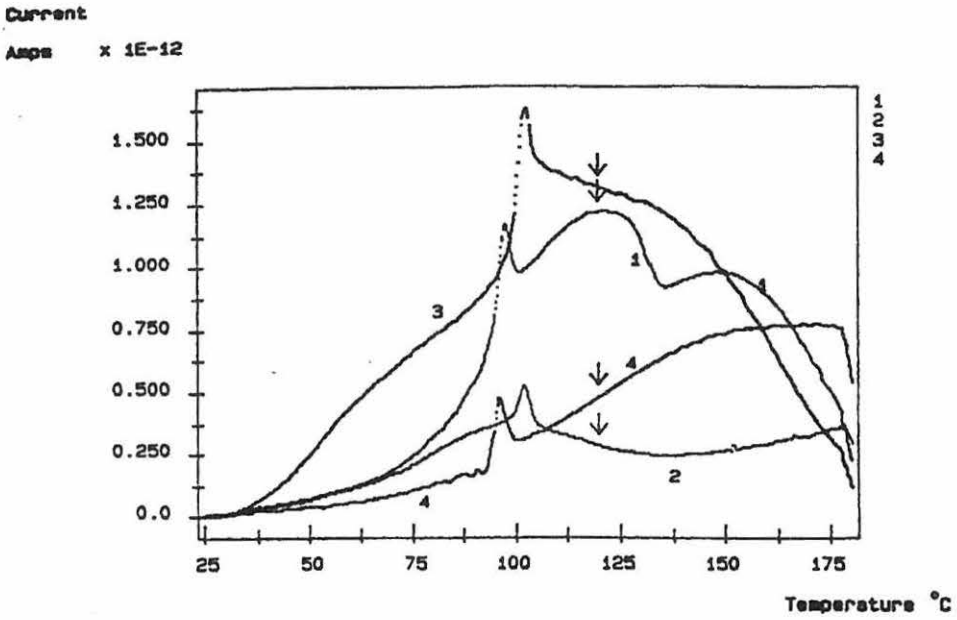

Figure 5.8. TSC spectra of crosslinked PE copolymers (from [8], figure 4).

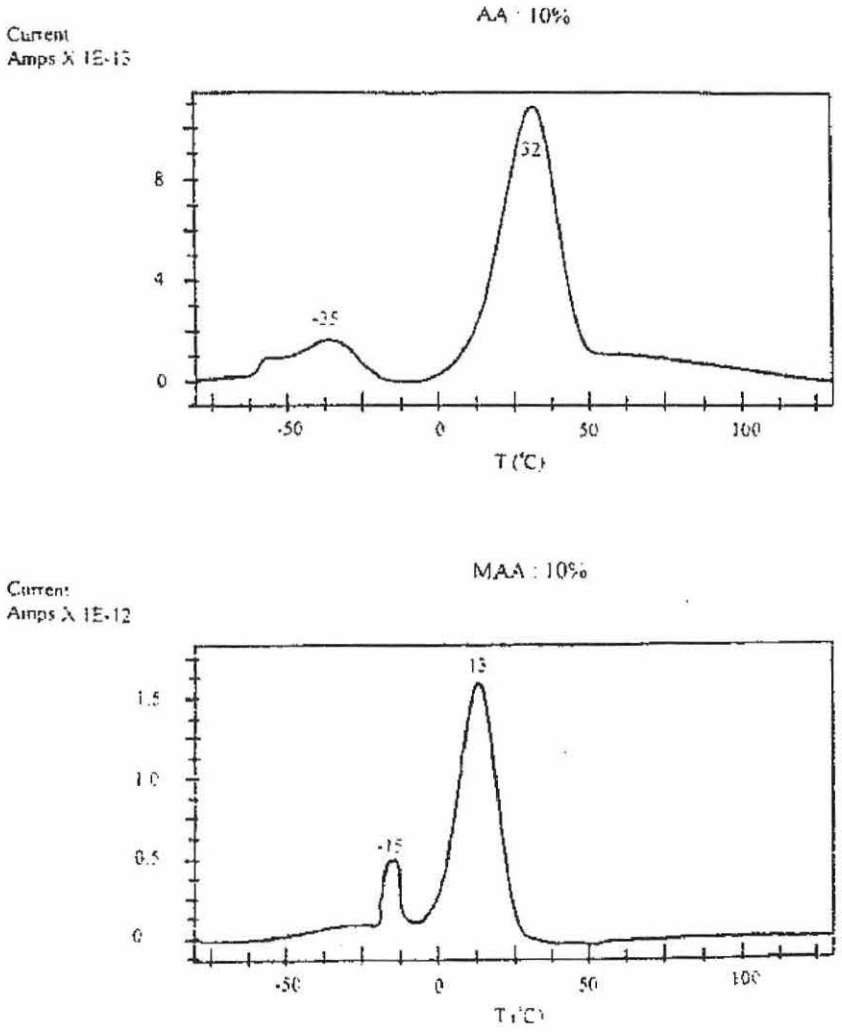

Figure 5.9. (from [9], figure 12).

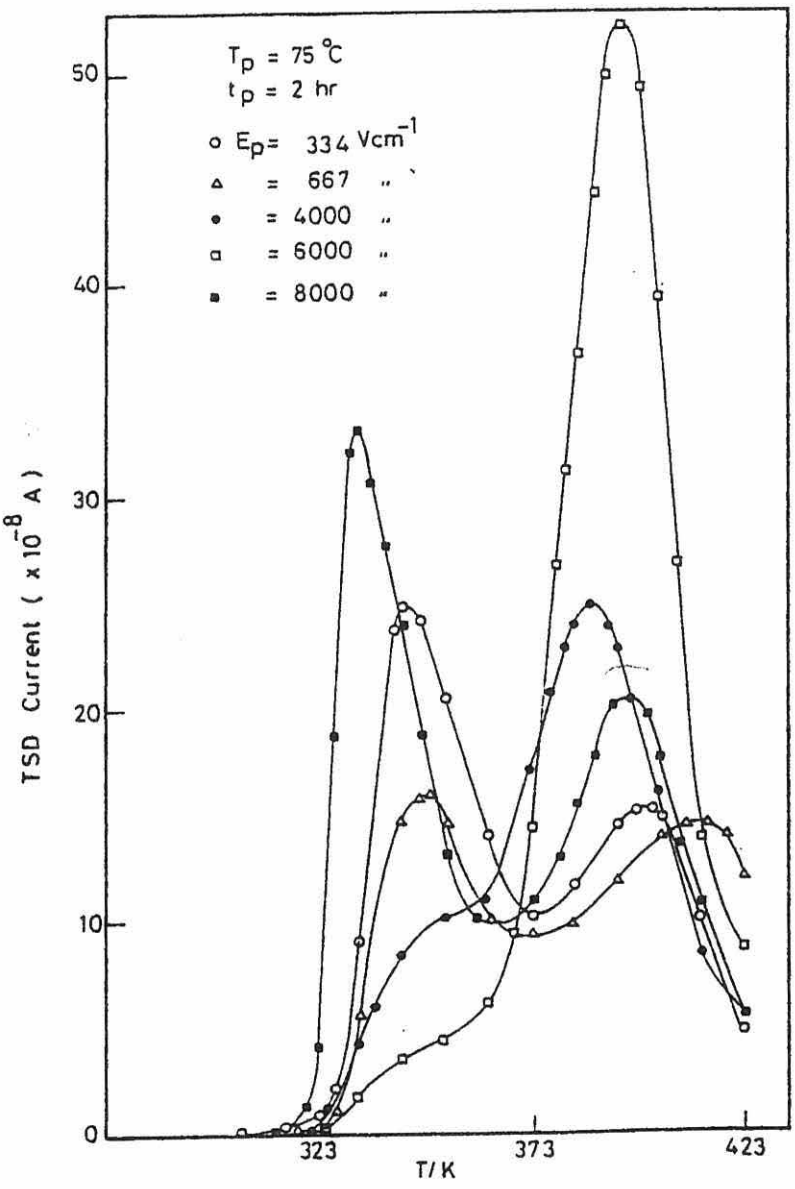

Figure 5.10. (from [10], figure 5).

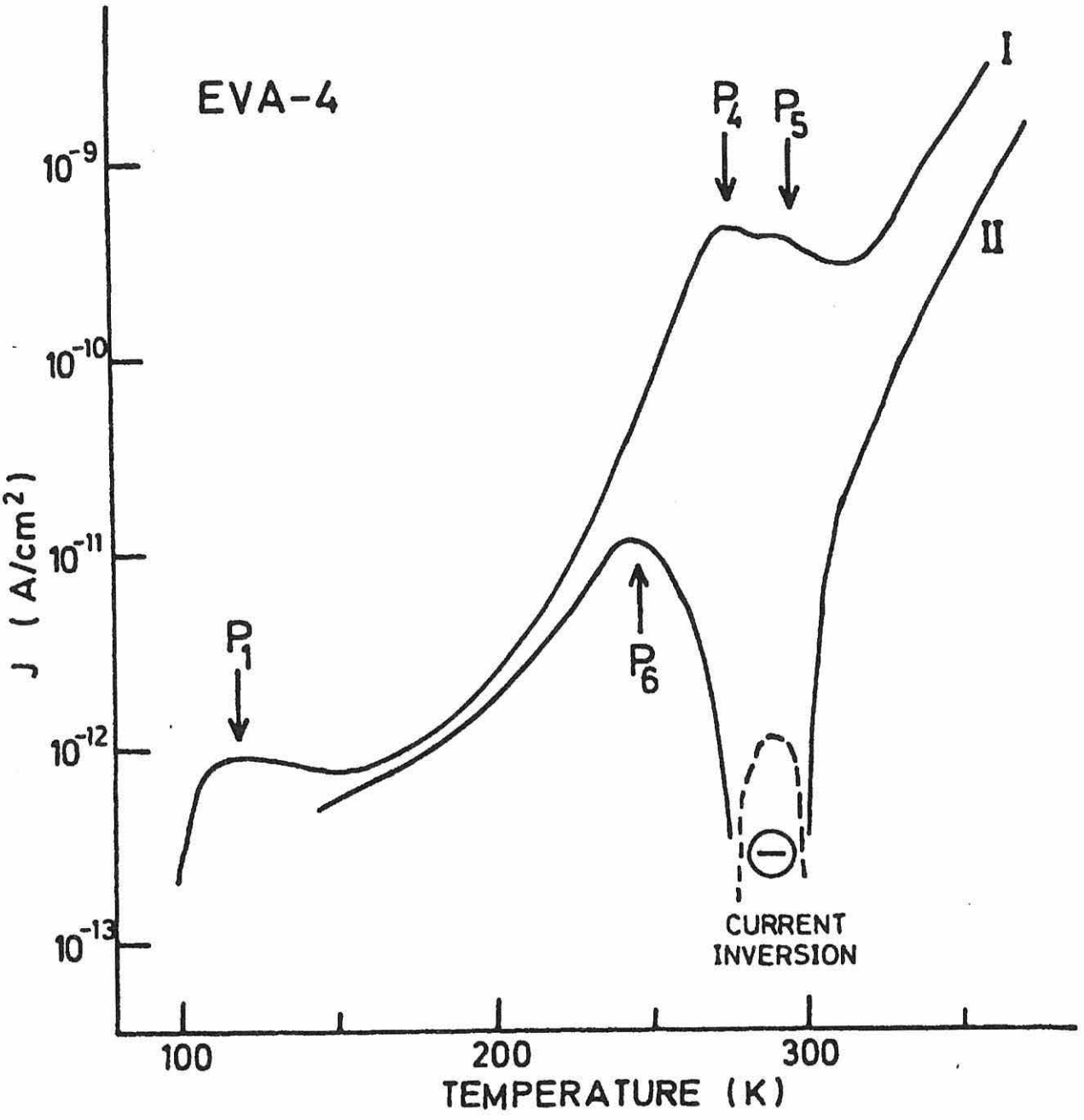

Figure 5.11. (from [11], figure 6).

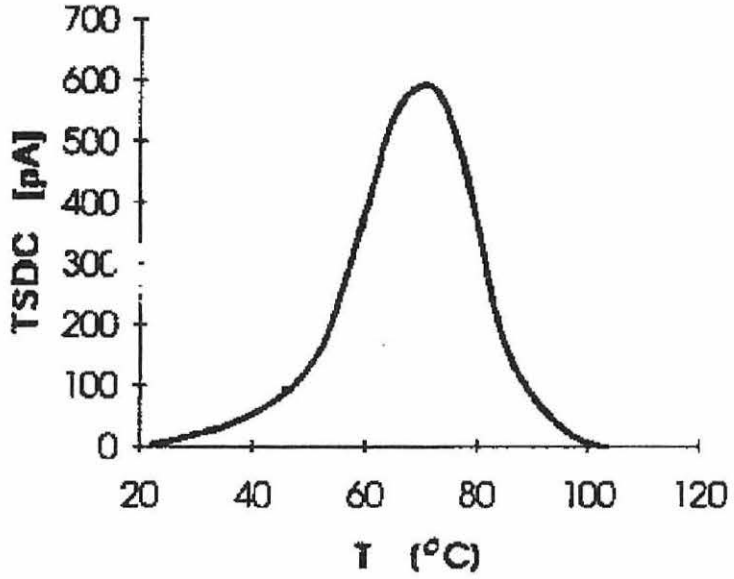

Figure 5.12. (from [12], figure 2).

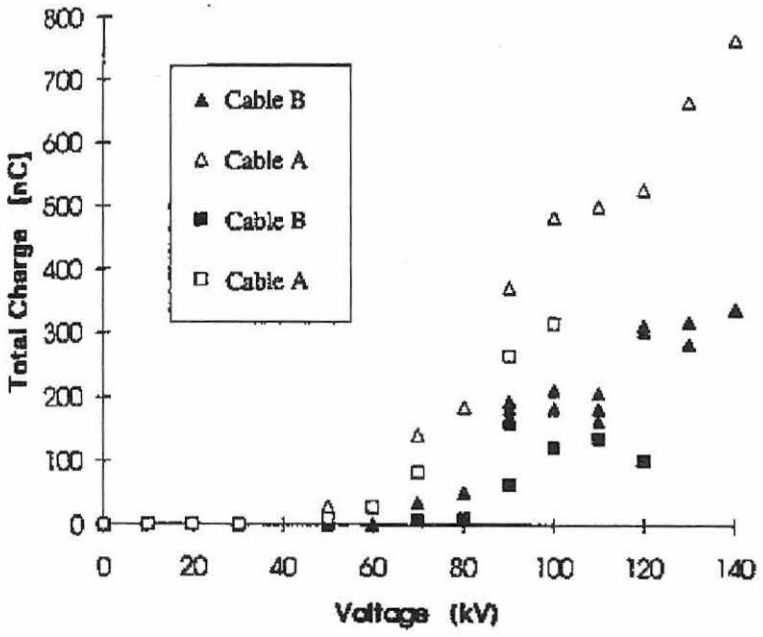

Figure 5.13. (from [12], figure 3).

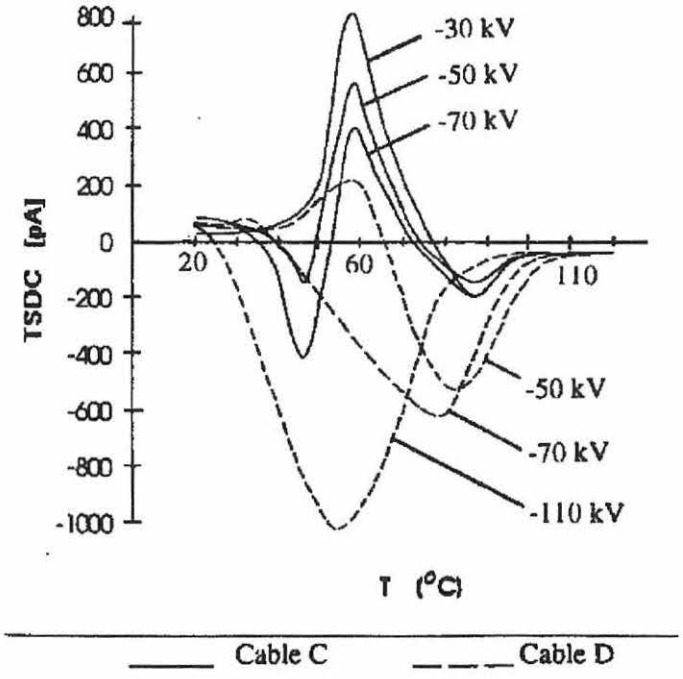

Figure 5.14. (from [12], figure 4).

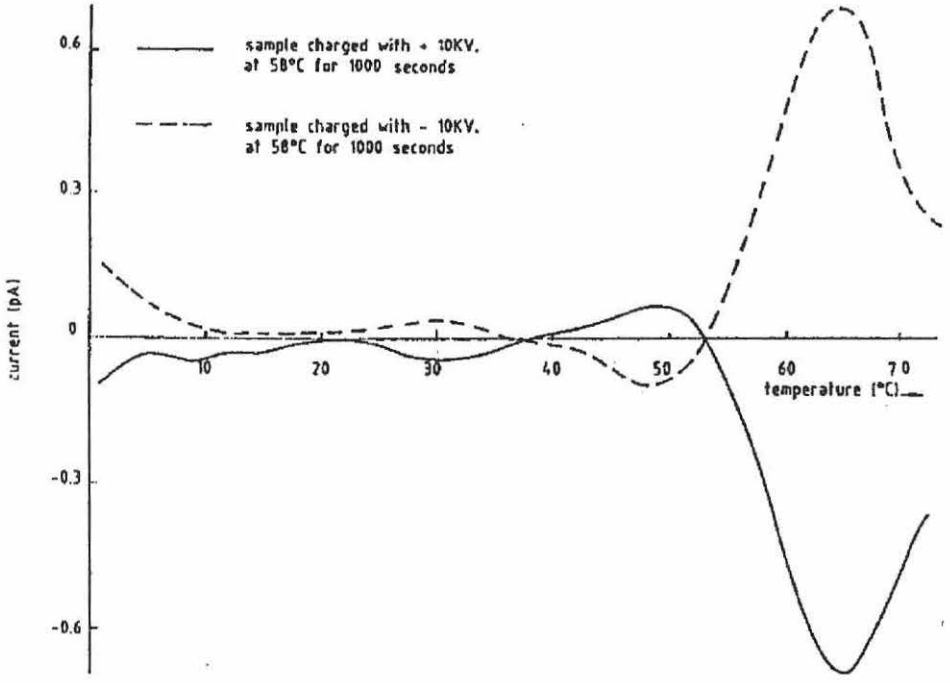

Figure 5.15. (from [13], figure 3).

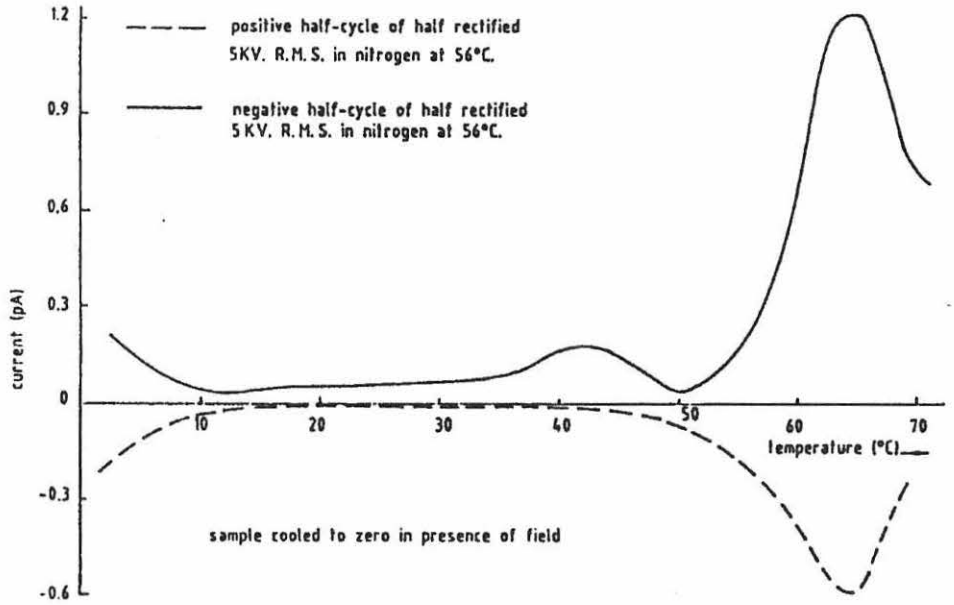

Figure 5.16. (from [13], figure 4).

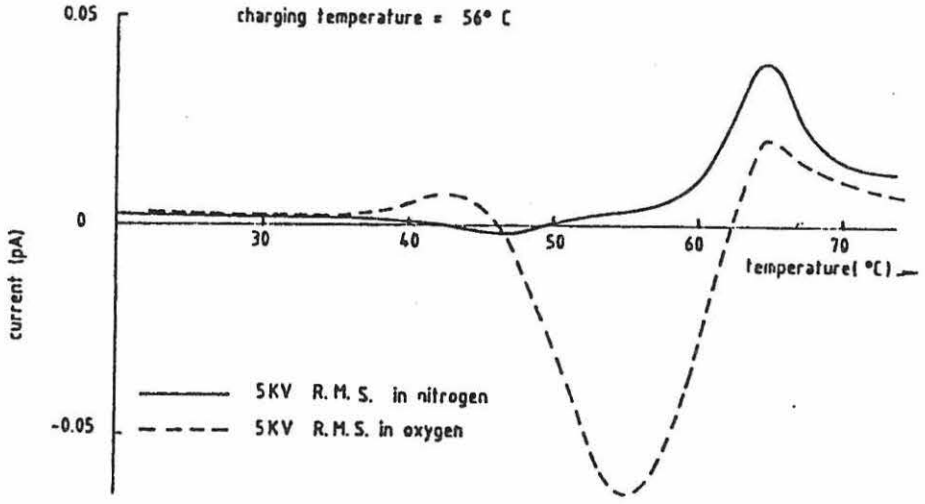

Figure 5.17. (from [13], figure 5).

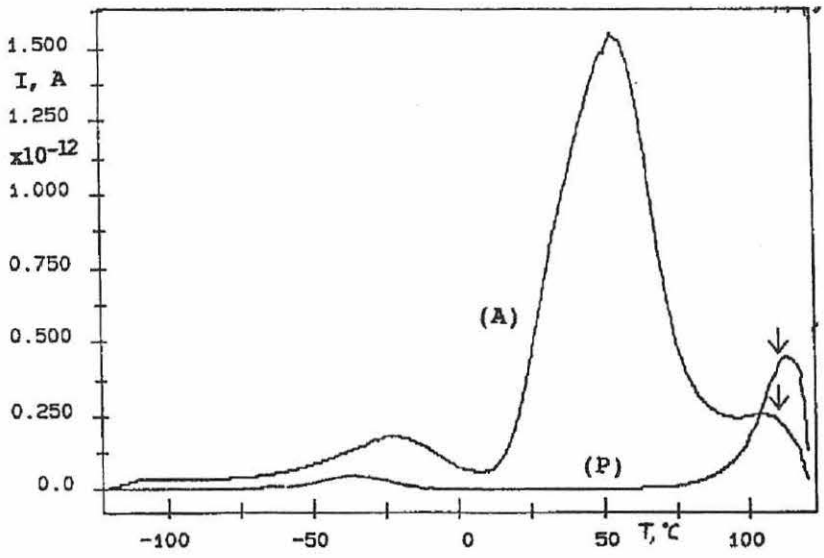

Figure 5.18. (from [14], figure 1).

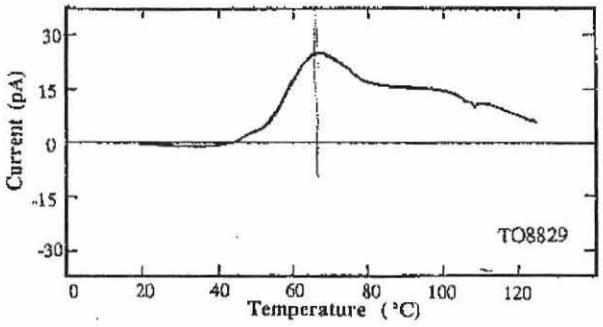

Figure 5.19. (from [4], figure 5b).

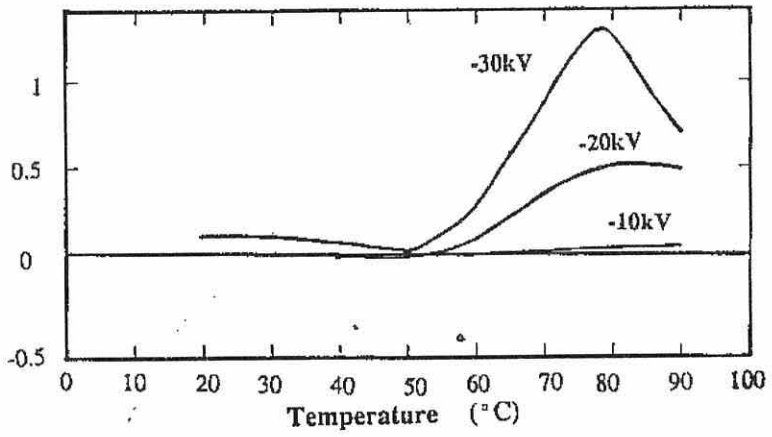

(a) low electric field

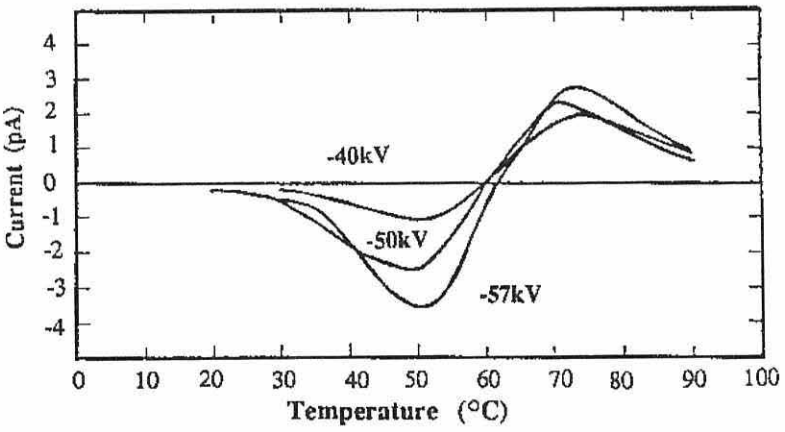

Figure 5.20. (from [4], figure 10).

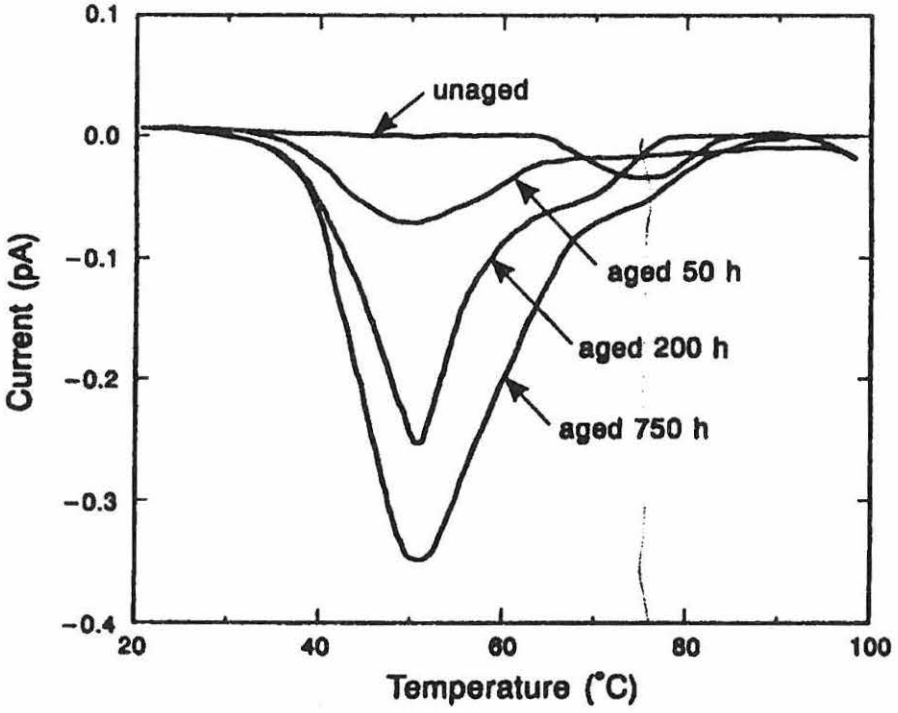

Figure 5.21. (from [15], figure 2).

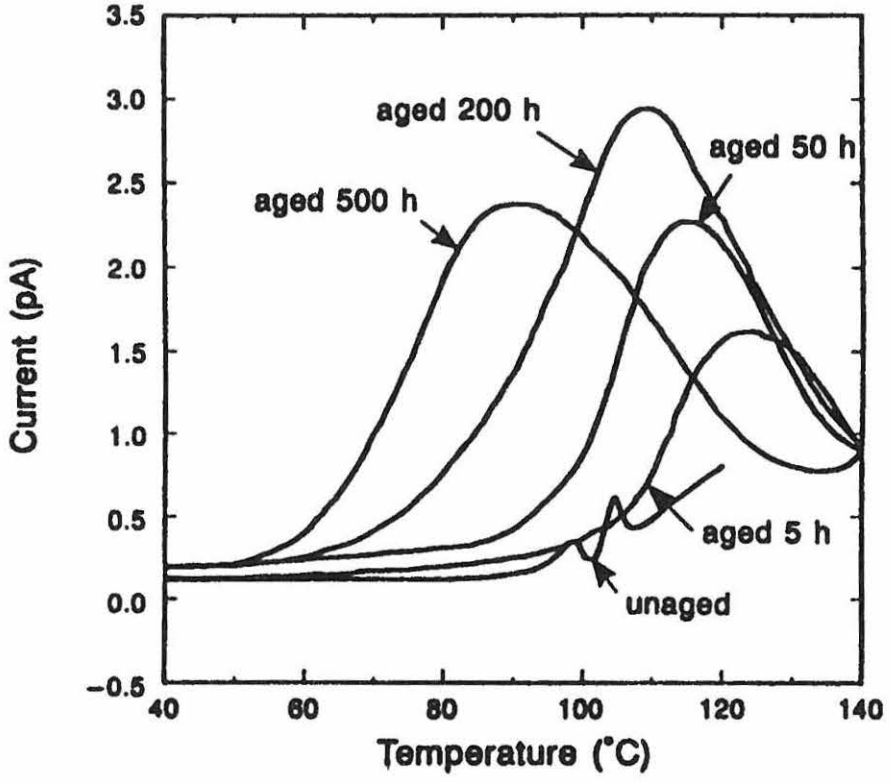

Figure 5.22. (from [15], figure 5).

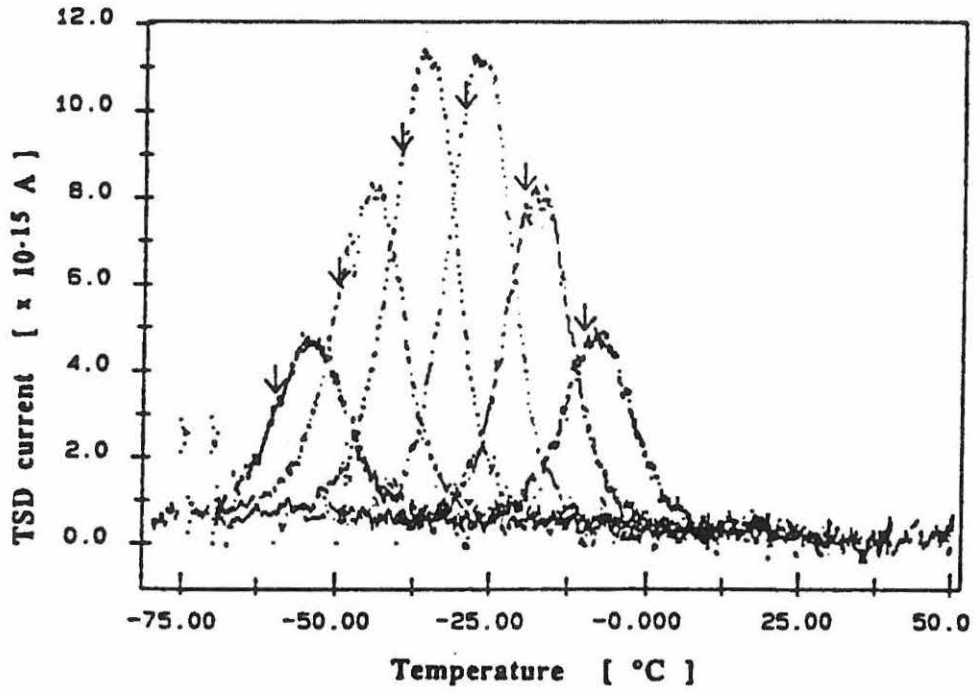

Figure 5.23. (from [16], figure 2).

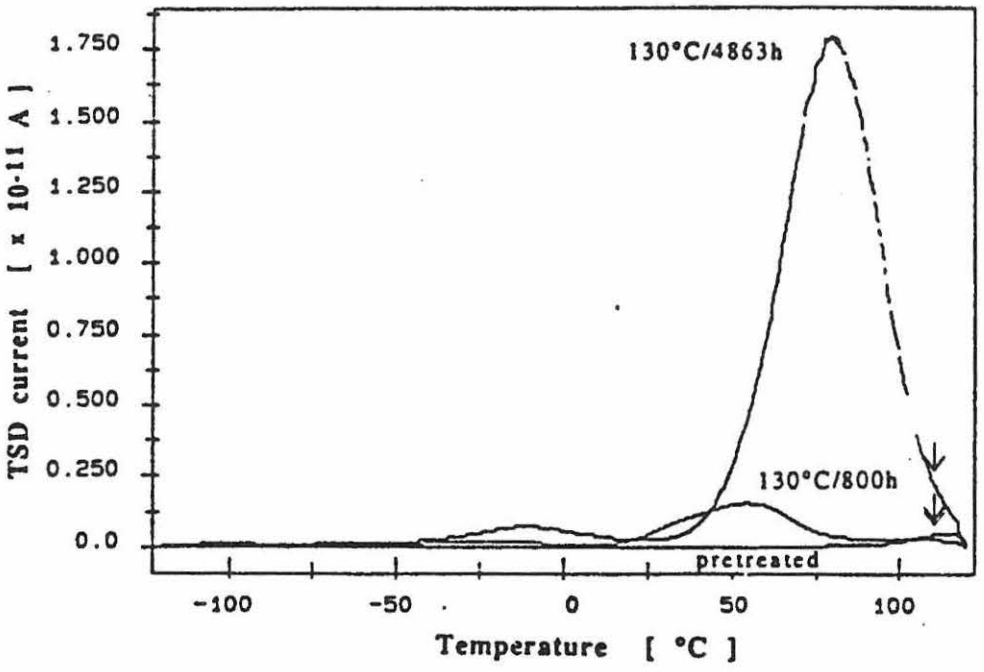

Figure 5.24. (from [16], figure 5).

Chapter 6

Experimental TSC Procedures

6.1 Cable Samples

The cable samples, each $\approx$ 1.2m long, were cut from various medium voltage 15kV cables and supplied by BICC Supertension and Subsea Cables Limited. Figure 6.1 shows a cable cross-section. A central multi-stranded aluminium core

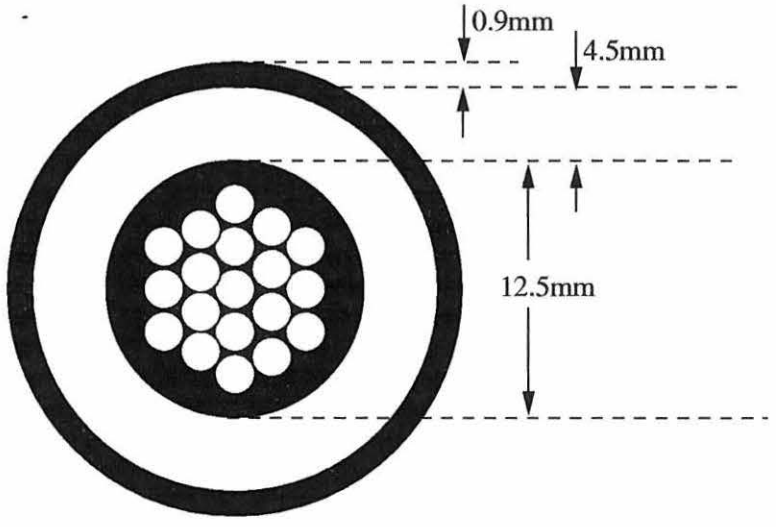

Figure 6.1. Schematic cross-section of a cable sample

is surrounded by an extruded semicon layer to a diameter of $\approx$ 12.5mm. Co-extruded with this layer is the XLPE dielectric insulation, which covers the inner semicon layer and has an optimum thickness of $\approx$ 4.5mm. A final semicon layer of $\approx$ 0.9mm is extruded around the XLPE. All three polymer layers are formed at the same time around the central core in a single co-extrusion process.

The ends of the cable samples were prepared as follows (figure 6.2a). 275mm of the outer semicon layer was stripped from each end to reveal the XLPE insulation. This increased the length of the air-insulation interface between the outer and inner semicon electrodes and reduced the chance of unwanted electrical discharges. 25mm of the XLPE insulation and inner semicon was then removed to expose the inner conductor for electrical connection purposes. With this arrangement a triple junction between the outer semicon, insulation and surrounding air still existed at A, and the high stress at this point was reduced by placing specially-shaped pre-formed stress cones there (figure 6.2b). The high stress at the cable end B was relieved by 40mm metal spheres placed over the exposed conductor. Finally, a layer of copper braiding was wrapped around the outer semicon layer between the stress cones to provide a good electrical contact to the semicon and to facilitate a more even temperature distribution when heating the cable sample.

Electrical heating tapes were next wound uniformly around the sample between the stress cones. A thermocouple was attached centrally between the cones and in direct contact with the outer semicon layer, to allow the sample temperature to be monitored. The sample was then thermally insulated with cotton wool and placed in a plastic tube which held the insulation in place. The tube was coated

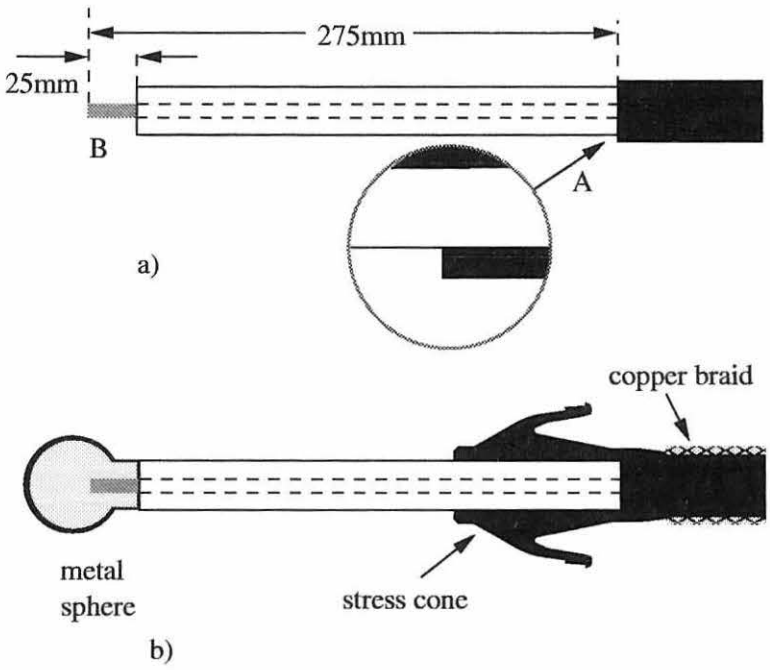

Figure 6.2. Modifications to cable ends.

with aluminium foil which was earthed to electrically screen the cable sample. A lead connected to the sample copper braiding was brought out of the tube and connected to a ground point. The heating tapes were connected to a low-voltage power supply which was switched by a Eurotherm temperature controller type 63e, operating in conjunction with the thermocouple. The system was arranged to provide a linear heating rate to the sample, which is essential for the TSC procedures. After the sample was polarised (figure 6.3), the isothermal and thermally stimulated currents were measured using a Keithley k602 electrometer connected between the inner and outer electrodes (figure 6.4). The electrometer output is recorded on a personal computer (PC) via an analogue-to-digital conversion unit and data-logging software.

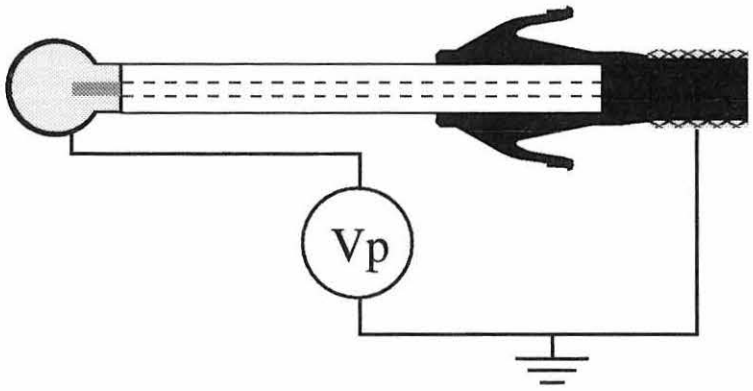

Figure 6.3. The outer electrode is shorted and the polarisation voltage $\pm V_p$ is applied to the aluminium core.

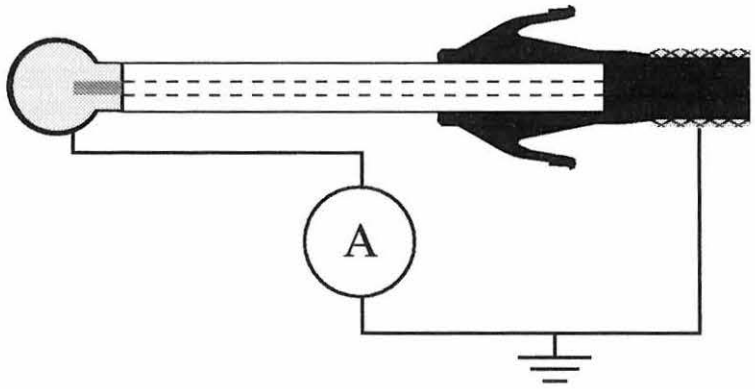

Figure 6.4. The current is measured between the inner and outer electrodes.

6.2 Procedures

The cables have been investigated using two TSC procedures which are shown diagrammatically in figures 6.5 and 6.7.

In procedure I (figure 6.5), the cable sample is first heated to the poling temperature T_p= 107°C before the poling voltage V_p is applied. The sample is then allowed to cool naturally overnight to room temperature T_0 (17–20°C). The rate of cooling is not linear; a typical time-temperature curve during cooling is shown in figure 6.6. V_p is then removed and the sample is shorted through the electrometer. The current is recorded for 2 hours, stage B, allowing a quasi-steady state charge condition to be established. At the end of this period, the sample is heated at a linear rate $\beta = 0.5°\text{C.min}^{-1}$ (stage C) and the thermally stimulated current is recorded up to a maximum temperature $T_{\max} = T_p$. The sample is then maintained at a maximum temperature $T_{\max}$ for approximately 2 hours while the current continues to be recorded. At the end of this stage, the electrometer is disconnected. The procedure may now be repeated from stage A as required, possibly with a different polarising voltage V_p.

In procedure II (figure 6.7) the polarisation stage A is substantially different. The sample is heated to a temperature $T_{\max}$ but then cooled to a temperature T_p between $T_{\max}$ and T_0. Cooling is then arrested. The poling voltage V_p is applied for a time t_p and then removed. The sample is then allowed to cool overnight to room temperature T_0 before stage B begins as before. This is followed by stages C and D which are the same as for procedure I except that the temperature is now taken up to $T_{\max}$, rather than T_p.

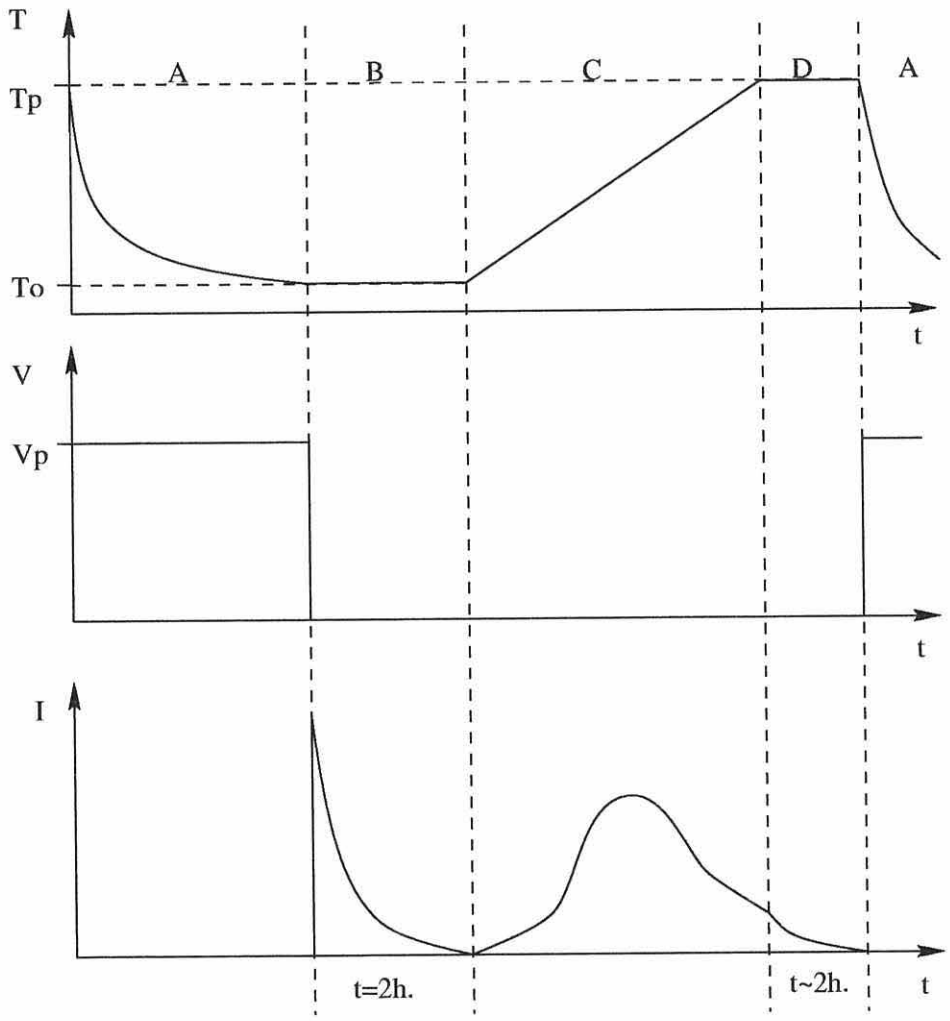

Figure 6.5. TSC experimental procedure I.

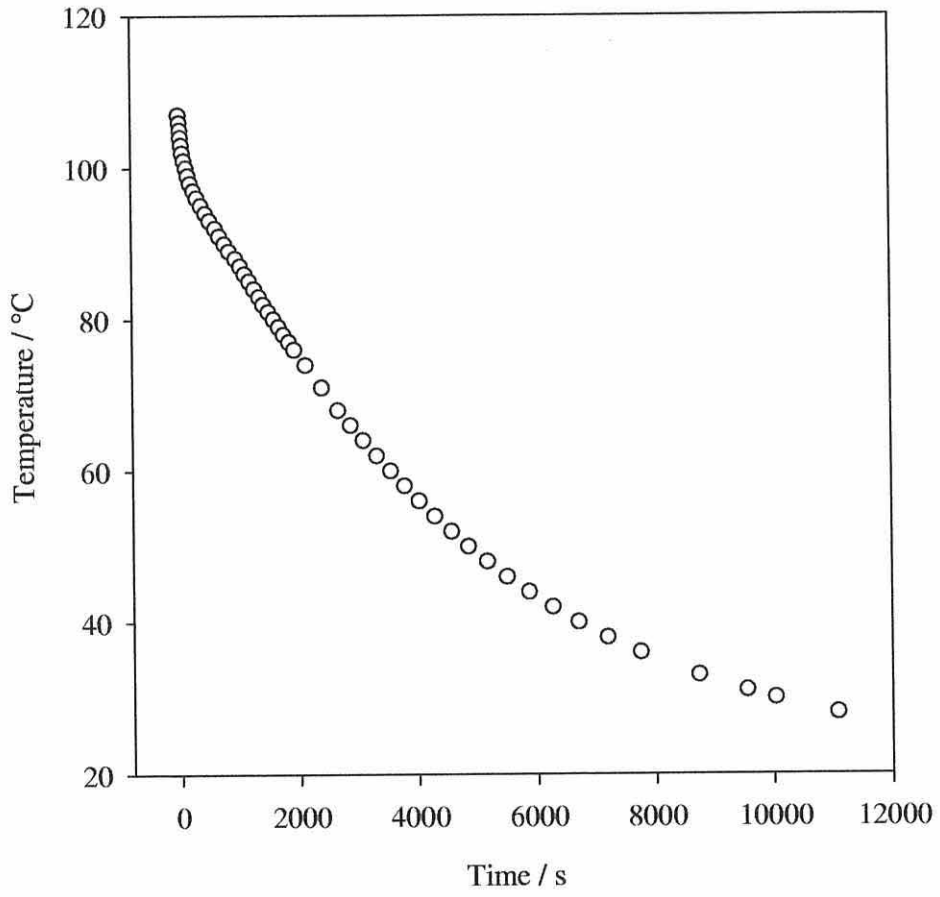

Figure 6.6. Non-linear cooling of model cable samples during stage A of the TSC procedures I and II.

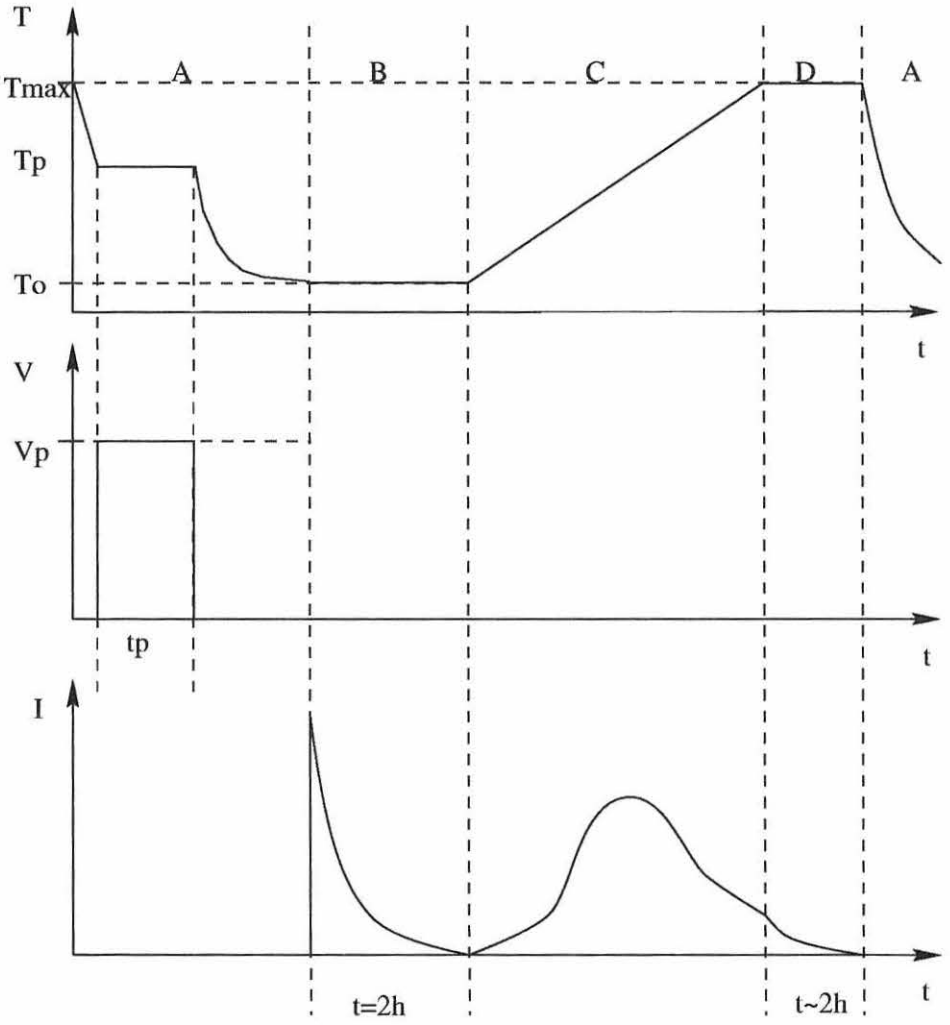

Figure 6.7. TSC experimental procedure II

Chapter 7

TSC Results

In this chapter, the results of the TSC experiments performed on cable models are described and some comments made. A more complete discussion will then appear in chapter 9.

7.1 Cable Types and Numbering

Cables may be one of several types, and each type will have a certain XLPE insulation, semicon base polymer and semicon carbon black. The cable samples were provided by BICC Cables Limited, Erith with, unfortunately, a confusing array of sample numbers. To aid the identification and comparison of cable types, a simplified numbering system has been adopted.

Each cable type will be designated by a number, followed by an upper case and lower case letter, for example "1Aa". The number ("1") identifies the type of insulation, the (pper case letter ("A") indicates the semicon base resin, and the lower case letter ("a") identifies the type of carbon in the semicon. To identify

multiple samples of the same cable, a sample number will be appended. For example, 1Aa/3 is the third sample of cable type 1Aa.

The full list of cable types is given in table 7.1.

Cable Type	Insulation Type	Semicon	
		Resin	Carbon Type
1Aa	FE1139	EBA	supersmooth
1Ab	FE1139	EBA	furnace black
1Ba	FE1139	EVA	supersmooth
2Ba	FE1137	EVA	supersmooth
3Ab	S4201	EBA	furnace black

Table 7.1. Cable types upon which TSC measurements have been made.

7.2 Field Distribution within a Cable

Since the cable samples have a concentric cylindrical geometry, the field F in the insulation is not uniform and varies across the cable radius r according to the law

$$F(r) = -\frac{dV}{dr} = \frac{V}{r\ln(\frac{r_o}{r_i})} \tag{7.1}$$

where r_i and r_o are the inner and outer radii of the cable insulation, and V is the potential difference between the inner and outer conductors, i.e., $V = V_i - V_o$. For the cable models employed here, r_i =5mm and r_o =9.5mm and so $F(r_i) = -0.3125.V$ (kVmm^{-1}) and $F(r_o) = -0.164.V$ (kVmm^{-1}), while the mean field $\bar{F}$ would be $-0.238.V$ (kVmm^{-1}), where V is in kV. Thus the field at the inner semicon interface is almost twice as great as that at the outer semicon. This is likely to have a strong influence on charge injection processes and on the charge and field distribution following poling. It must be remembered, however, that

these are geometric hypothetical values because charge injection will immediately upset the field at the semicon-insulation interfaces.

7.3 Isothermal Measurements

As with much of the published literature, the thermally stimulated currents are of primary interest to this thesis. However, a large quantity of space charge is also released during both the initial isothermal Stage B and, in much smaller quantities, the final isothermal Stage D prior to poling and cooling.

During these isothermal stages, polarised dipoles and space charges that have an activation energy lower than or close to the ambient temperature of the cable sample are released with an exponential, time-dependent characteristic, as previously described in chapter 4. The typical room temperature isothermal current curves shown in figure 7.1 are very similar for different V_p. By integrating these curves with time, the charge released during the isothermal period can be determined, and larger variation between different magnitude V_p can be observed. Figure 7.2 shows the isothermal charge released for each of cable types 1Aa, 1Ab and 1Ba at different magnitudes and polarities of V_p. It is interesting to note that there is only a small variation between the total charge released for different cable types. Note also the existence of a threshold in the region of poling voltage magnitude $|V_p| = 35$kV at which the total charge increase from one voltage to the next is reduced. This feature is also observed in the thermally stimulated measurements, as will be described later in this chapter.

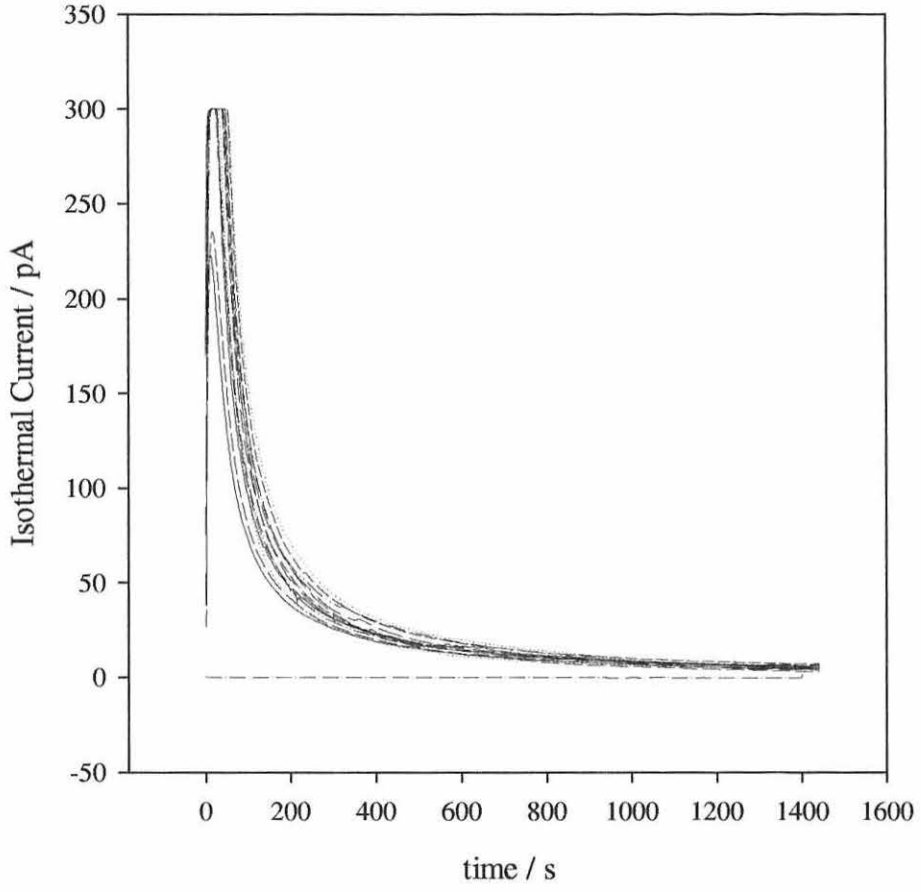

Figure 7.1. A set of typical isothermal current curves, obtained from cable type 1Aa.

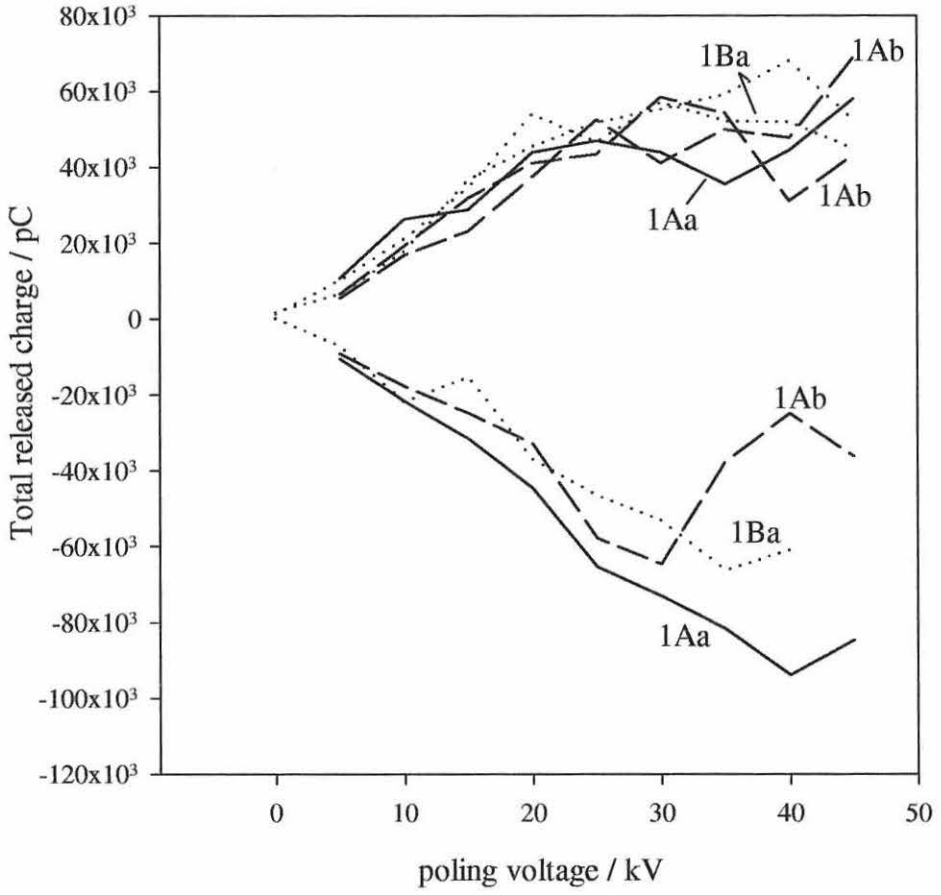

Figure 7.2. Total charge released during the isothermal Stage B for the three main cable types at a range of both positive and negative poling voltages. A net negative charge was released during $+V_p$ poling, while a net positive charge was released during $-V_p$ poling for these cable types.

7.4 TSC Procedure I

7.4.1 Cable Type 1Aa

Cable type 1Aa has an experimental insulation, an ethyl-butyl acrylate copolymer semicon base resin and a supersmooth carbon black in the semicon.

Sample 1Aa/1

The measurements made using Procedure I on sample 1Aa/1 for a range of V_p from -5 to -45kV are shown in figure 7.3. As the magnitude of V_p increases, the temperature, T_{peak}, at which the current peak occurs decreases steadily for all values of V_p. The corresponding maximum current I_{peak} also steadily increases, until V_p reaches ~ -25kV, beyond which I_{peak} first decreases, before resuming an increasing trend. This surprising behaviour is repeatable only on previously unpoled samples, as demonstrated in later sections of this chapter.

Measurements were next made on the same sample using positive V_p as shown in figure 7.4. In this series, four repeat measurements were made at $V_p = +5$kV, followed then by a sequence of measurements made at each value of V_p increasing from $+10$kV to $+60$kV in $+10$kV steps. As noted in section 7.2, the geometric field will be less at the outer electrode, which is the cathode for positive V_p. As electron injection was expected to be the main process in the formation of these peaks, significantly lower peak magnitudes were expected when using positive V_p than when using negative V_p. It was somewhat surprising, therefore, to observe current peaks in the $+V_p$ series to be of similar magnitude to those

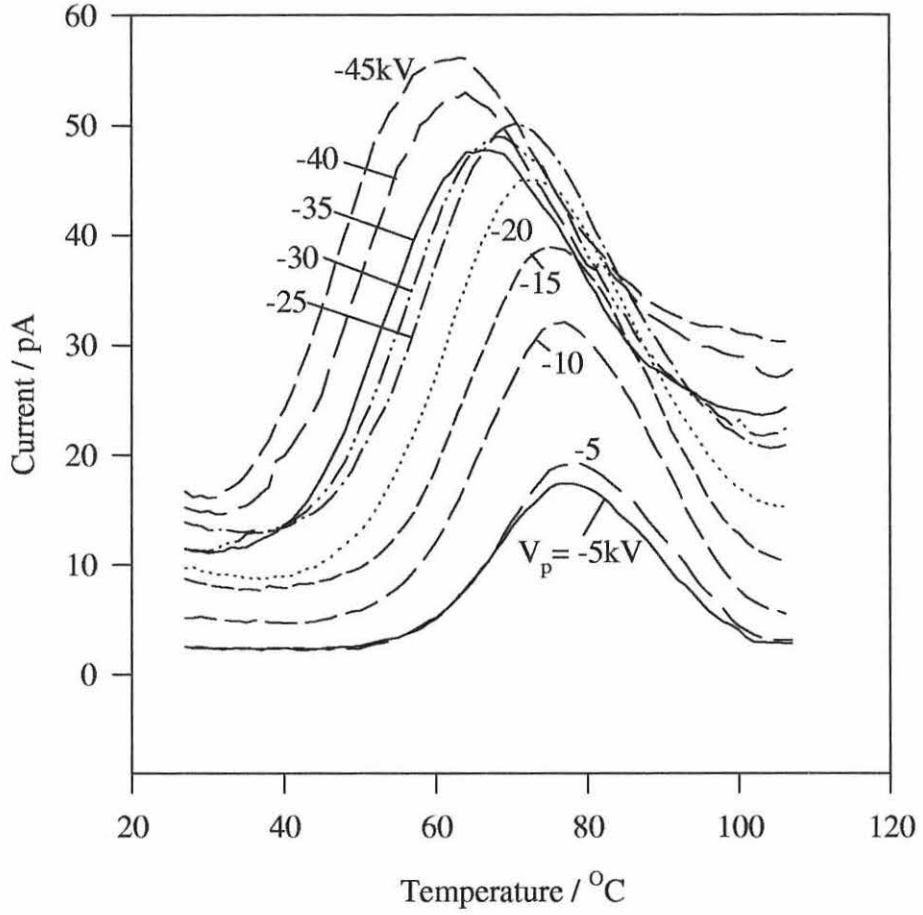

Figure 7.3. TSC measurements made using procedure I and negative V_p on sample 1Aa/1. The values of V_p are indicated. All V_p refer to the inner conductor, as previously defined in figure 6.3.

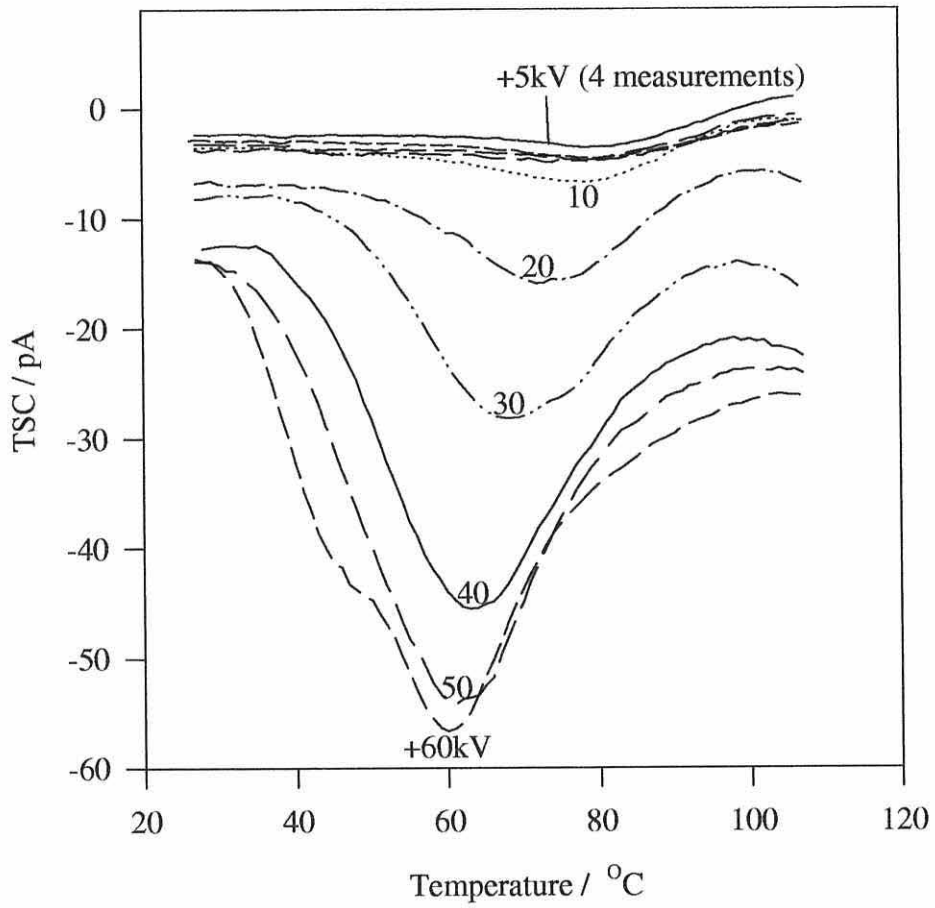

Figure 7.4. TSC measurements made using procedure I and positive V_p on sample 1Aa/1. The values of V_p are indicated.

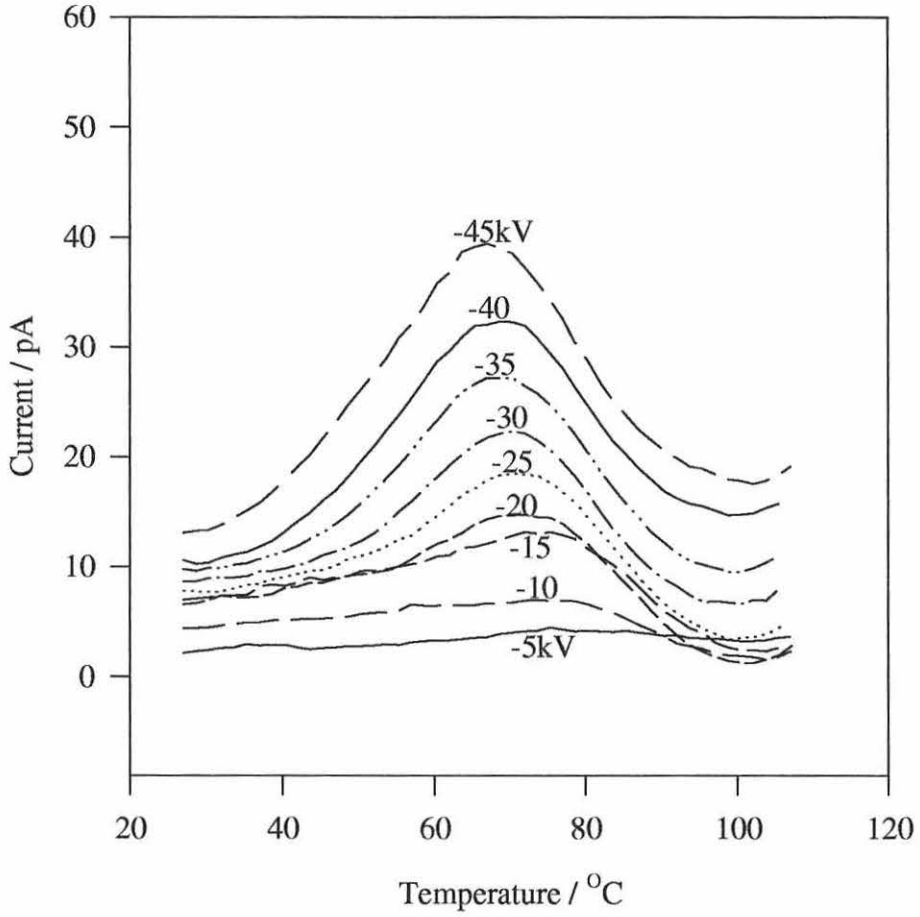

Figure 7.5. Repeat TSC measurements made using procedure I and negative V_p on sample 1Aa/1. V_p are shown.

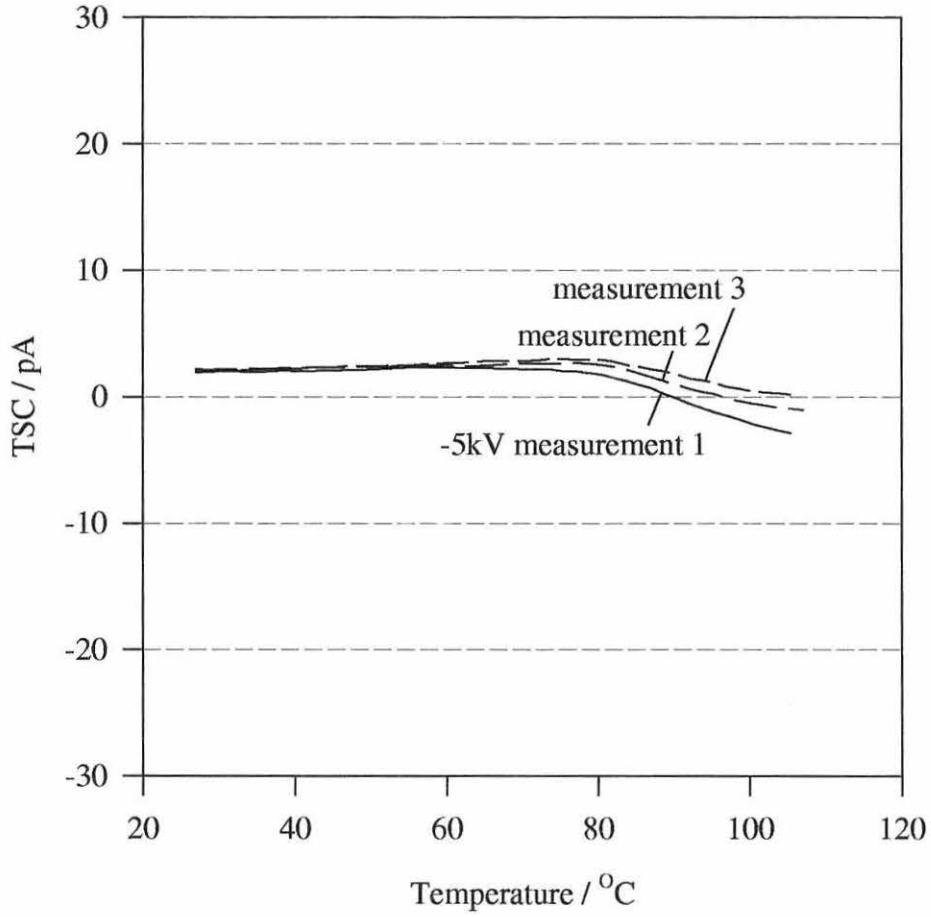

Figure 7.6. Three repeated procedure I measurements on sample 1Aa/1 using $V_p = -5$kV.

in the $-V_p$ series (figure 7.3). This forced a radical re-appraisal of the expected mechanism of space charge generation, as will be discussed in the next chapter.

A further series of measurements were then made on sample 1Aa/1 using negative poling voltages again, with the result shown in figure 7.5. Following this sequence, repeat procedure I measurements were then made on this sample with $V_p = -5$kV (figure 7.6) in the hope that the peak at $\sim$ 80°C originally observed when poling with $V_p = -5$kV (figure 7.3) would be recovered. It is clear that the TSC response has now been altered considerably as a result of the experimental procedure, in that there is now a significant negative-going current at temperatures above 80°C. This is similar to the phenomena observed by Gubanski *et al* [8] for their copolymer samples, as noted earlier in chapter 5. The magnitude of the $T > 80$°C peak does not regain the shape seen in figure 7.3, but does increase slightly upon repetition. It is more important to note that the repeat TSC curves have changed *shape* markedly from those seen for $V_p = -5$kV in figure 7.3.

Fresh Sample 1Aa/2

To verify some of the features observed for the procedure I TSC measurements on sample 1Aa/1, and to determine the effect of thermal cycling on a sample, two series of similar experiments were performed on a previously unused ("fresh") sample 1Aa/2. In the first series, very similar results were seen to those shown in figure 7.3. The first series procedure I measurements (figure 7.7) show that the peak occurring in the 70–80°C temperature region at low negative poling voltages ($V_p < -30$kV) moves progressively to lower temperatures as V_p becomes more

negative. Note also that I_{peak} initially increased with more negative V_p until about -30kV was reached. For $V_p = -35$kV however, I_{peak} is less, but then increases again for $V_p = -40$kV and -45kV. At these higher poling voltages, there is also a marked change in the characteristic above 80°C, a phenomenon which is discussed later (chapter 9).

The second series of procedure I TSC measurements were made on this sample immediately after the first and are shown in figure 7.8. The 80°C peak previously seen for $V_p = -5$kV, figure 7.7 has now changed appreciably in shape, being smaller and broader and has shifted to $T \sim 100$°C. The dominant peak seen in the first measurement series (figure 7.7) at $V_p \sim -30$kV has also disappeared now. It would appear that this dominant peak, seen only in the first measurement series, is probably associated with the 80°C peak of the first series. Note that now in the second series the high temperature behaviour for all V_p follows the $V_p > -30$kV characteristic of the first series; the 80°C peak previously identified at low V_p has now disappeared for all V_p.

To better illustrate the differences noted above, the peak maximum, I_{peak} (figure 7.9) and the temperature, T_{peak} at which the peak occurs (figure 7.10) have been plotted as a function of V_p from the measurements shown in figures 7.7 and 7.8.

Figure 7.9 shows the reduction in the overall peak magnitude on repetition of the TSC measurement series. It also illustrates well the inflexion point in I_{peak} at $|V_p| = 35$kV for the first series and it's notable absence during the second series.

The shift in position of the current peak T_{peak} upon repetition of the TSC

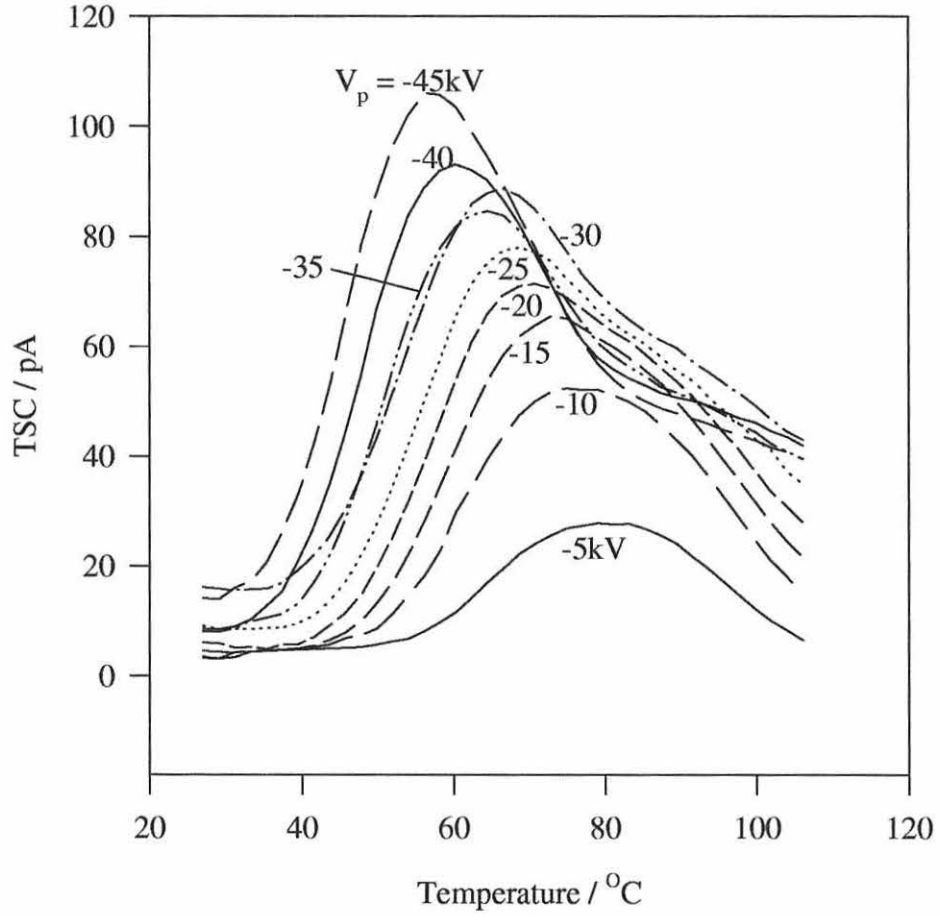

Figure 7.7. Procedure I TSC measurements made on a fresh sample 1Aa/2 using negative V_p. Note the decrease and significant shift in T_{peak} in the region of $V_p \sim$ 30kV.

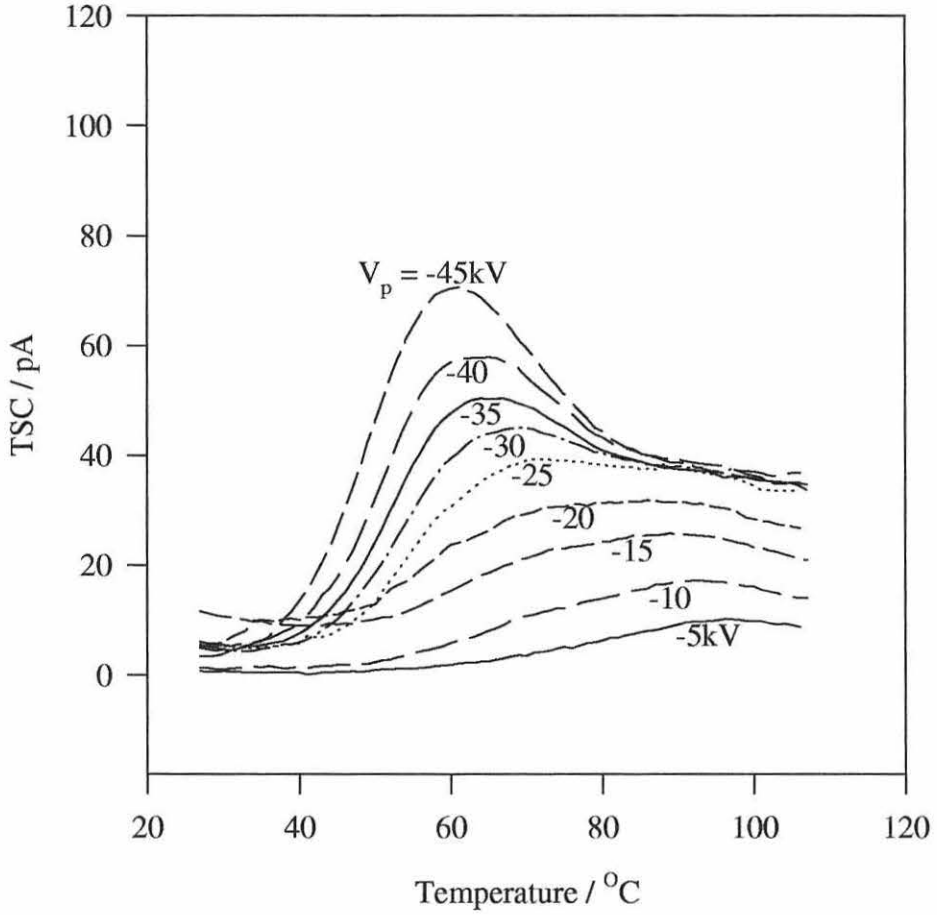

Figure 7.8. Repeat of the procedure I TSC measurements on sample 1Aa/2 using negative V_p.

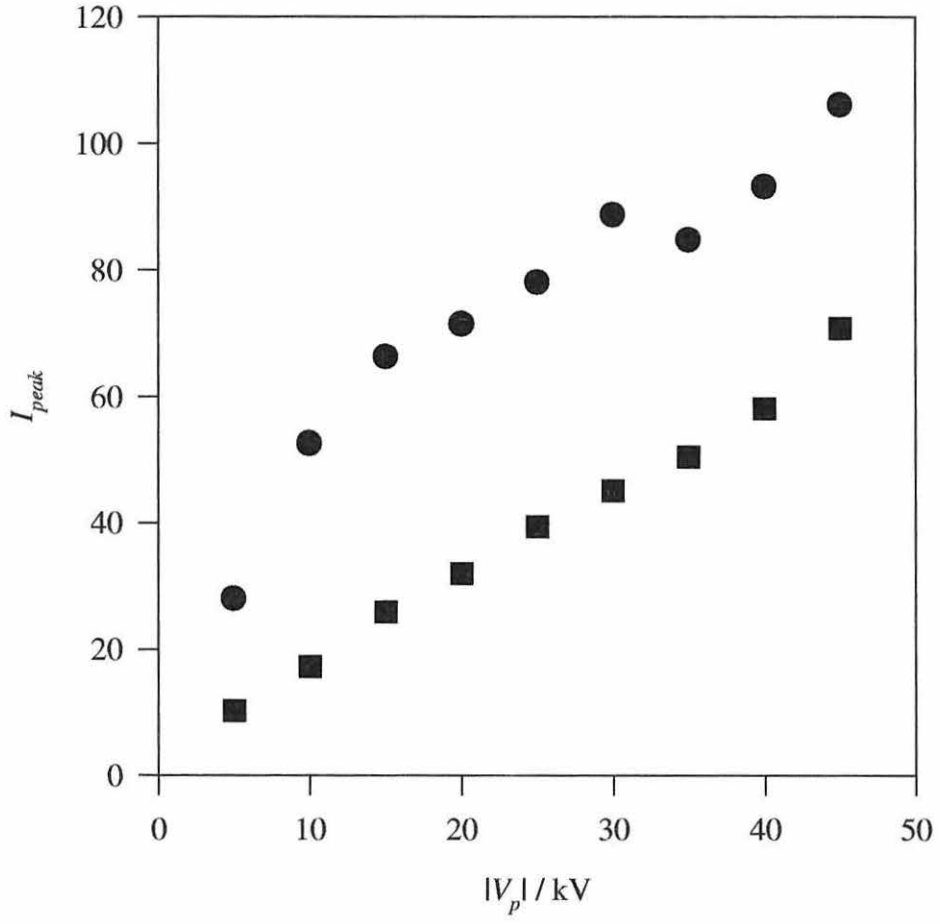

Figure 7.9. Values for I_{peak} versus V_p from figures 7.7 and 7.8. The circles show the data from the first negative-V_p TSC series (figure 7.7), while the squares show those of the repeat series (figure 7.8).

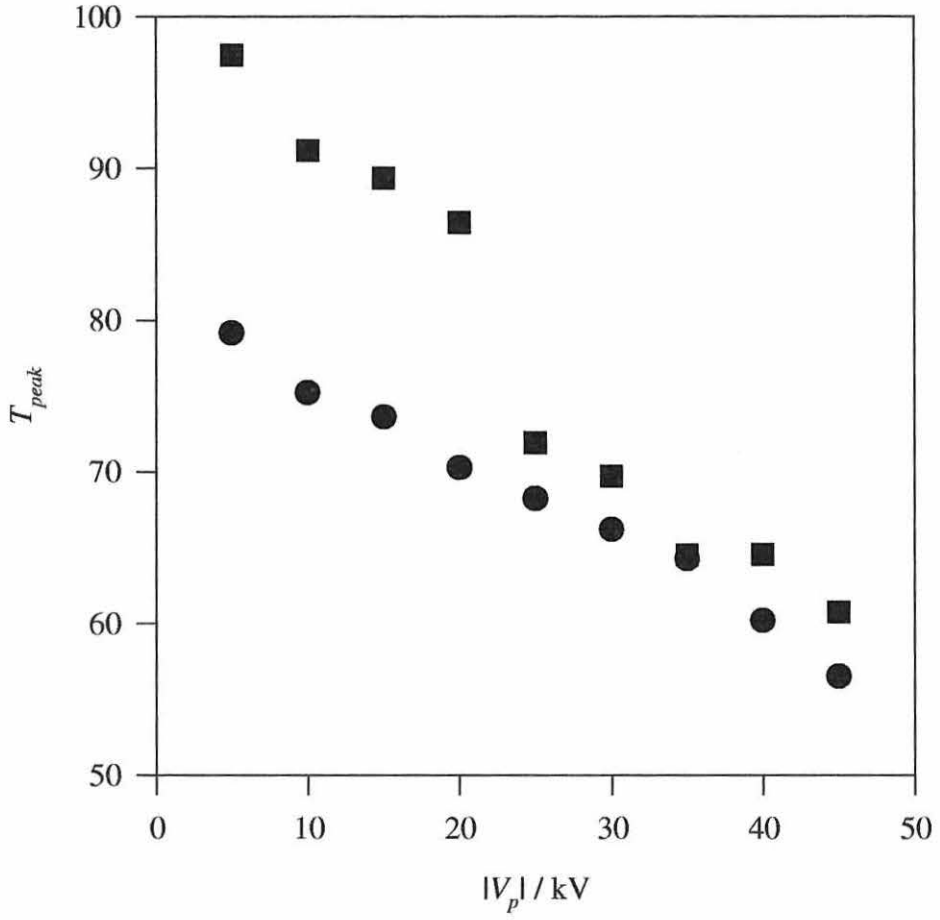

Figure 7.10. Values for T_{peak} versus V_p from figures 7.7 and 7.8. The circles show the data from the first negative-V_p TSC series, while the squares show those of the repeat series.

measurement series can clearly be seen in figure 7.10. T_{peak} is also higher for the second series than the first for $|V_p| \geq 25$kV. For values of $|V_p|$ below this, T_{peak} appears to be significantly higher on repetition by as much as 20°C. However, this change in T_{peak} may be considered to be artificial because the current peak is now very broad and of a very low magnitude under these conditions.

Fresh Sample 1Aa/3

A series of measurements was also made on another fresh sample, 1Aa/3, this time using positive V_p in the range +5 to +45kV, as shown in figure 7.11. At first glance, the TSC appear to be almost the mirror image in the T-axis of the negative V_p measurements for sample 1Aa/2 (figure 7.7). However, there are several important differences. For $V_p = +5$kV, the high temperature peak appears at $T_{\text{peak}} \sim 85$°C, approximately 5°C higher than the similar peak for $V_p = -5$kV (figure 7.7). It is a coincidence that the temperature variation across a sample of the type examined here has been measured to be $\sim$ 4°C. The consequences of a temperature variation across a sample will be discussed in chapter 9.

Although the position of the peak seen at $T_{\text{peak}} = 80$°C for $V_p = -5$kV is polarisation-dependent, the position of T_{peak} as $|V_p|$ increases becomes *polarity independent*, which suggests that the peak at $\sim$ 60°C resulted from dipole relaxation, or charge injection and ejection, at both interfaces, irrespective of the field there. This point will be discussed later in chapter 9. As found earlier (see $V_p = -5$kV, figure 7.7) the measurements made using $+V_p$ shown in figure 7.11 also exhibit a) the reduction in the magnitude of I_{peak} at high $|V_p|$, although for

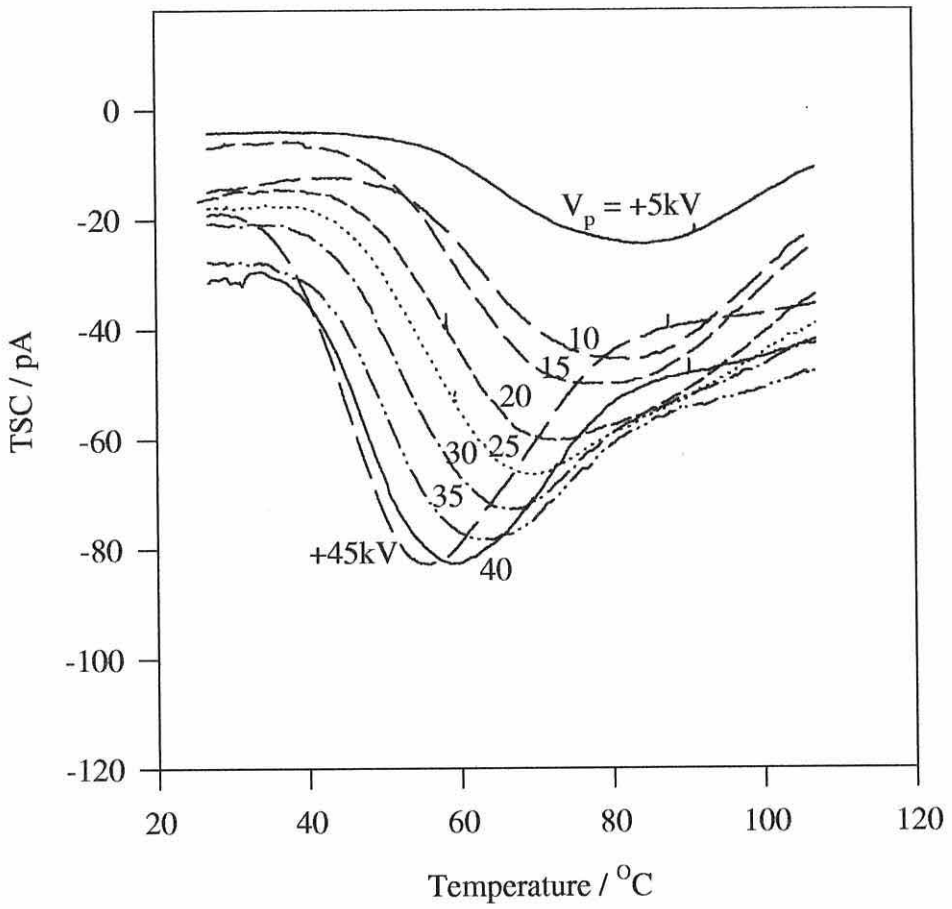

Figure 7.11. Positive V_p Procedure I TSC measurements made on fresh sample 1Aa/3. V_p are indicated.

this sample and voltage polarity the reduction occurs above $V_p = +40$kV; and b) the flattening of the response above 80°C as $|V_p|$ increased. It is most probable that these two phenomena are related, and coincide with the disappearance of the 80°C peak observed when $|V_p| = 5$kV, as before.

7.4.2 Cable Type 1Ab

Cable type 1Ab has the same insulation and semicon base resin (EBA) as type 1Aa, but with furnace carbon black rather than a supersmooth carbon filling.

Sample 1Ab/1

The measurements made on sample 1Ab/1 for V_p between -5 and -45kV are shown in figure 7.12. The TSC of this sample of 1Ab did not exhibit the large shift in T_{peak} seen previously in fresh samples of 1Aa because poling voltages in excess of -30kV had previously been applied to the sample. However, the low broad peak ($V_p = -5$kV) at $T \sim 100$°C was still present and as V_p increased a second peak appeared in the region of 65°C. At $V_p = -45$kV, this second peak eventually became quite large (approximately 80pA) when compared to the 40pA peak produced by similar conditions for cable type 1Aa (figure 7.5).

Sample 1Ab/2

As previously for type 1Aa, it was deemed necessary to perform further experiments on fresh samples of 1Ab to ascertain the effect of thermal cycling. Two series of negative polarity V_p measurements were made on sample 1Ab/2. For the

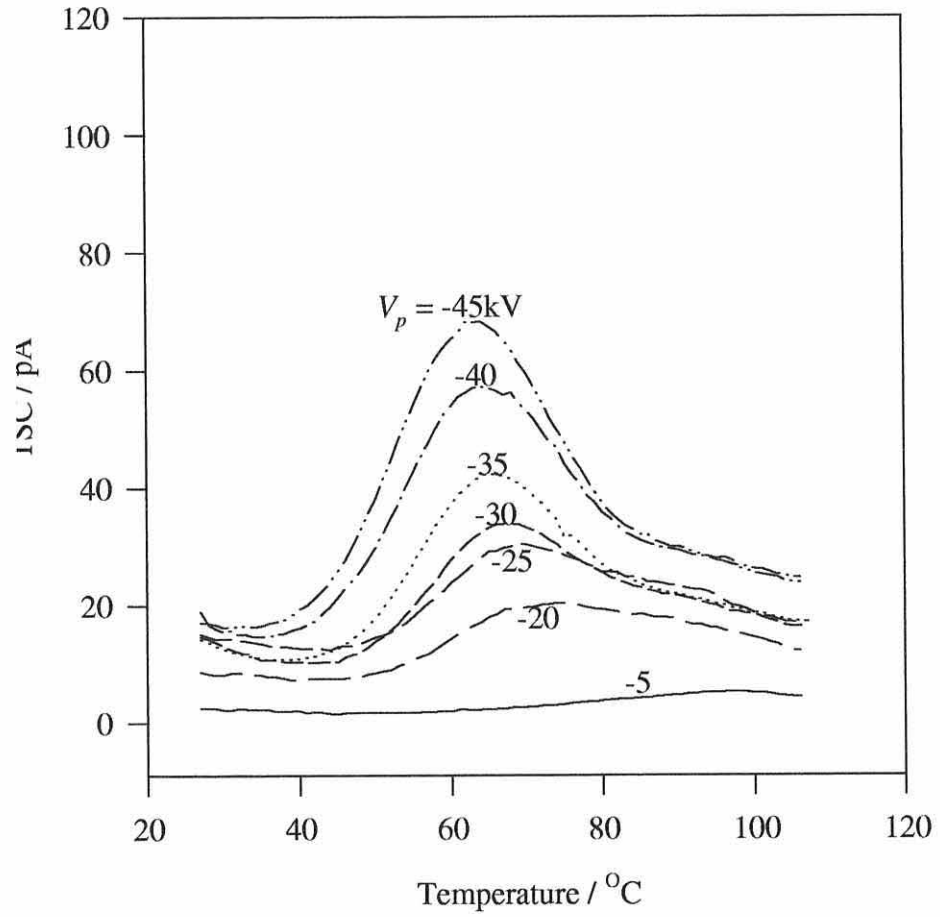

Figure 7.12. Early TSC measurements made on cable sample 1Ab/1. V_p are indicated.

first series (figure 7.13) the low V_p peak appeared at $\sim 75°C$ and again decreased steadily as $|V_p|$ was increased, as seen in the fresh samples of 1Aa. The poling voltage at which I_{peak} decreased before increasing again, was observed to be in the region of -25kV. However, the TSC for $V_p = -45$kV appeared to reach a slightly lower T_{peak} of $\sim 55°C$.

A repeat series of measurements is shown in figure 7.14. The low V_p peak appeared at a slightly higher temperature of $\sim 90°C$, with the beginnings of the lower temperature peak appearing on the low temperature side of the 90°C peak. As V_p increased, so T_{peak} once more decreased until reaching $T \sim 65°C$ for $V_p = -45$kV. The extra high peak that was present at 45°C in the first measurement series (figure 7.13) has now disappeared to leave a smooth single peak at $T \sim 65°C$. This second TSC series is very similar in form and shape to the second negative series previously observed for cable sample 1Aa/2 (figure 7.8), although the respective values of I_{peak} are again slightly larger in magnitude.

Sample 1Ab/3

Positive polarity V_p measurements were also made on a fresh cable sample of type 1Ab. The resultant TSC are shown in figure 7.15. There does not appear to be a significant peak shift at $|V_p| \sim 40$kV, although the initial current at $T \sim 27°C$ when $V_p = +45$kV decreases contrary to the TSC measurements made at lower V_p. 1Aa/3 (figure 7.15) exhibits a similar shift in current. Note that $I_{peak} = -120$pA at $V_p = +45$kV, 50% larger than the similar I_{peak} seen for sample 1Aa/3. The significance of this observation will be discussed in chapter 9.

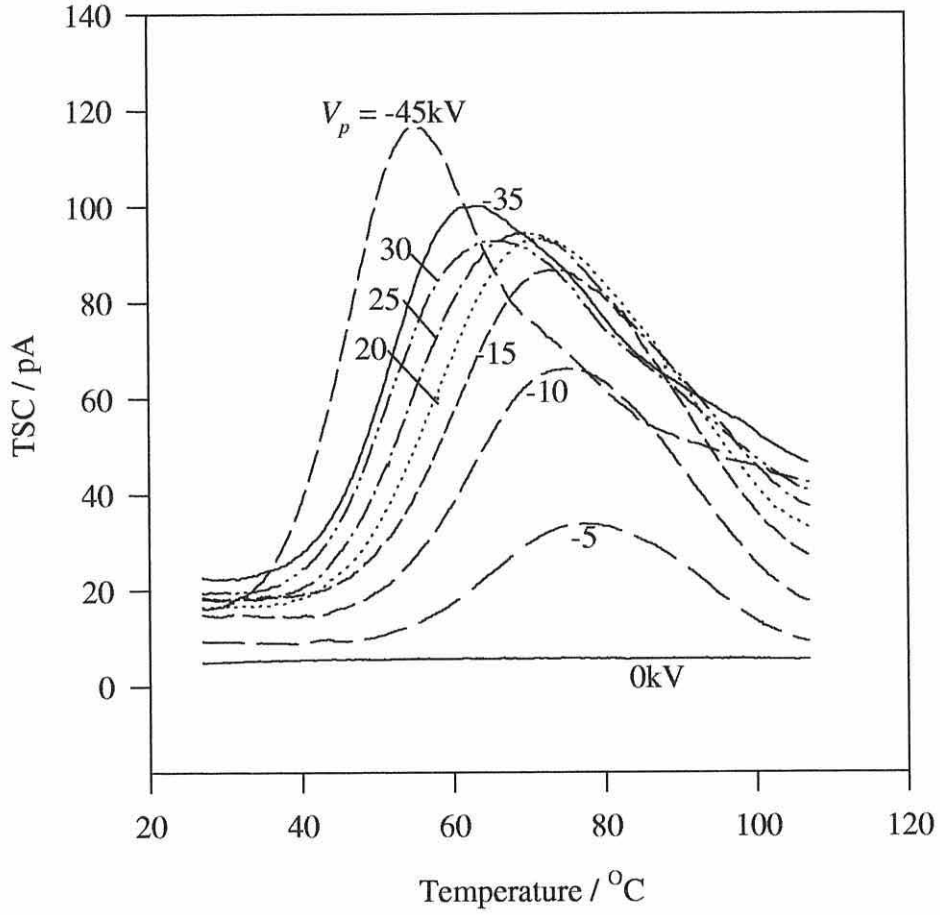

Figure 7.13. First series of procedure I TSC measurements on fresh sample 1Ab/2.

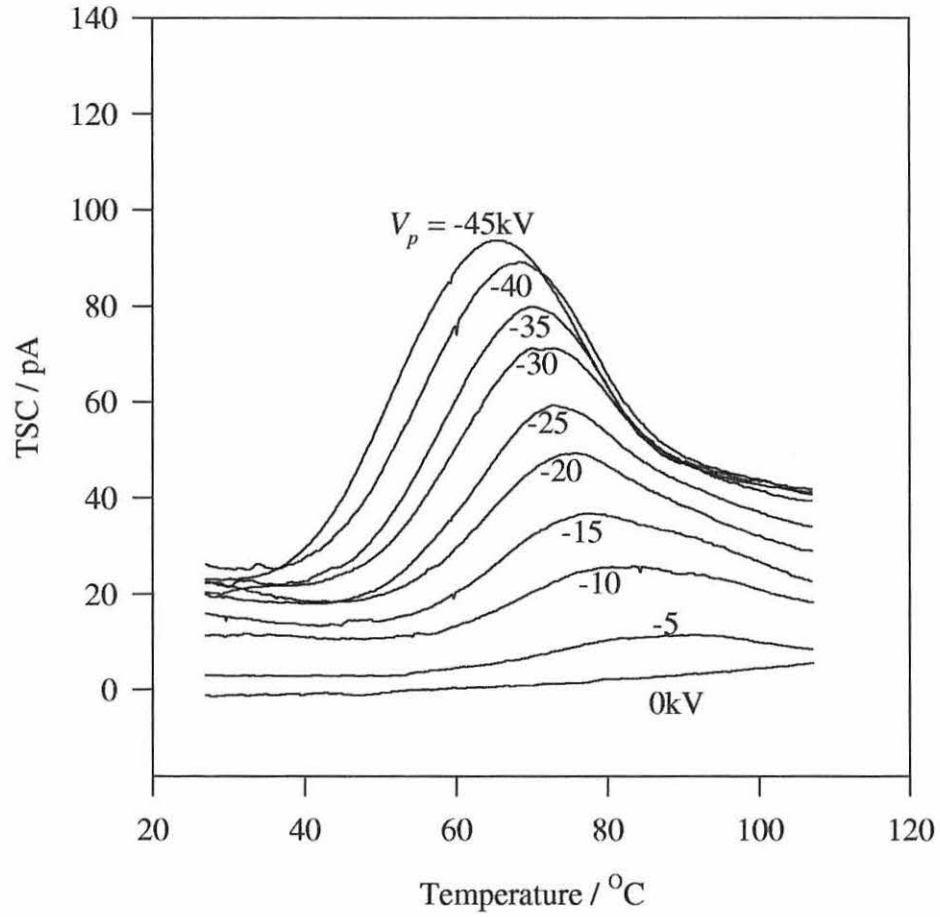

Figure 7.14. Repeat of the measurements made on sample 1Ab/2 and shown in figure 7.13

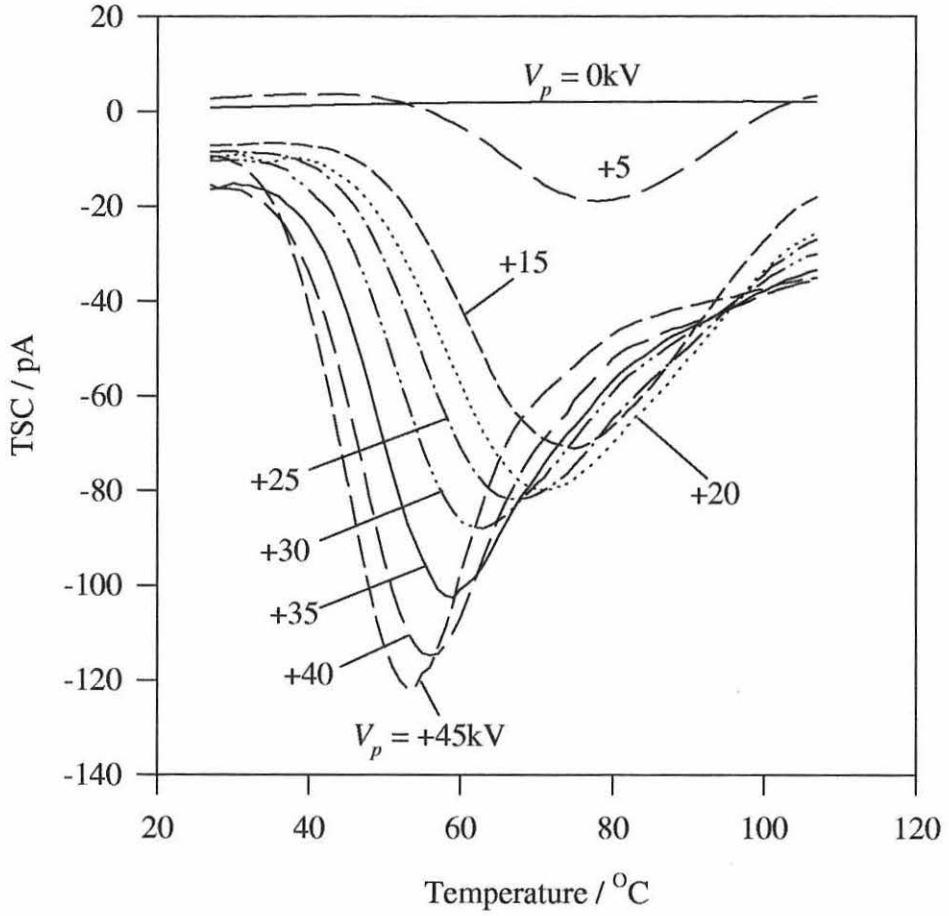

Figure 7.15. Positive V_p Procedure I TSC measurements made on fresh sample 1Ab/3. V_p are indicated.

7.4.3 Cable Type 1Ba

Cable type 1Ba has the same insulation type as cable types 1Aa and 1Ba. The semicon base polymer is an ethylene-vinyl acetate (EVA) copolymer which contains the same supersmooth carbon black as cable type 1Aa.

Sample 1Ba/1

The measurement series made on cable sample 1Ba/1 using procedure I is shown in figure 7.16. The responses are distinctly different from those of cable types 1Aa (for example, figure 7.3) and 1Ab (figure 7.12). A notable feature of the TSC in figure 7.16 is the almost constant current level found above $T = 80°C$. This sample was used for a number of preliminary experiments, so it is possible that the history of this sample has influenced the TSC (this will be verified below with repeat measurements made on fresh samples of this type). A low temperature peak appears at $T \sim 50°C$, and a trough at $T \sim 65°C$ before the current reaches a constant level. However, the trough may actually be caused by a peak of opposite polarity, a possibility which is investigated in section 7.4.4.

Sample 1Ba/2

As for the other cable types, procedure I measurements were performed next on a fresh sample of cable type 1Ba. The results are shown in figure 7.17. The TSC peaks exhibit more detail, but less peak temperature variation, when compared to those of the previous cable types 1Aa and 1Ab. A peak appears at $T \sim 50°C$ for V_p as low as -10kV, and the peak remains within $\sim 5°C$ of this temperature for all

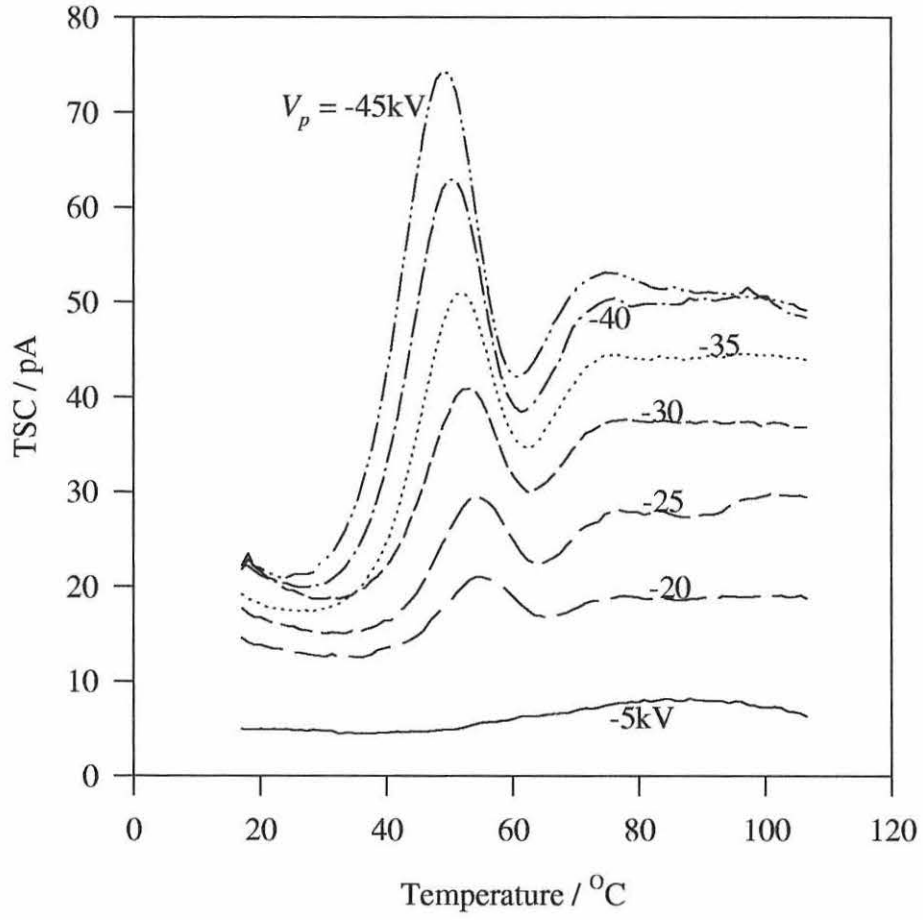

Figure 7.16. Procedure I negative V_p TSC measurements made on sample 1Ba/1. V_p are indicated.

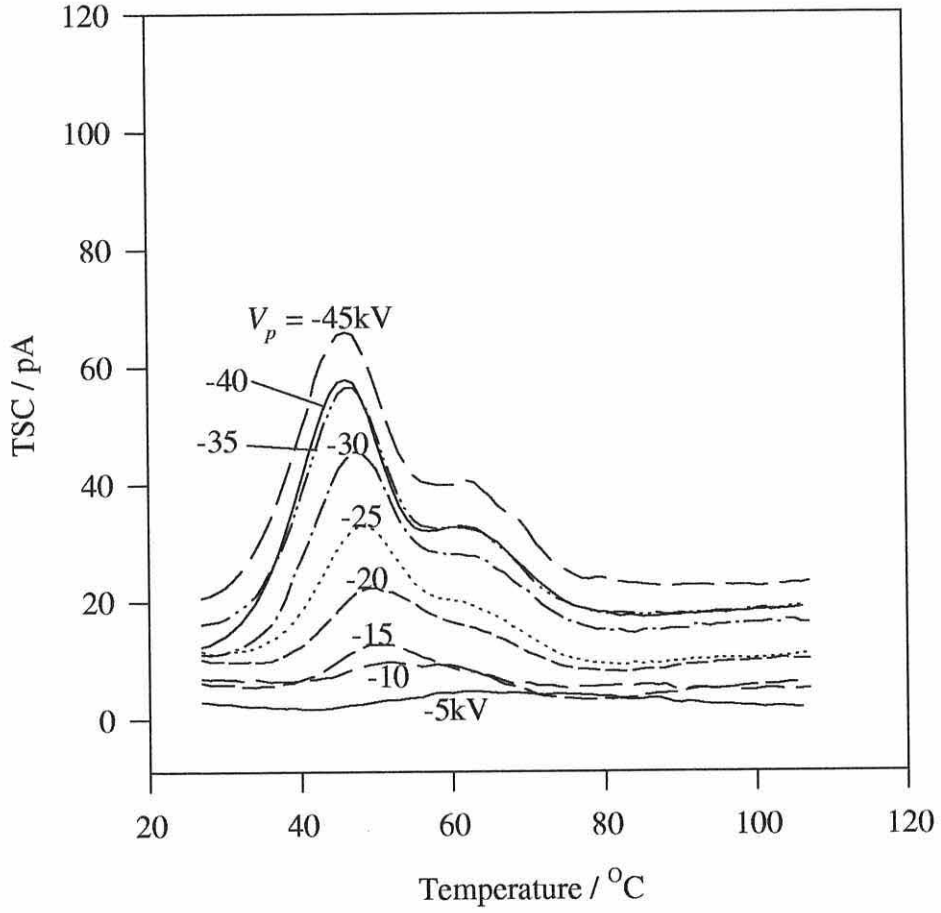

Figure 7.17. TSC measurements made on fresh sample 1Ba/2 using $-V_p$ and procedure I.

negative values of V_p. There also appears to be a second peak at $T_{\text{peak}} \sim 65°\text{C}$ for $V_p > -20\text{kV}$. However, there is a possibility that these two peaks were actually a broad peak of one polarity with a smaller peak of an opposite polarity at $T \sim 55°\text{C}$. This suggestion will be confirmed, to a certain degree, as a characteristic of the EVA semicon base resin type by experiments performed on cable type 2Ba (section 7.4.4). Note that the high temperature current response is very flat, as for sample 1Ba/1, but is of a much lower magnitude. As noted above, the TSC peak did not shift in temperature appreciably, and there was no significant increase in I_{peak} when $|V_p|$ increased from 35kV to 40kV. This may be an indication of the same effect in this cable type as the peak inflexion previously seen in the first series of negative polarity measurements made on types 1Aa (figure 7.7) and 1Ab (figure 7.13).

Repeating the negative V_p series (figure 7.18) on sample 1Ba/2 did not create any obvious changes in the TSC. However, closer examination of the results revealed an increase in the magnitude of the 65°C peak, and it now first appears when $V_p$is -10kV instead of -20kV. The peak at $T = 50°\text{C}$ does not move in temperature during the repeated cycle. The high temperature current ($T > 80°\text{C}$) also is now greater in magnitude following repetition, in agreement with the corresponding current seen in sample 1Ba/1.

Sample 1Ba/3

Positive polarity V_p measurements were made on cable sample 1Ba/3, and these are shown in figure 7.19.

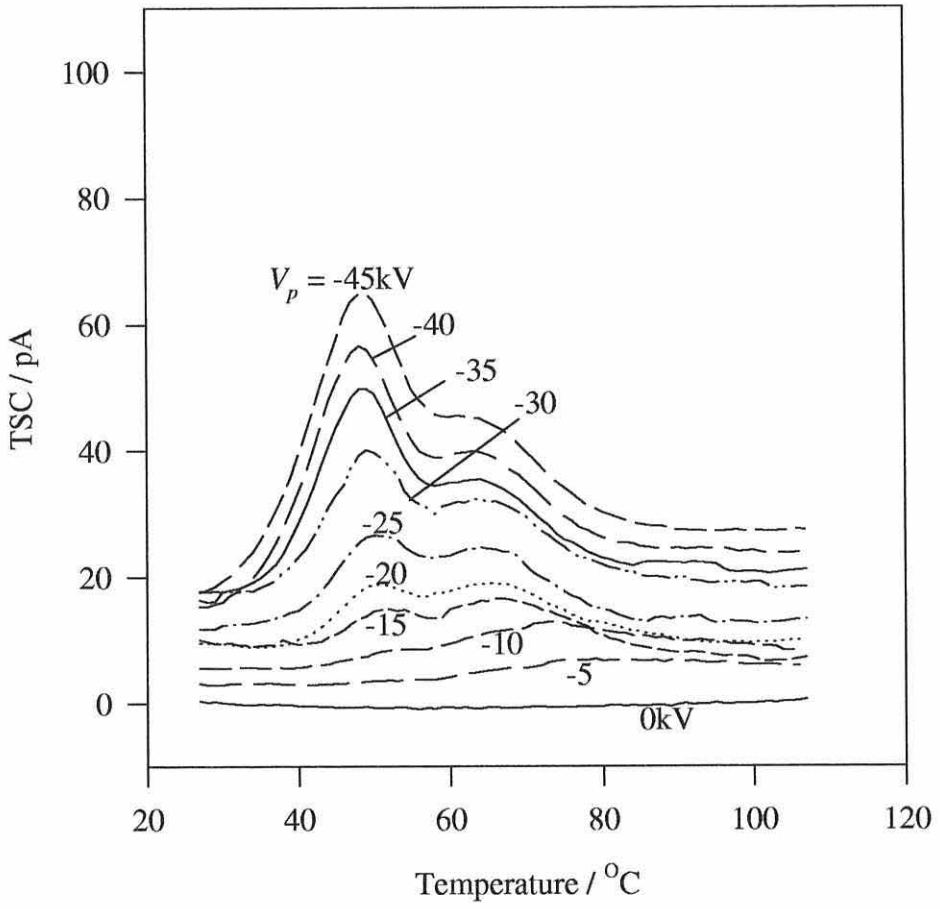

Figure 7.18. Repeat of procedure I TSC measurements made with negative V_p on cable sample 1Ba/2. V_p is indicated.

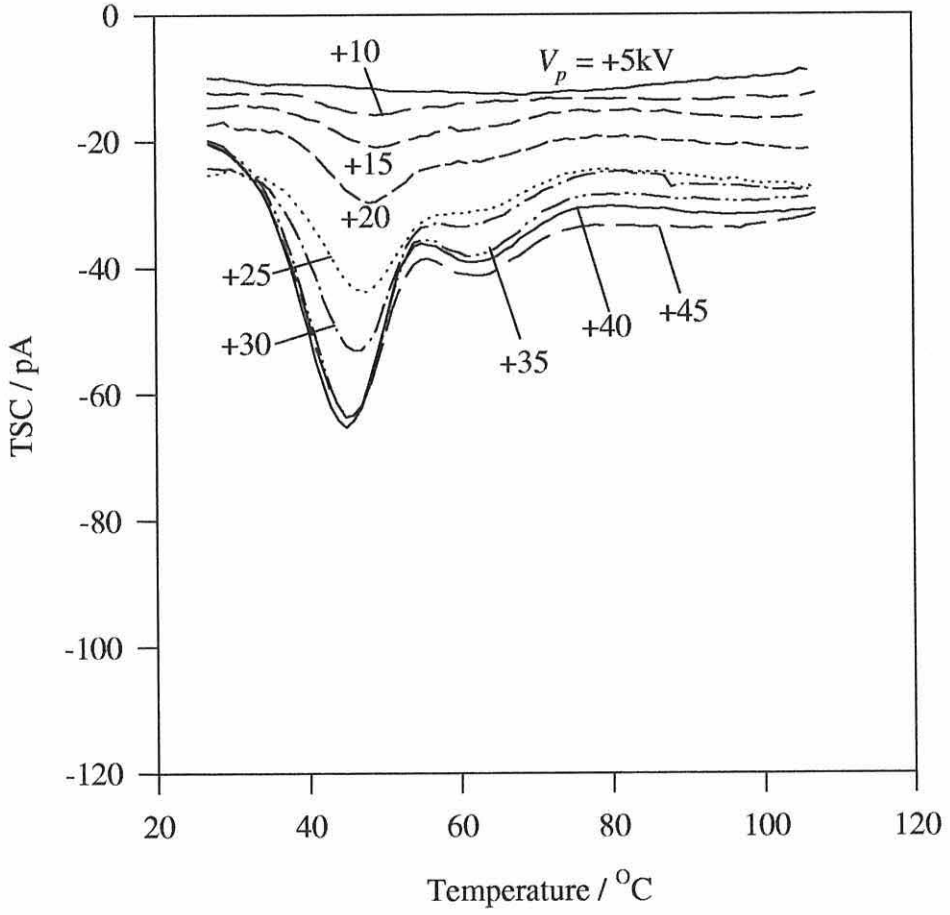

Figure 7.19. procedure I TSC measurements made on cable sample 1Ba/3 using positive V_p as indicated.

The TSC steadily increases with V_p. A peak first appears at $T \sim 45°C$ when $V_p = +10kV$. As V_p increases to +20kV, the second peak at $T = 65°C$ begins to appear. The peak at 45°C increases until $V_p = +35kV$, when it attains a constant magnitude of around −65pA. By comparison, the peak at 65°C increases steadily until V_p reaches +35kV, slows when $V_p = +40kV$, then increases by a larger amount when V_p progresses to +45kV. This suggests that there is a voltage at which a change occurs, similar to the voltage seen in TSC series of 1Aa and 1Ab. As previously observed in these other types, this change occurs at $|V_p|$ of 35 to 40kV for positive poling voltages and is slightly higher than for their negative counterparts. The alternative behaviour of the 1Ba type (arrest in the increase of peak height, as opposed to the peak shift seen in types 1Ab and 1Aa) is also evident.

7.4.4 Cable Type 2Ba

The Procedure I measurements performed on sample type 2Ba reveal a very low TSC current. It is interesting to note the appearance of a trough at $T \sim 55°C$ for $V_p \geq -35kV$, indicating a threshold field at this V_p. A second notable feature is the high temperature TSC, which becomes increasingly negative as the high values of V_p are used. This indicates the presence of a different, negative peak, just outside of the measured temperature range, which could be attributed to the insulation type. To investigate this high temperature peak, an extra Procedure I measurement was then performed (figure 7.21). for this measurement, $V_p = -45kV$ and $T_p = 107°C$, as for a standard Procedure I measurement. However,

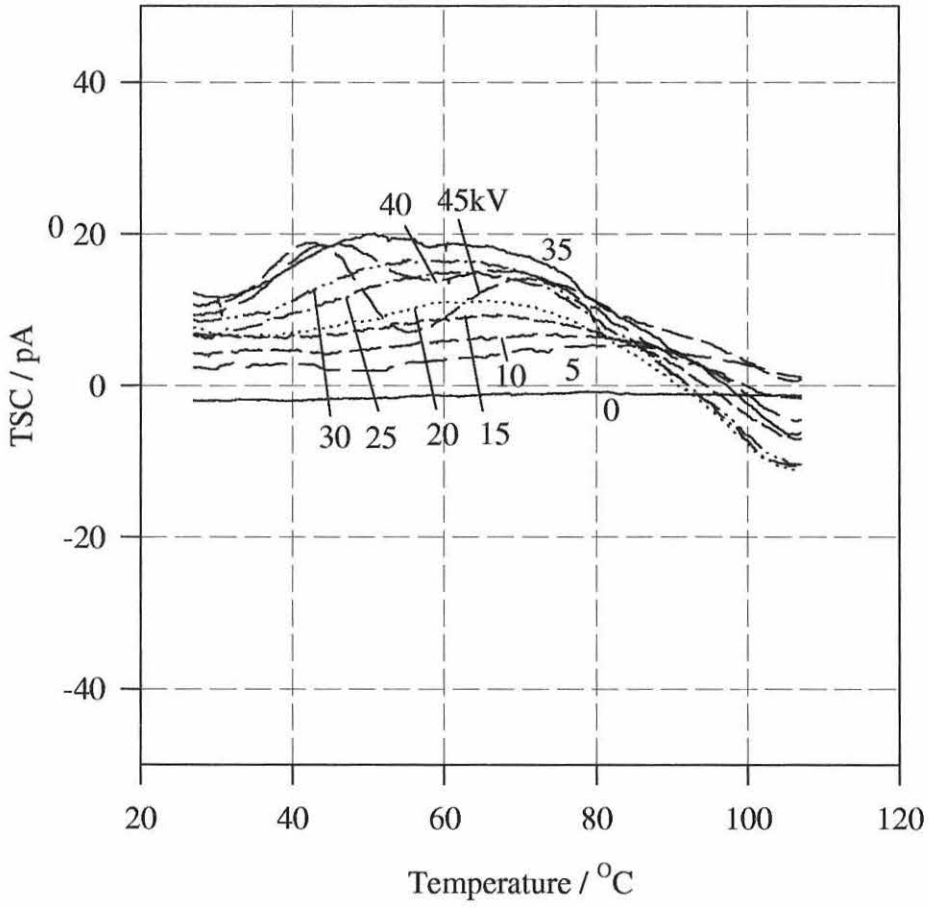

Figure 7.20. Procedure I measurements made on cable type 2Ba using negative polarity V_p. V_p are indicated.

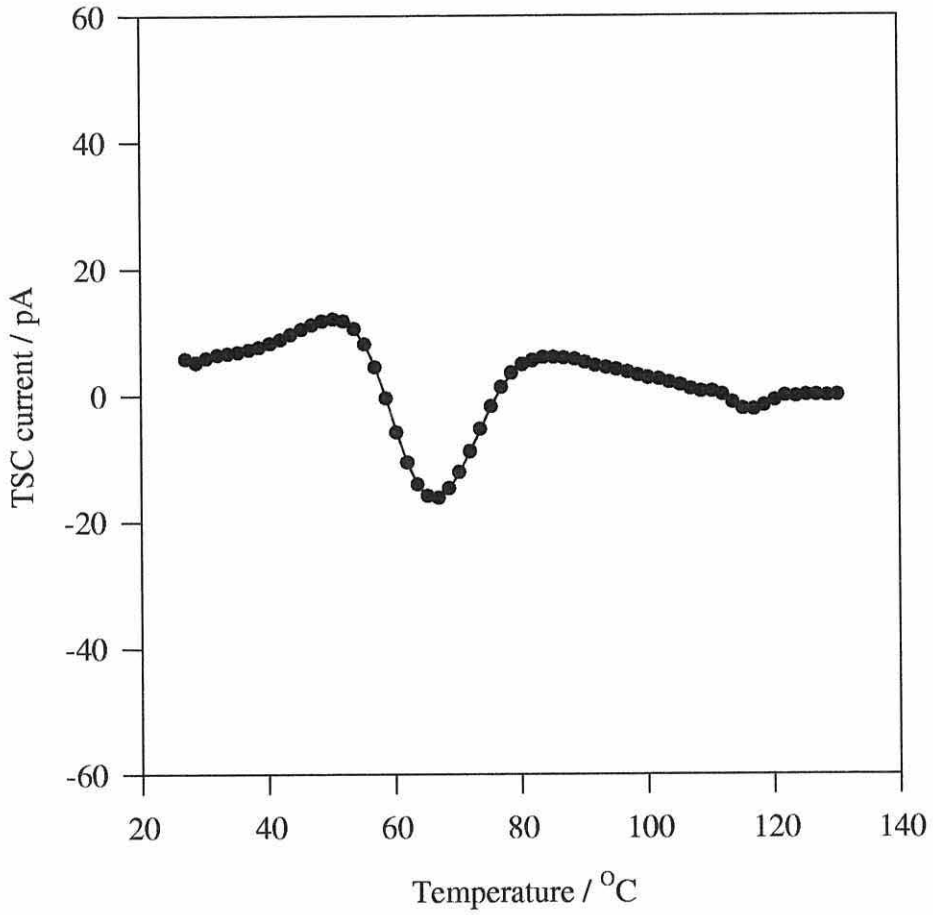

Figure 7.21. Final TSC measurement made on cable type 2Ba. $T_p = 107°C$, $T_{max} = 130°C$.

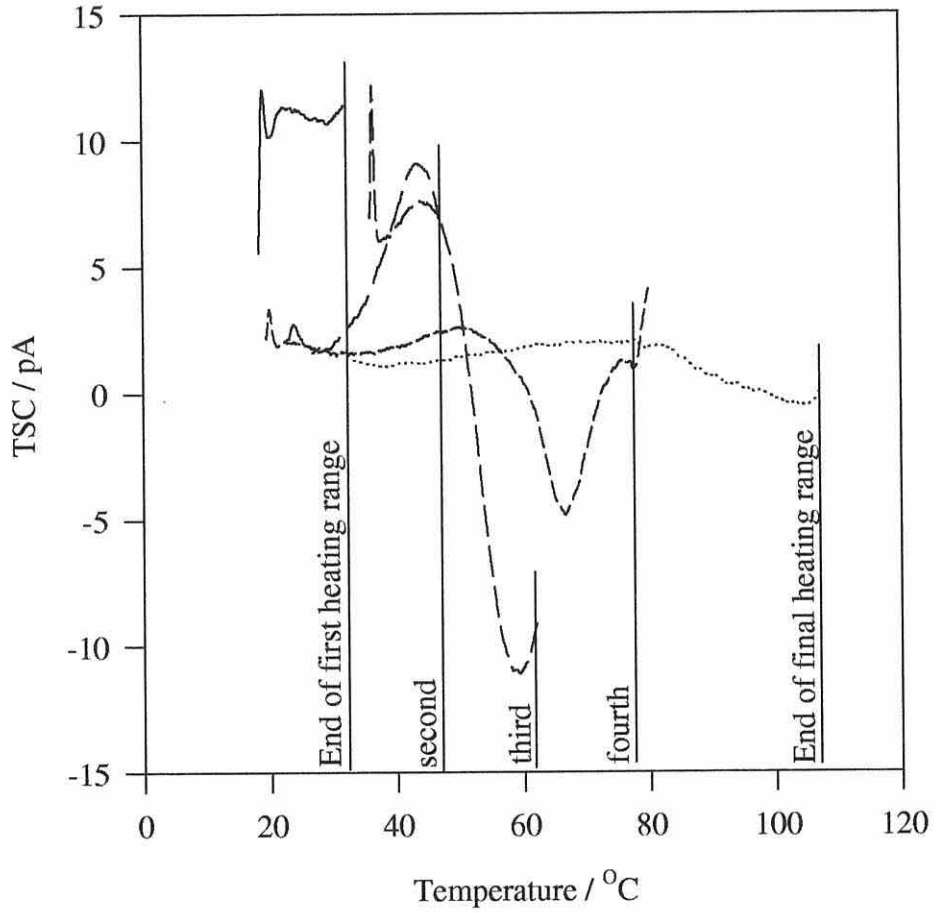

Figure 7.22. Partial heating TSC measurement on cable type 2Ba.

T_{max} was increased from the usual 107°C to 130°C, so that the peak suspected to exist above 107°C could be observed. However, this TSC measurement showed no further peaks above 107°C under these poling conditions.

Following the Procedure I and Procedure II (§7.5.4) measurements made on sample type 2Ba, investigations into the feature appearing at $\sim$ 55°C were performed. It was uncertain whether the "trough" seen at this temperature was indeed a trough, or was actually a peak of opposite polarity charge. To test this, a modified Procedure I technique called "Partial Heating" was used. This involved poling and cooling the cable as before, but during the TSC measurement, the cable was only heated a part of the way to T_{max} before being cooled again. This allowed the relaxation of the easily-activated charge, while leaving the deeper-trapped charge poled. The technique is also known as "Peak Cleaning", as the lower temperature peaks are cleaned out to allow other peaks to be observed more readily.

After performing several partial heating steps on cable type 2Ba, the partial heating TSC in figure 7.22 was obtained, which allowed the true nature of the "trough" to be revealed as a negative charge peak. This has important consequences for the analysis and interpretation of the TSC measurements, and will be discussed fully in chapter 9.

7.5 Procedure II Measurements

The experimental procedure known as Procedure II has previously been described in chapter 6. It is important to notice that during Procedure II the samples are poled with a voltage V_p at a single temperature T_p for a fixed poling period t_p, after which V_p is removed *before* allowing the sample to cool to room temperature (circa 17°C). This procedure permits a 'window' of polarisation, such that space charge (unipolar and dipolar) with a small range of activation energies are polarised. As suggested by Hobdell *et al* [61], poling in this manner prevents activated processes below a certain energy depth from being polarised during t_p, as the space charge will possess too much energy to remain in the polarised state. It should be noted that $V_p = -45\text{kV}$ for all of the results presented in this section, unless otherwise stated.

7.5.1 Cable Type 1Aa

The Procedure II TSC measured in cable type 1Aa are shown in figure 7.23. It can be seen that an $I_{\text{peak}} = 55\text{pA}$ occurs at $T \sim 65°\text{C}$ after poling at $T_p \sim 47°\text{C}$. The current at $T \sim 100°\text{C}$ appears to vary little with T_p. The TSC response can be considered to originate from a single process, and hence values of the symmetry factor μ_g (section 4.3.1) can realistically be considered. μ_g can be determined best from the $T_p = 47°\text{C}$ peak, giving a value of $\mu_g = 0.54$, a value which is equivalent to that for a process obeying second order kinetics. This will be discussed further in chapter 9.

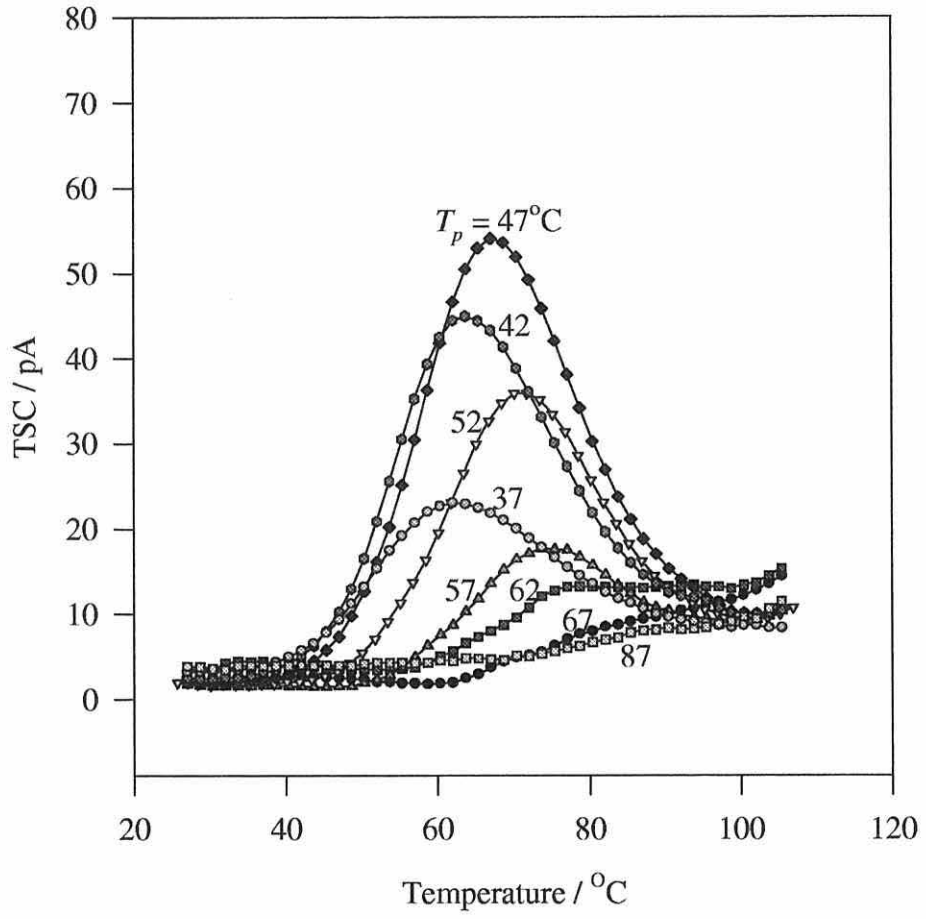

Figure 7.23. Procedure II measurements made on type 1Aa. T_p are indicated, t_p is 2 hours.

7.5.2 Cable Type 1Ab

The procedure II TSC for cable type 1Ab are shown in figure 7.24. This cable type exhibits a large peak at $T \sim 65°C$ that is similar to that seen in type 1Aa, but with a smaller I_{peak} of $\sim$ 75pA. Again, the peak is best reproduced by poling at $T_p = 47°C$, but the magnitude of the peak when $T_p = 42°C$ compared to $T_p = 53°C$ suggests that the optimum T_p for the largest peak would be nearer to 45°C. There is also a minor peak at $T \sim 100°C$ which is present for most of the higher T_p measurements. However, this minor peak is absent when $T_p = 37°C$.

A realistic value of the symmetry factor, μ_g, for this series of TSC curves cannot be obtained due to the presence of the 100°C peak. However, qualitative observation shows the main peak at 65°C to be too broad to be of first order kinetics. This broadness suggests a range of trapping levels or activated processes as per the models described previously in chapter 3, and hence a non-first order space charge kinetic.

7.5.3 Cable Type 1Ba

The Procedure II measurements obtained from cable type 1Ba, figure 7.25 are very different from those for types 1Aa and 1Ab. At the high T_p of 87°C, there is a broad peak which appears to reach a maximum value at a temperature > 100°C and beyond the range used here. For values of T_p between 27 and 47°C, there are two peaks. As noted on several previous occasions, the feature seen here is most likely a small negative polarity peak superposed upon a larger positive polarity

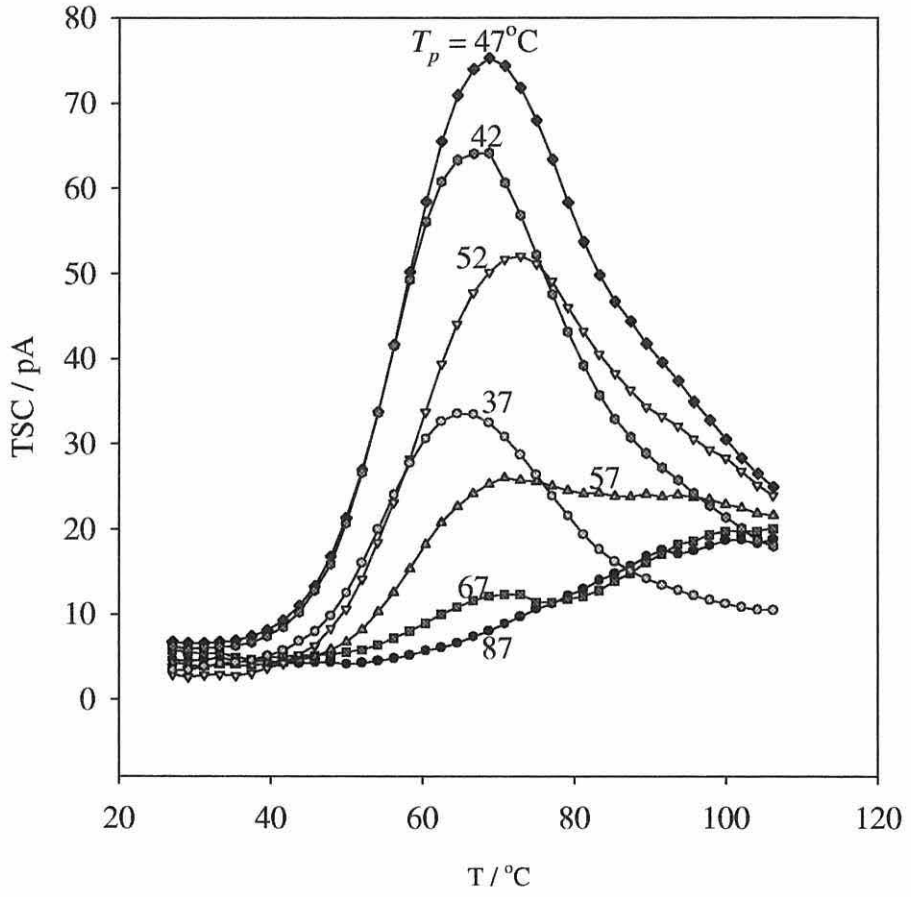

Figure 7.24. Procedure II measurements made on type 1Ab. T_p are indicated, t_p is 2 hours.

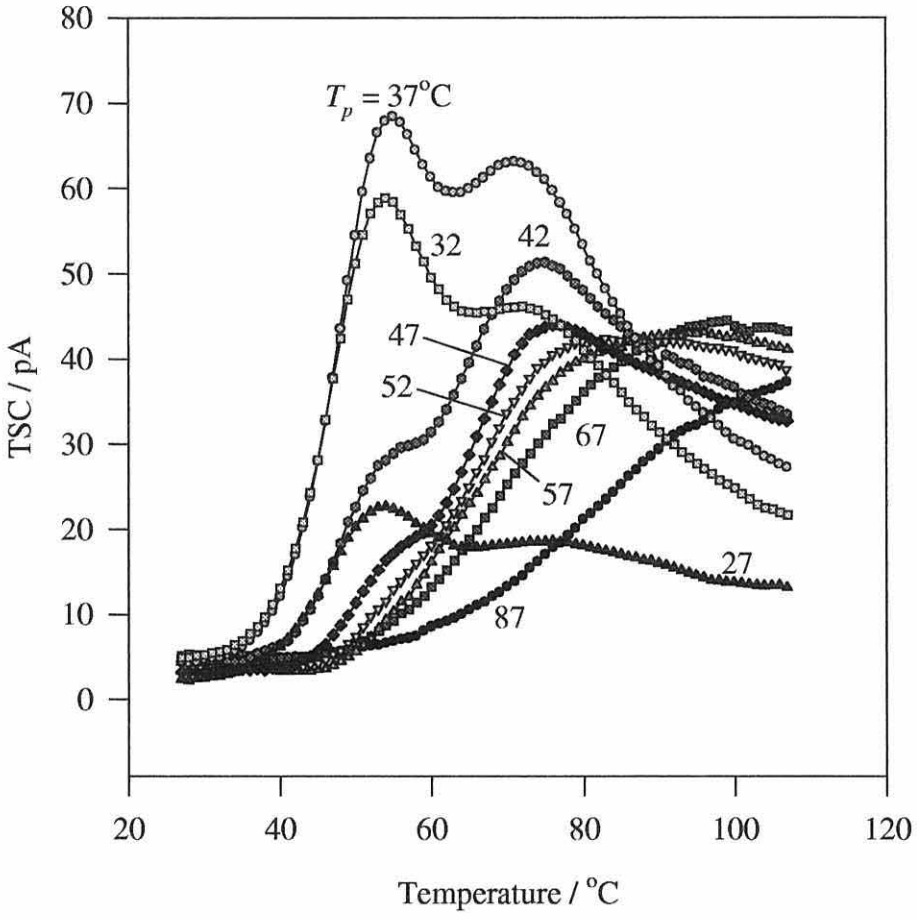

Figure 7.25. Procedure II measurements made on type 1Ba. T_p are indicated, t_p is 2 hours.

peak (section 7.4.4). It is obvious that a value of μ_g cannot be obtained from these curves due to the complex nature of the peaks.

7.5.4 Cable Type 2Ba

The procedure II measurements performed on 2Ba are plotted in figure 7.26. They show an interesting progression as T_p changes. The most notable feature of these TSC curves are their very low magnitudes. The $T_p = 27°C$ TSC is featureless and flat. Conversely, the $T_p = 47°C$ measurement exhibits the same negative polarity peak superposed on a broad positive peak as that seen in the procedure II measurements for 1Ba above. It will be argued in Chapter 9 that this negative peak is characteristic of semicon Ba.

The TSC at $T_p = 67°C$ and $87°C$ exhibit a broad peak at $T \sim 90°C$, a peak that is somewhat similar to that observed in the TSC of 1Ba at these temperatures.

7.5.5 Cable Type 3Ab

The first procedure II measurements made were performed on cable type 3Ab. The poling time t_p was only 1 hour, half of the time used for the procedure II measurements on other cable types. Despite this difference, qualitative observations can still be made of the type 3Ab results.

Figure 7.27 shows the TSC measurements using procedure II on cable type 3Ab. The TSC for $T_p = 27°C$ is characterised by a very low current magnitude. This is as expected: the temperature is not high enough to allow charge to be

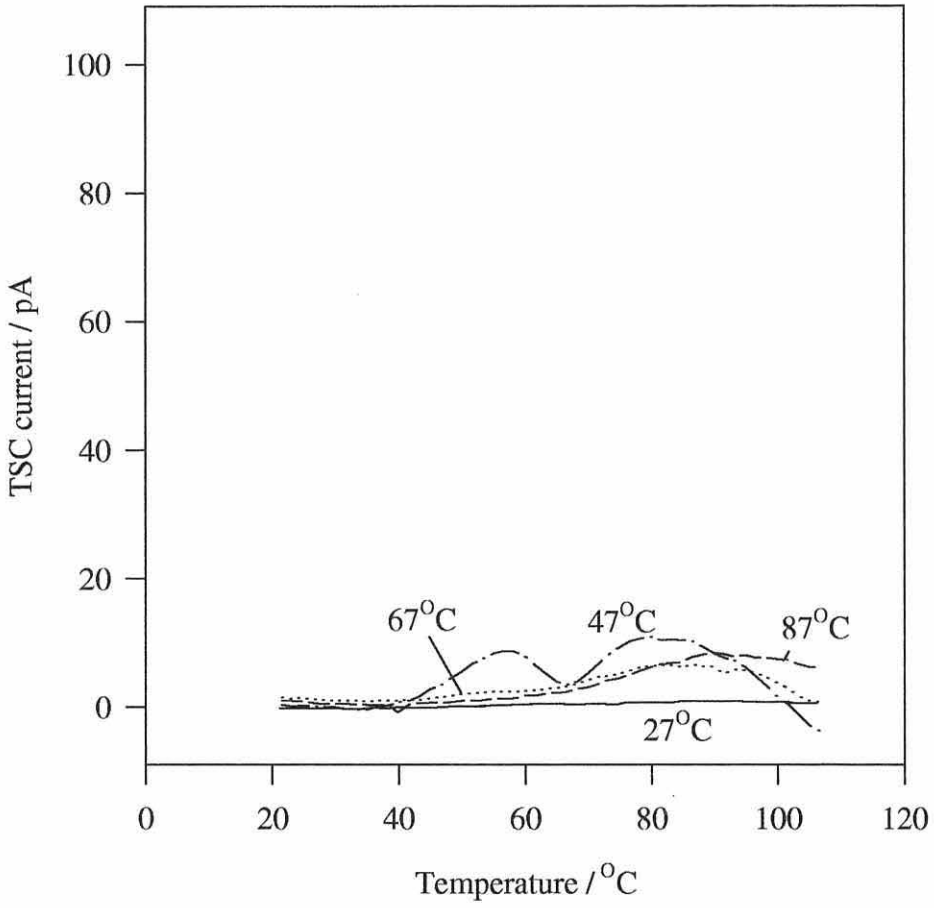

Figure 7.26. Procedure II TSC measurements made on cable type 2Ba.

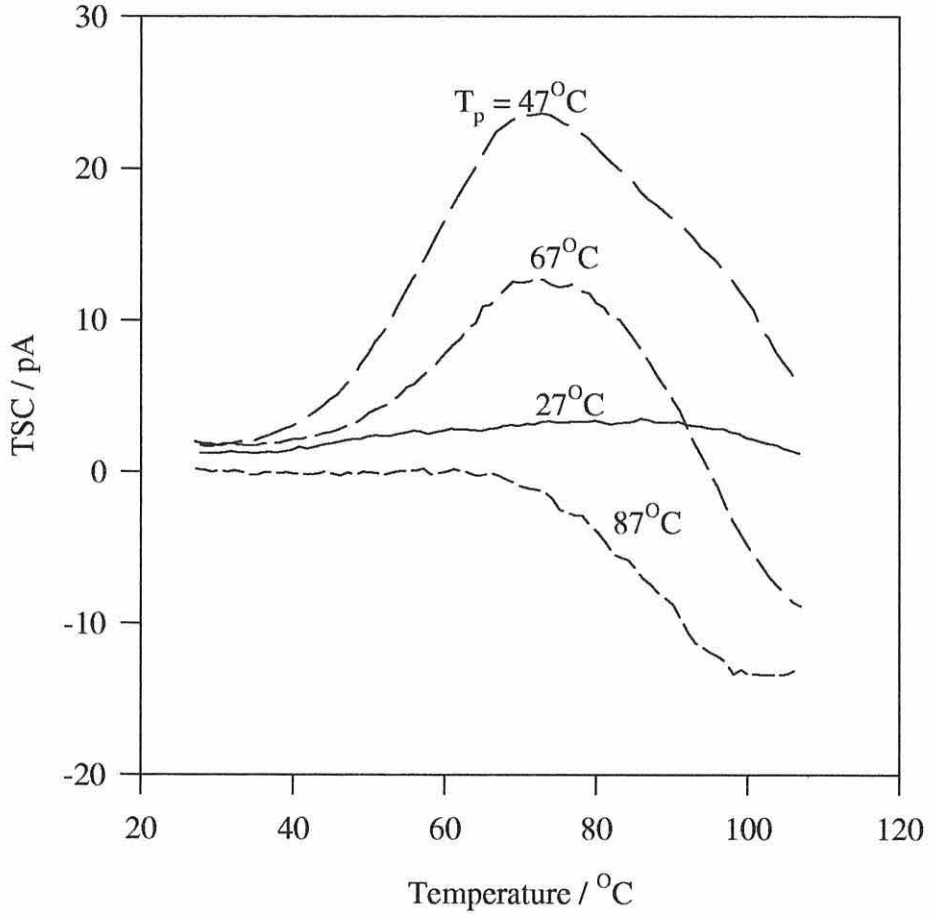

Figure 7.27. Procedure II measurements made on type 3Ab. T_p are indicated, t_p is 1 hour.

energetically injected into the XLPE, and any polarisation would relax as soon as the poling voltage is removed. This point will be discussed in chapter 9. As T_p increases to 47°C, a curve is obtained that is similar in shape to that for type 1Ab at this same T_p: a curve with a main peak centred at $\sim$ 70°C with a minor peak appearing on the high temperature side of the main peak at $T \sim$ 100°C. However, as T_p increases to 67°C, a negative peak appears in the high temperature region which reaches T_{peak} above 107°C. As T_p increases further to 87°C, the low temperature positive peak at $t \sim$ 70°C disappears completely and a high temperature negative peak at $T_{\text{peak}} \sim$ 104°C now dominates the curve.

The magnitudes of these TSC are similar to those seen for 2Ba in figure 7.26, although the poling time t_p employed during these measurements was significantly shorter than those of 2Ba. This suggests that the TSC of 3Ab would be larger if t_p had been longer.

Chapter 8

The Electrokinetic Effect

It is understood that poling, as in the TSC procedure, will leave a cable sample with some degree of persistent polarisation and/or space charge, which is then released in the TSC experiment. Space charge in particular will leave the cable sample with an internal electric field, the presence of which might be detectable using a novel measurement technique, which has been called the electrokinetic method [62]. Space charge detected in this way could then be correlated with the TSC measurements.

8.1 The Electrokinetic Measurement Technique

In principle, the electrokinetic (EK) measurement technique is very simple. Application of a steady bias voltage, V_b, together with a small alternating signal v, where

$$v = v_o \sin(\omega t) \tag{8.1}$$

has been shown to induce measurable mechanical displacements in a range of materials [62, 63].

Application of the combined signal $V_b + v$ induces displacements in the sample with components at zero frequency, at the fundamental frequency ω and at the second harmonic 2ω, such that the displacement at a given point is given by:

$$D = C.V_b^2 + A.V_b v \sin(\omega t) + B.v^2 \sin(2\omega t). \tag{8.2}$$

It can be seen from equation 8.2 that the fundamental component of D is proportional to both V_b and v, and that the second harmonic is proportional to v^2 alone.

The displacements D_ω and $D_{2\omega}$ of a point on the surface of a coaxial model cable sample at frequencies ω and 2ω, respectively, can be measured using a Michelson interferometer, as shown schematically in figure 8.1. The coherent light beam from the Helium-Neon (HeNe) laser, with a wavelength $\lambda = 632.8$nm, is split into two by a beam splitter and travels to two mirrors, one of which is attached to the sample surface and the other is servo driven. The two beams are then reflected back and produce an interference pattern in the region of the photo-diode, which then converts the light level to a voltage V. The two light paths are approximately the same length. If the sample mirror is kept stationary but the servo mirror is displaced by an amount x, then a change in the interference pattern will be detected by the photo-diode (figure 8.2). If the servo mirror is displaced by a distance $x = \frac{\lambda}{2}$ then the interference pattern is displaced by exactly one "fringe", as indicated in figure 8.2. Constructive interference of the light causes a voltage V at the diode to reach a maximum value of V_0, while destructive interference causes a minimum $-V_0$. The voltage generated at the photo-diode as a function

of mirror displacement is

$$V = V_0 . \sin\left(\frac{2\pi}{\frac{\lambda}{2}}.x\right) \tag{8.3}$$

and its differential is

$$\frac{dV}{dx} = V_0 . \frac{2\pi}{\frac{\lambda}{2}} \cos\left(\frac{2\pi}{\frac{\lambda}{2}}.x\right). \tag{8.4}$$

The maximum sensitivity of the interferometer occurs at the crossover points, i.e., at the maximum of dV/dx, and has a value

$$|\frac{dV}{dx}|_{max} = \frac{4\pi V_0}{\lambda} \text{ when } \frac{4\pi x}{\lambda} = 0, \pi, 2\pi \ldots, \tag{8.5}$$

Measurements of displacement are therefore made at the crossover points, where a sufficiently small change in displacement Δx produces a corresponding linear change in the photo-diode voltage ΔV:

$$\Delta x = \frac{\lambda}{4\pi V_0}.\Delta V = \frac{\lambda}{2\pi}.\frac{1}{2V_0}.\Delta V \tag{8.6}$$

$$\simeq 101 . \frac{\Delta V}{2V_0} \text{ nm.} \tag{8.7}$$

The servo mirror only responds to noise at a frequency less than ω, so that any signal measured at a frequency of ω or 2ω can be attributed to movement at the surface of the cable sample mirror. The lock-in amplifier (figure 8.1) is used to measure the amplitude of the components of the signal at the fundamental frequency ω and the second harmonic 2ω. These voltage amplitudes can then be converted into displacements using equation 8.7. The sensitivity of the interferometer enables sample displacements in the picometre range to be measured at the frequencies ω and 2ω. Note that the static displacement at zero frequency ($C.V_b^2$) cannot be detected by the interferometer.

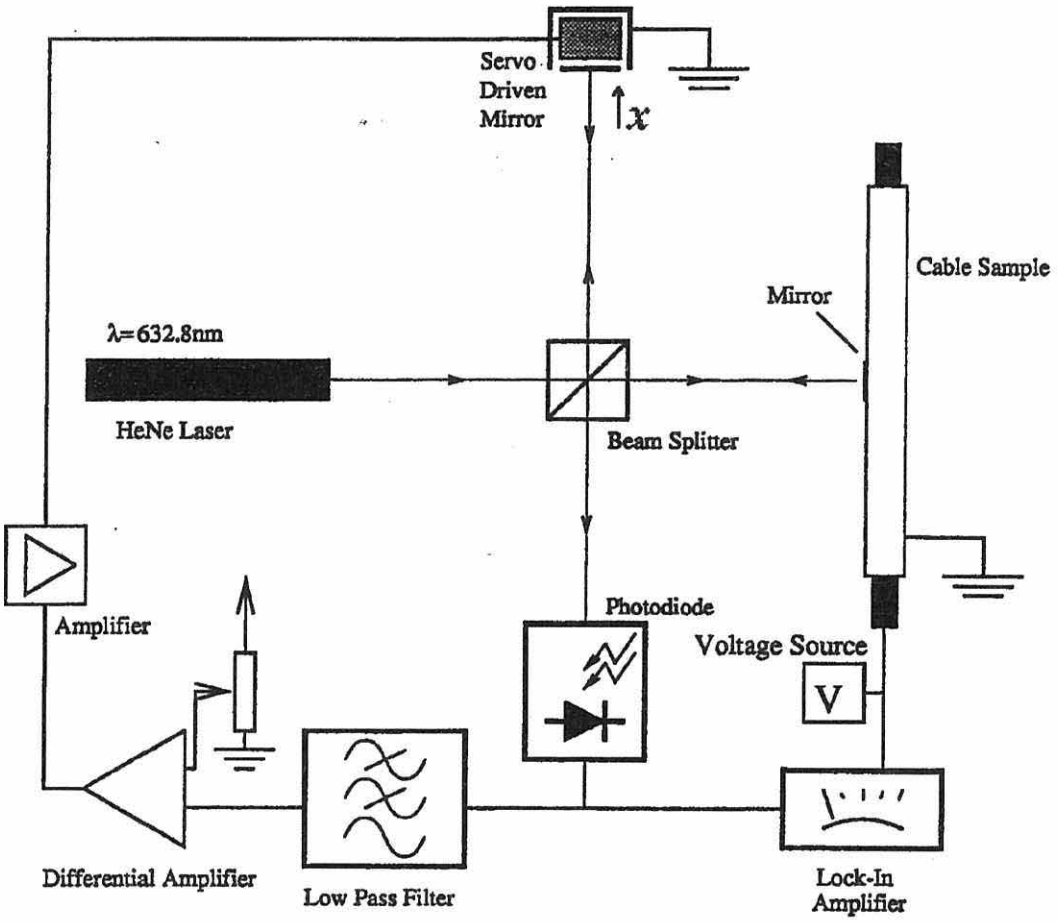

Figure 8.1. Schematic diagram of the Michelson interferometer used to measure picometer displacements in model cable samples.

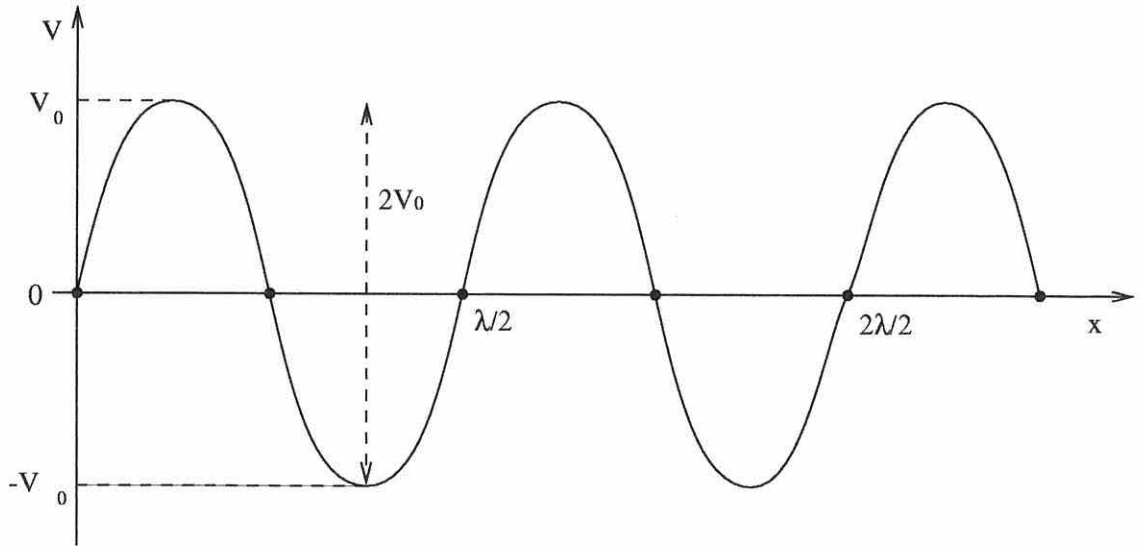

Figure 8.2. The variation of the photo-diode output voltage V with the position x of the sample mirror.

The next step taken, which was novel, was to consider that quasi-static space charge induced in a sample as a result of poling would generate a field equivalent to that which would be produced by external application of a steady bias voltage V_b. It was then argued that in this case, the displacements D_ω and $D_{2\omega}$ would still be measured when only an alternating signal v was applied to the sample.

The gradient dD_ω/dv was expected to be constant and equal to $A.V_b$ and therefore directly related to the space charge present within the sample. On the other hand, $D_{2\omega}$ would be independent of space charge. $D_{2\omega}$ could then be expected to follow a square-law dependency on v and be characteristic of the cable type. Observations made during preliminary measurements showed $D_{2\omega}$ was not independent of space charge, however. The theoretical model was then reappraised [64] to accommodate space charge induced variations in $D_{2\omega}$. As a consequence, it was now no longer possible to simply characterise a cable type by the $D_{2\omega}$ measurement, as $D_{2\omega}$ would change due to space charge in a similar manner to D_ω.

A number of difficulties with the experimental apparatus prevented a full and extensive investigation from being made of the EK effect in model cable samples. However, some results have been obtained that are nevertheless interesting.

8.2 EK Measurements

EK measurements were made as follows.

A small mirror of approximately 2mm in diameter was mounted on a cable

sample as one arm of the Michelson interferometer (figure 8.1). An alternating voltage V was then applied to the inner conductor of the sample at a frequency, $f = 220$Hz, where

$$f = \frac{\omega}{2\pi}. \tag{8.8}$$

As erratic displacements were often recorded during the first 30s of measurement, the lock-in amplifier voltage reading was permitted to settle before several measurements were recorded at one second intervals over a period of between 30 and 60 seconds. The lock-in amplifier was then switched to monitor the second harmonic, $2f$, of 440Hz, while v remained at 220Hz. Again, the equipment was allowed to settle before several measurements were recorded. The voltage measurements were later converted to picometer displacements using the conversion equation 8.7.

The alternating voltage v was increased in 1kV steps from 0 to 10kV, and then reduced in 1kV steps back down to 0kV. Measurements of D_f and D_{2f} were made at each value of v.

Measurements were made on cable samples 1Aa/3, 1Ab/3 and 1Ba/3, after they had previously been used for the TSC measurements reported in chapter 7. As such, the samples had all experienced similar poling, discharge and thermal cycles. The samples were not polarised prior to the EK measurements. The measurements reported here were performed on the samples directly after the TSC measurements were made. The EK responses are therefore due to residual space charge within the samples, most likely permanent dipoles and charge at semicon-insulation and at crystalline-amorphous interfaces. They can also be interpreted

as resulting from the composition of the cable samples after annealing.

As only one of each cable type has been investigated, the samples will only be referred to by the cable type in the following text, not by the individual sample number.

8.3 Results

Typical EK responses for type 1Aa are shown in figure 8.3a-c. The measurements were repeated, such that the voltage v was raised from 0kV up-to 10kV and then down to 0kV in 1kV steps for each measured EK response. Three sets of EK data were recorded in this way.

Although the graphed data is useful for obtaining a "feel" for the response of a cable sample, more indicative results can be obtained by performing regression and curve fitting analyses of the data. As noted above, the f data varies linearly with v while the $2f$ data has a square-law dependency on v. So if the f data can be fitted with both linear regression and curve fitting techniques using

$$D_{1f} = m_{1f}v + c. \tag{8.9}$$

It should be noted here that linear regression and curve fitting are essentially the same measurements. However, the software package used to fit the curves approaches the two methods slightly differently, i.e., the curve fitting method can be customised more fully by the operator than linear regression technique. For this reason, then, using both methods permits an extra verification route for the analyses. Additionally, the curve fitting technique provides comprehensive error

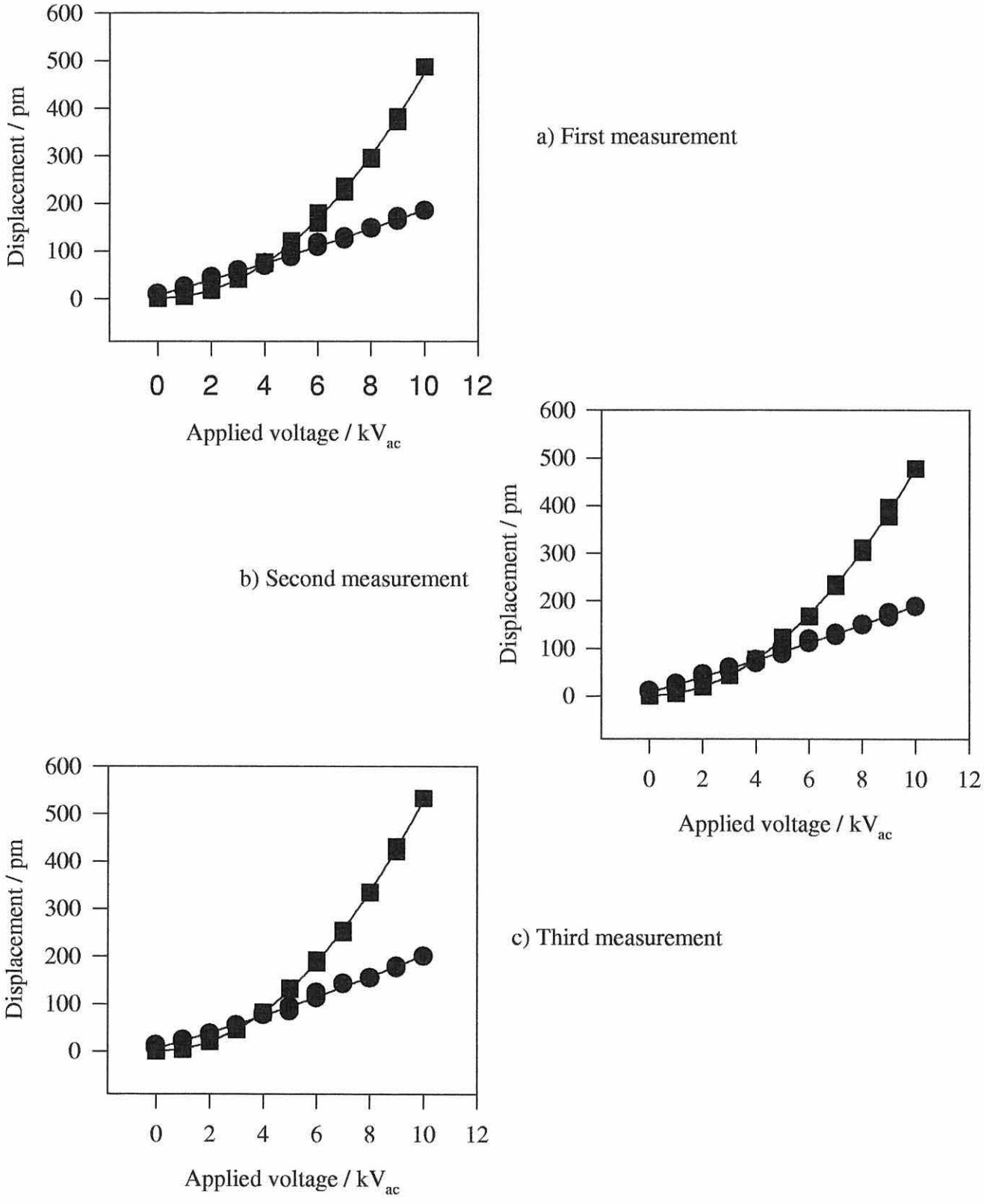

Figure 8.3. EK measurements performed on cable type 1Aa. ●: D_f; ■ : D_{2f}.

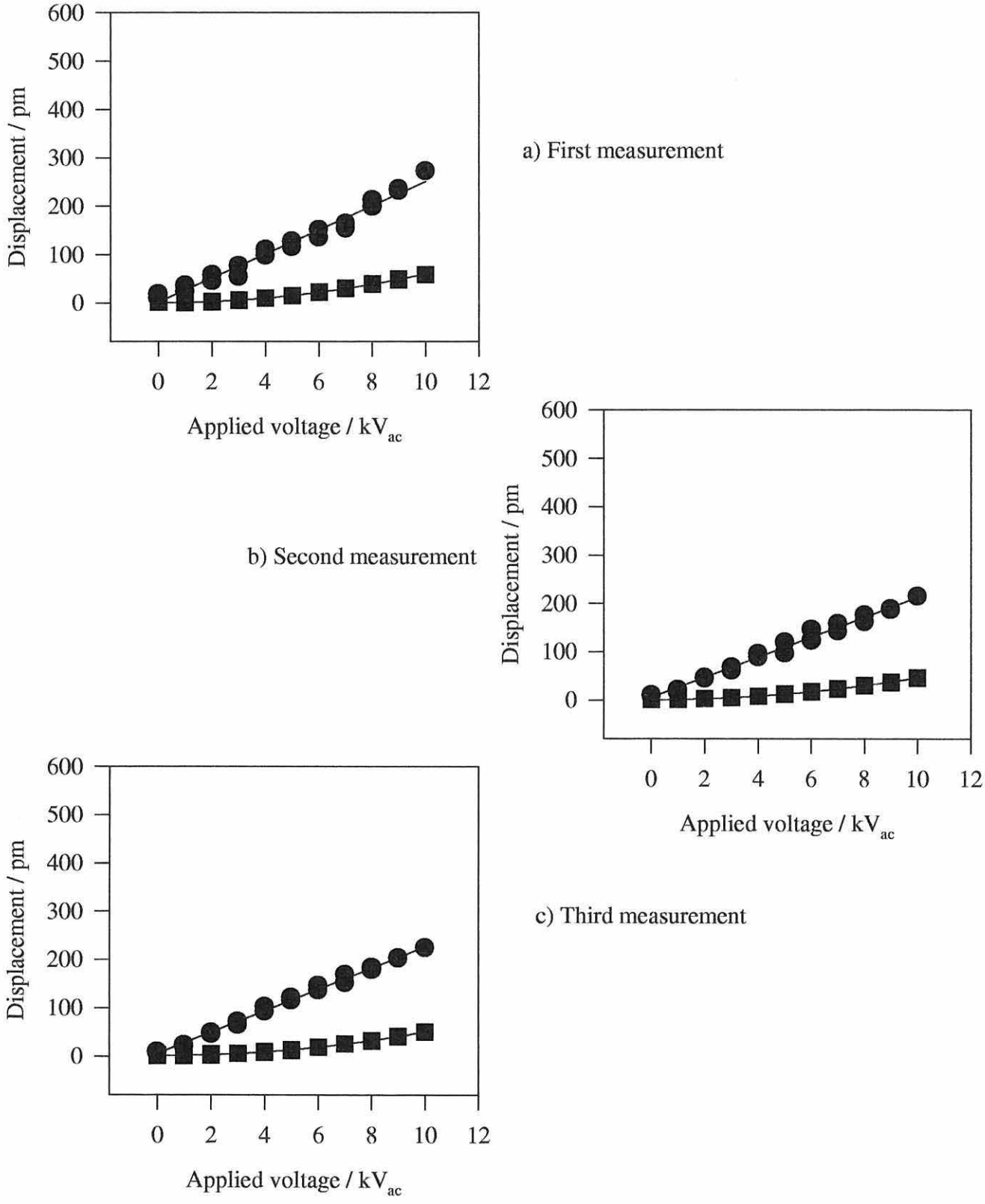

Figure 8.4. EK measurements performed on cable type 1Ab. ●: D_f; ■ : D_{2f}.

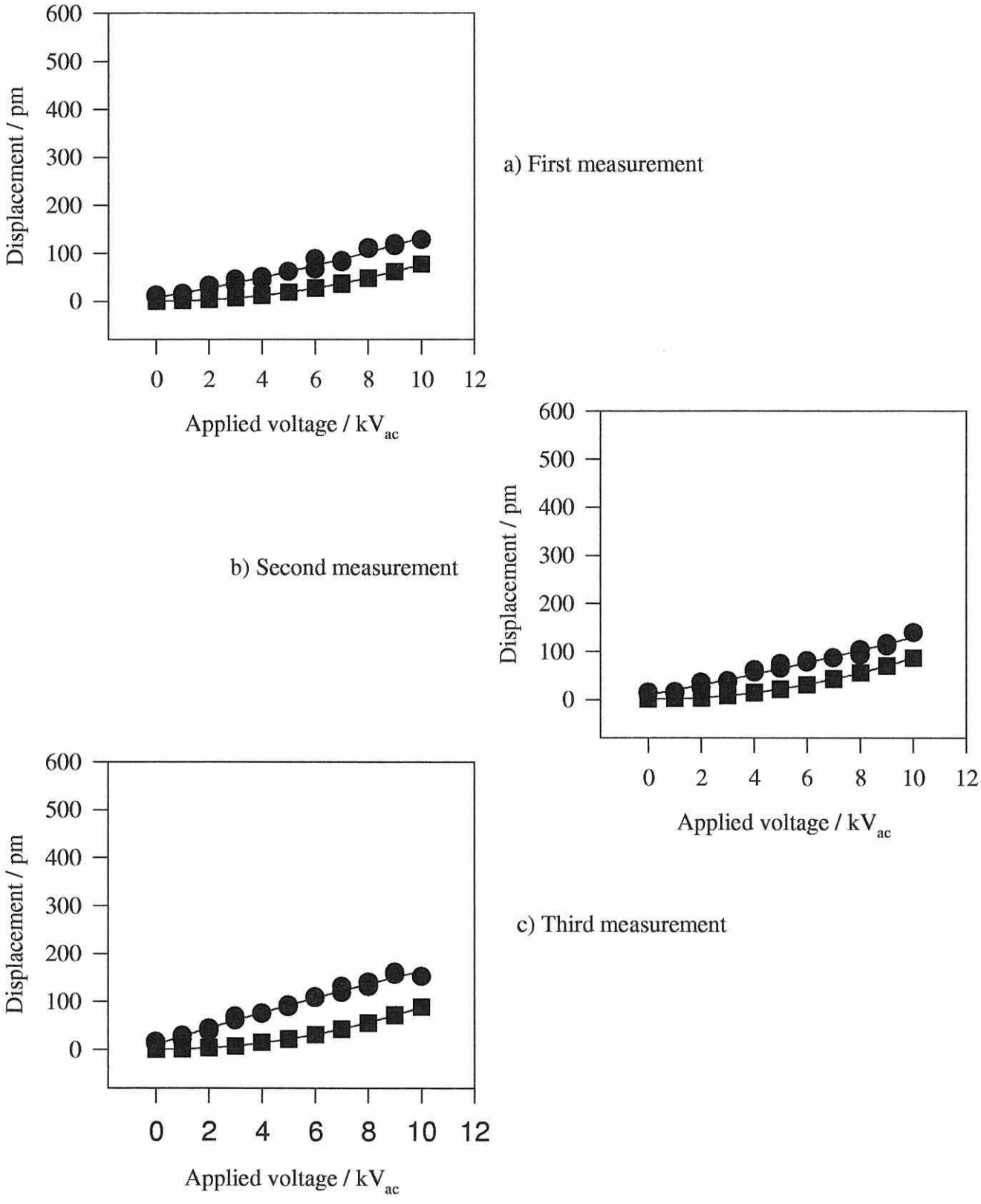

Figure 8.5. EK measurements performed on cable type 1Ba. ●: D_f; ■ : D_{2f}.

analysis functions, while the linear regression provides a regression coefficient which directly relates to goodness of fit.

The $2f$ data can be fitted using a curve fitting algorithm of

$$D_{2f} = m_{2f}v^2 + c \tag{8.10}$$

or a square-law regression of

$$D_{2f} = m_{2f}v^2 + nv + c. \tag{8.11}$$

The results of the data analysis are shown in tables 1 and 2. r^2 in table 1 is the regression analysis confidence parameter. The error in the curve fitting parameters are variable: c typically has a large error of between 40% and several 100%. Conversely, m_{1f} and m_{2f} have a very low error of only 1 or 2%. This indicates that the curve shape can be fitted accurately, but determination of the initial ($v = 0$) offset value is difficult. It would be desirable to determine the value of the displacement D at $v = 0$, as this would then directly relate to the space charge in a sample.

The shape parameters, m_{1f} and m_{2f}, are the parameters of most interest here. The values of m_{1f} determined by both analytical techniques for D_{1f} are similar, indicating the usefulness of either technique.

The variation in the analysis parameters derived from the D_{2f} data is not unexpected, as the fitting equations for each technique (equations 8.10 and 8.11) are slightly different. Despite this difference, m_{2f} is surprisingly similar for both techniques, indicating that the linear parameter n is not significant.

Sample	Repetition	D_{1f}			D_{2f}			
		c	m_{1f}	$r^2/\%$	c	n	m_{2f}	$r^2/\%$
1Aa	1	4.4	17.8	99	2.682	-2.006	4.915	100
1Aa	2	4.5	18.2	99	1.483	-0.336	4.799	100
1Aa	3	0.4	19.5	99	1.345	-1.402	5.414	100
1Ab	1	2.0	25.0	98	0.800	0.024	0.590	100
1Ab	2	4.9	20.8	99	0.674	0.077	0.452	100
1Ab	3	5.0	22.2	99	2.332	0.059	0.493	100
1Ba	1	3.5	12.3	97	0.87	-0.28	0.79	100
1Ba	2	6.7	12.0	97	1.04	-0.27	0.89	100
1Ba	3	13.5	15.4	99	1.32	-0.47	0.92	100

Table 8.1. Linear regression results from analysis of the EK data from the given sample measurements.

Sample	Repetition	D_{1f}		D_{2f}	
		c	m_{1f}	c	m_{2f}
1Aa	1	4.4	17.8	-0.7	4.7
1Aa	2	4.5	18.2	0.9	4.8
1Aa	3	0.4	19.5	-1.0	5.3
	Error	$> 18\%$	$< 4\%$	$> 30\%$	$< 1\%$
1Ab	1	2.0	25.0	0.8	0.6
1Ab	2	4.9	20.8	0.8	0.5
1Ab	3	5.0	22.2	1.3	0.5
	Error	$> 60\%$	$< 5\%$	$> 16\%$	$< 1\%$
1Ba	1	3.5	12.3	0.4	0.8
1Ba	2	6.7	12.0	0.6	0.9
1Ba	3	13.5	15.4	0.5	0.9
	Error	$> 40\%$	$< 2\%$	$> 100\%$	$< 1\%$

Table 8.2. Curve fitting results from analysis of the EK data from the given sample measurements.

8.4 Consistency of m

8.4.1 Cable Type 1Aa

When the EK measurements were repeated on cable type 1Aa, values of both m_{1f} and m_{2f} increased (tables 8.1 and 8.2). As the voltage v used during the measurement was relatively low, it is expected that the change in EK response resulted from migration of space charge — and hence, a change in the electrical field — within the sample, and not from injection of further space charge.

A noteworthy feature of the EK response (figure 8.3) is that the D_{2f} measurements at $v = 10$kV are approximately three times larger than D_{1f} at this v. This will be discussed in chapter 9.

8.4.2 Cable Type 1Ab

The EK measurements made on cable type 1Ab (figure 8.4) showed no definite trend in their m-parameters. This suggests that the charge within the sample is very mobile, and the space-charge-induced electric field distributions return to an equilibrium one in a short period of time after perturbation by the voltage v. Despite the EK response originating from the presence of a field arising from persistent DC charges within the sample, the high mobility of the charge suggests that this charge may be a different type to the long-term charge released during the TSC measurements.

As can be seen in tables 8.1 and 8.2, type 1Ab has the largest values of m_{1f},

but the smallest values of m_{2f}. This is notable in the discussion, when comparing the EK and TSC measurements.

8.4.3 Cable Type 1Ba

EK displacements measured in 1Ba (figure 8.5) at first glance appear to increase in magnitude from the first to third measurement. Indeed, the error margins of the first two values of m_{1f} shown in table 8.1 overlap, suggesting no change in the internal field of the sample. The third m_{1f} shows a 25% increase for both analysis methods, although the final two measurements of m_{2f} using the curve fitting technique could be argued to be statistically identical, with a difference of only 0.02 between them.

8.4.4 Summary

There are clearly differences between the EK responses of the three types of cable and these will be discussed and correlated with the TSC responses in chapter 9.

8.5 The Effect of Poling

EK Measurements were also made on sample 1Aa/1 under different poling conditions. Initial EK measurements made after poling in the TSC apparatus failed to produce any identifiable change in the EK response, probably because that poling method allowed charge to migrate and the electric field, upon which a good EK measurement depends, would have reached equilibrium. The aim was to create

poled and unpoled states which were significantly different, and the field would be in different states approaching the equilibrium charge distribution and field. To this end, the samples were heated *in-situ* in the EK apparatus.

Figure 8.6, plot 1, shows measurements after 1Aa/1 had been maintained at a temperature of $T \sim 50°C$ for 48 hours and subsequently cooled to room temperature while electrically shorted. This was done with the intention of removing all space charge from the sample. Measurements were made for voltages v up to $5kV_{ac}$ and not $10kV_{ac}$ as in the previously reported measurements. Even so, the responses for sample 1Aa/1 in figure 8.6, plot 1, are of similar magnitudes to those seen in figure 8.3 illustrating good correlation between samples of the same cable type.

Sample 1Aa/1 next was re-heated to $T \sim 50°C$ while short-circuited, to simulated the discharge measurement of a TSC procedure. The sample was poled at this temperature and $V_p = -45kV$ for a period of $2\frac{1}{2}$ hours and was then cooled to room temperature. The cable sample was then short-circuited while at room temperature for a period of 1 hour, again to simulate the TSC procedure, and another EK measurement was made. The results of this measurement (figure 8.6, plot 2) show a marked increase in dD_{1f}/dv — a three-fold increase in the magnitude of m_{1f} was observed, as confirmed from the linear regression analysis results (table 8.3). D_{2f} increased only slightly, indicating it's relative independence of space charge when compared to D_{1f}. This is a good result, indicating a response due to the presence of space charge in the sample.

The cable was then re-heated once more, with the intention of returning

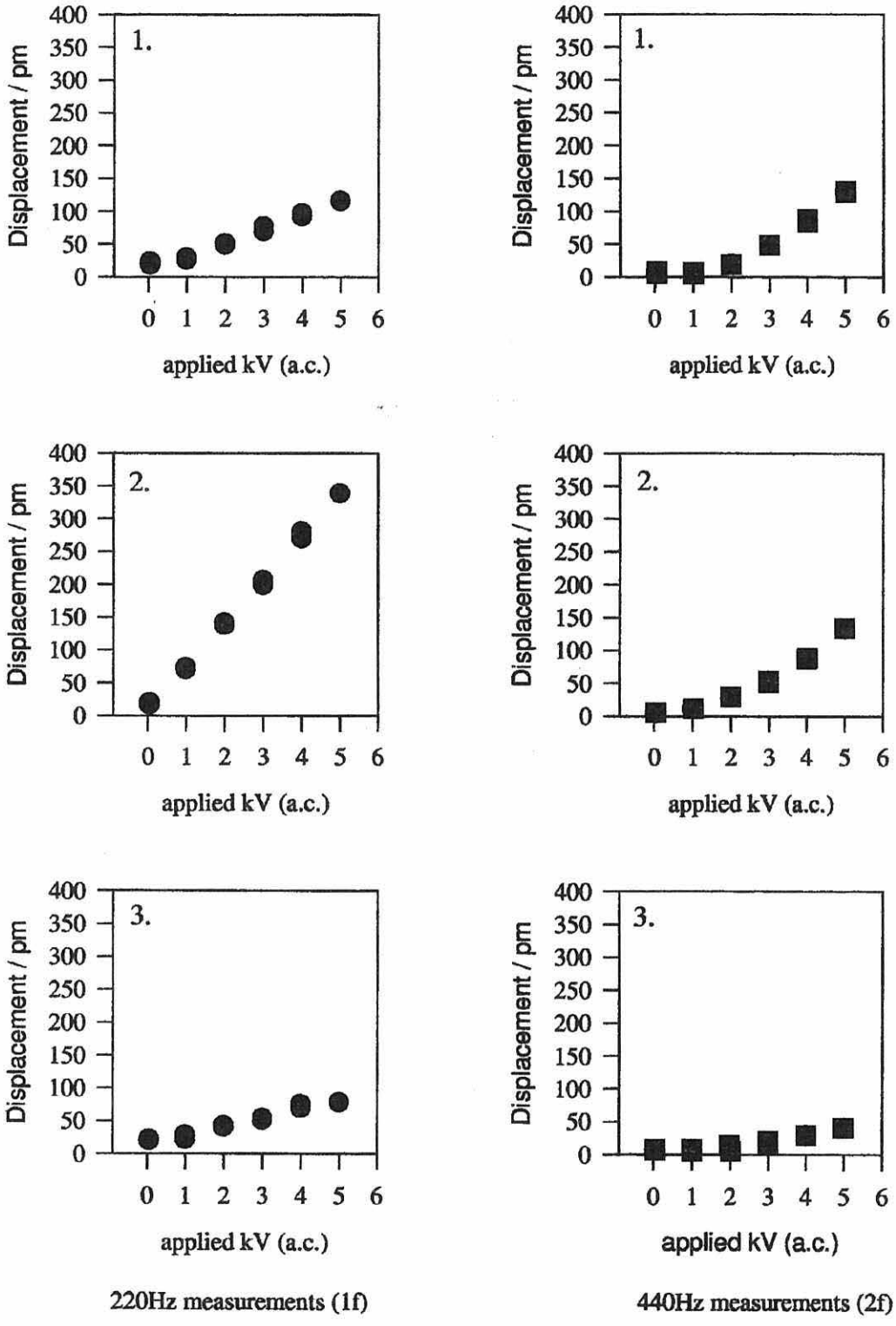

Figure 8.6. Measurements made after various poling stages on 1Aa/1. ●: D_{1f}; ■ : D_{2f}. the measurement number (1, 2 or 3) is indicated in the top-left of each plot.

1Aa/1 to the space charge state of the sample before the data in figure 8.6, plot 1 were obtained. The aim was to take the sample up to a temperature of $T \sim 100°C$, but the sample was erroneously heated to 130°C, in excess of the melting temperature of LDPE. This may have altered the morphology of the cable, although the previous thermal and electrical cycling performed during the TSC measurements should have fully annealed the sample already. Heating this high also has the effect of certainly removing any space charge in the sample. The sample was then cooled to room temperature and a third EK measurement was made (figure 8.6, graph 3). D_{1f}/dv had decreased significantly, indicating the removal of space charge. Linear regression analysis (table 8.3) showed m_{1f} to be lower for the third EK measurement than for the first. The coefficient m_{2f} of the D_{2f} measurement was also much reduced. This reduction in D_{2f} was interpreted as a morphological change in the sample, because D_{2f} depends on the mechanical modulus and dielectric constant of the cable insulation material.

As noted earlier in this chapter, D_{2f} was originally expected to be independent of space charge, and at first was assumed to be characteristic of the cable type. However, after the changes in D_{2f} reported above were observed, reappraisal of the EK theory showed that D_{2f} may also vary with space charge, and the D_{2f} measurement could no longer be interpreted as being cable-dependent.

The changes in D_{1f} and D_{2f} reported above indicate that there is a correlation between the poling condition of a cable and the measured EK response. However, the difficulties encountered while attempting to reproduce this effect suggest that the electric field, upon which D_{1f} depends, is not solely dependent

on the presence of space charge to produce a change in the EK effect. It would appear that the electric field distribution within the cable sample and, perhaps more importantly, at the semicon-insulation interface, has a greater influence over the results obtained with the EK measurement technique than the mere presence of space charge within the sample.

The results reported and the point raised above will be discussed further in chapter 9.

	D_{1f}			D_{2f}			
Plot Number	c	m_{1f}	$r^2/\%$	c	n_{2f}	m_{2f}	$r^2/\%$
1	13.9	19.9	98	5.3	-3.3	5.8	100
2	11.0	65.2	100	4.6	2.4	4.6	100
3	16.9	12.8	96	5.4	-0.9	1.6	100

Table 8.3. Linear regression analysis of data plotted in figure 8.6.

Chapter 9

Discussion

There are several interesting points that have arisen as a consequence of the TSC and EK measurements reported in chapters 7 and 8, respectively. In this chapter, these points will be discussed and consideration will be given to the main effects found in the various cable samples.

It is useful to recall the three main mechanisms involved in TSC, those of dipolar relaxation, the relaxation of displaced intrinsic space charge and the migration and relaxation of injected space charge. The injection of space charge has been reported [12] to occur mainly at electric fields that are much greater than the average macroscopic fields used in the present work. However, as noted in chapters 3 and 5, the roughness of the semicon-insulation interface may be sufficient to promote some space charge injection below this well-defined threshold level, perhaps providing an explanation of the effects found as $|V_p|$ approaches 45kV.

This leaves the other two mechanisms of dipole and intrinsic space charge relaxations to dominate the low $|V_p|$ measurements, where peaks in the TSC

arise due to charge effects at both the semicon-insulation and the morphological crystalline-amorphous interfaces.

The effects observed during the present work have had many different origins, e.g., semicon carbon, semicon base resin, thermal cycling, voltage cycling. An effort has been made to discuss each of these individually, but there is necessarily some overlap which, the author hopes, will neither confuse nor obscure the importance of the effects themselves.

The main concern of any experimental work is reproducibility of the results. Reproducibility of TSC results is possibly more difficult to define, given that the mere act of performing a TSC measurement will leave a sample in a different state. If the exact same measurement sequence is repeated on the same cable sample at the same poling voltage, then the TSC will change from one measurement to the next. Consequently the total time-integrated charge will change. Examples are the repeated TSC cycle measurements of 1Aa/1 (figures 7.7 and 7.8), and the TSC measurements of 2Ba performed at different times during the experimental programme (figures 7.20 and 7.21). By contrast, features of the TSC, such as peak temperature T_{peak}, will remain the same on repetition of TSC at a given poling voltage on a given sample, as shown in the aforementioned figures. Additionally, performing the same TSC measurement series by starting on a fresh sample will produce the same TSC at the same measurement in the series as on another similar sample. Deviation from the measurement series will necessarily introduce a deviation from the repeatability of the measurement series. The measurement is therefore repeatable as long as the measurement conditions are well-defined.

9.1 Effect of Polarity and Magnitude of V_p

Figures 9.1–9.3 show the total charge released for three cable types 1Aa, 1Ab and 1Ba respectively, determined by integrating the TSC with respect to time for V_p values of both sign.

It was originally expected that poling with negative V_p would provide larger total charge and higher TSC peaks than with positive V_p due to the combined effects of (a) dominant electron injection as described by several authors [3, 34, 65] and noted in chapter 5, (b) a geometric field enhancement at the conductor screen and (c) the observation [3] that in an aluminium-polyethylene-copper system, the charge injected was double when the aluminium electrode was the cathode. Figures 9.1–9.3 show that this is not the case in the present study, and that similar amounts of charge are present with either polarity V_p. This implies that the semicon electrodes do not act in the same manner as a metallic electrode such as aluminium or copper which inject only electrons efficiently. It seems that the semicon may permit ready injection of either positive or negative charge according to the polarity of V_p. This is in agreement with the findings of Sigmond and Hegerberg [34] who reported that semicon electrodes were found to inject both holes and electrons equally well into polyethylene. Additionally, the low voltage results reported in the present work agree with the low electric field measurements of Doughty *et al* [13] who also observed mirror-image TSC for opposite polarity poling voltages. However, if Doughty *et al*'s work is compared with that of Braun *et al* [66], it can be concluded that the space charge seen in the majority of the TSC reported in Doughty *et al*'s work do not originate from injected charge at all.

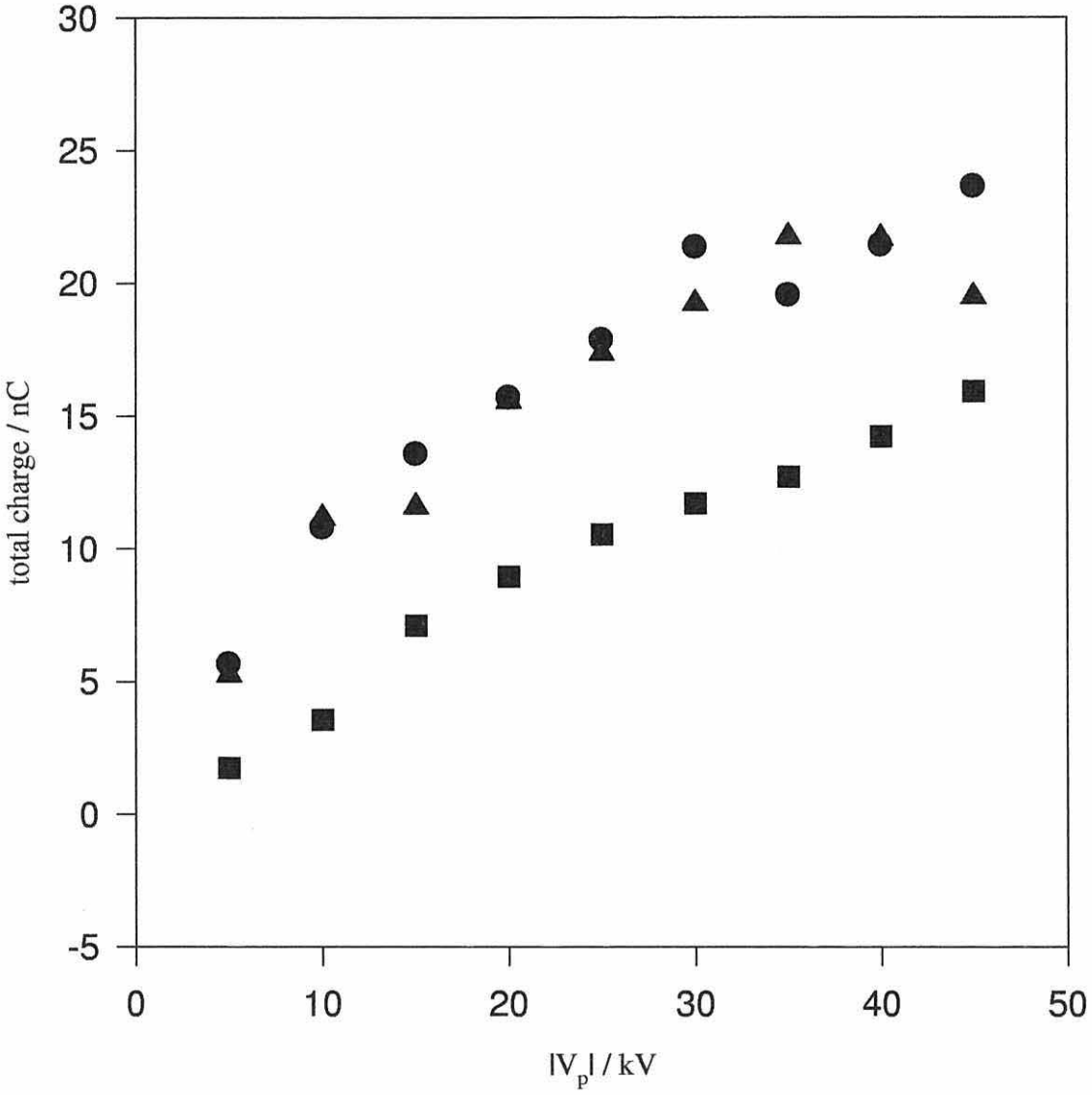

Figure 9.1. Magnitude of total charge from TSC measurements for cable type 1Aa. ▲, $+V_p$, data from figure 7.9; ●, $-V_p$, data from figure 7.5; ■, $-V_p$, data from figure 7.6.

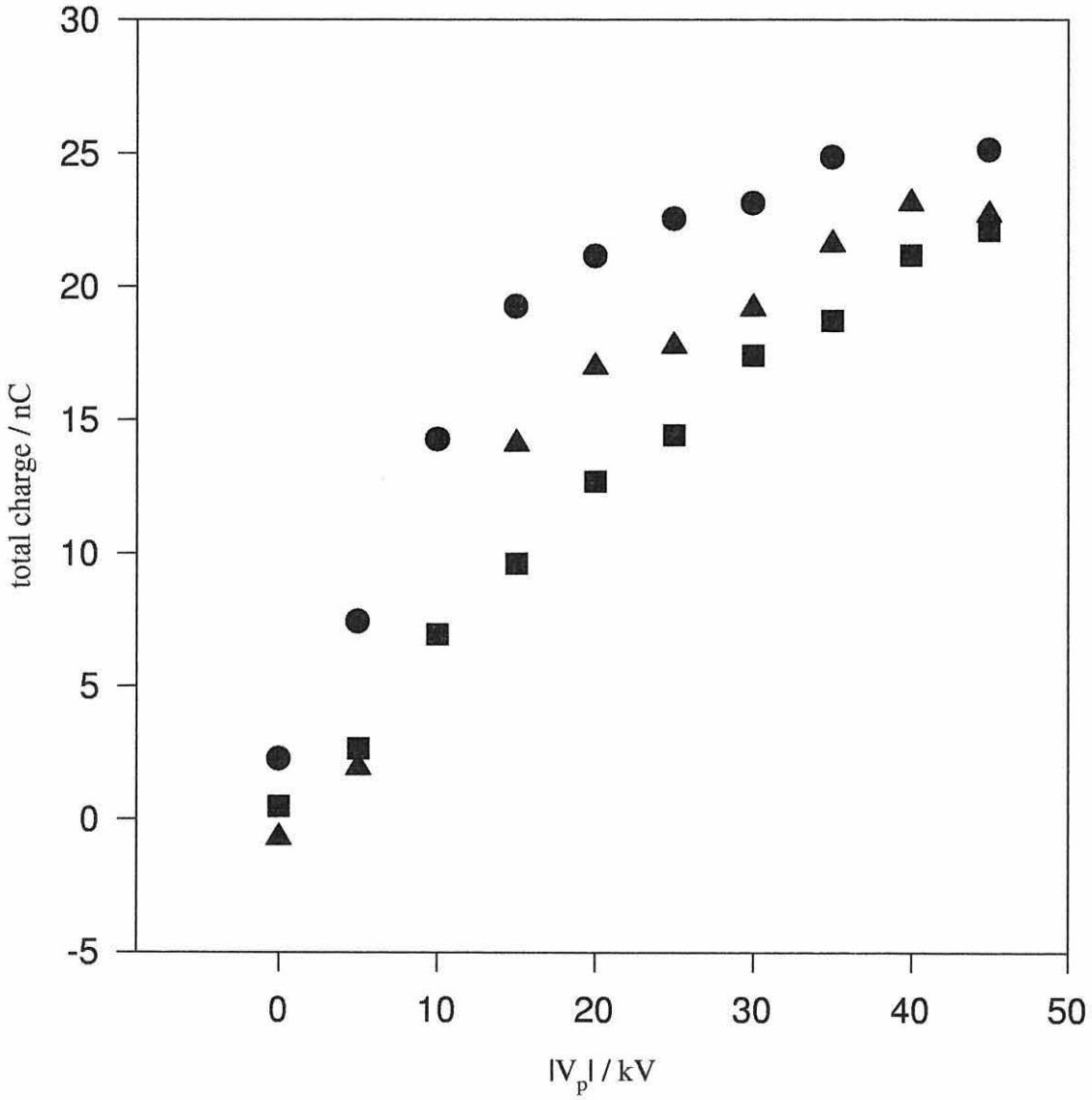

Figure 9.2. Magnitude of total charge from TSC measurements for cable type 1Ab. ▲, $+V_p$, data from figure 7.13; ●, $-V_p$, data from figure 7.11; ■, $-V_p$, data from figure 7.12.

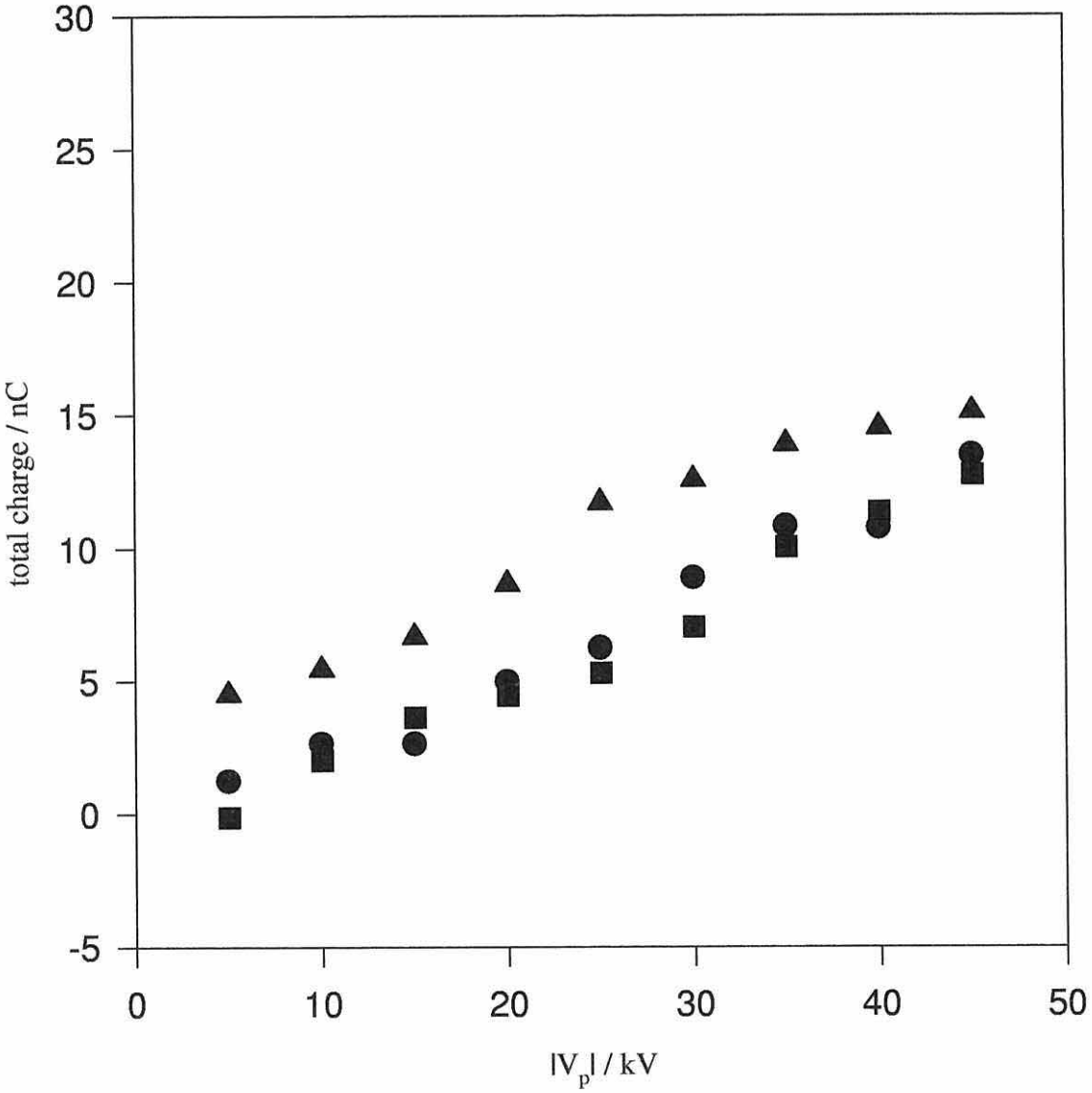

Figure 9.3. Magnitude of total charge from TSC measurements for cable type 1Ba. ▲, $+V_p$, data from figure 7.17; ●, $-V_p$, data from figure 7.15; ■, $-V_p$, data from figure 7.16.

As noted in chapter 5, Braun *et al* investigated samples with similar geometries to those studied here, and their work therefore has the most relevance to the present work. Their samples also had the same insulation type as sample 3Ab. They found a threshold field above which charge injection occurred in the neighbourhood of 12kV.mm^{-1}. For the samples used in the present work, the geometric field would reach this threshold value at the inner semicon electrode when $|V_p| = 38.4$kV, or at the outer electrode when $|V_p| = 73$kV; values well in excess of those employed.

It is therefore obvious that the measurements reported in chapter 7 were, at best, made at the threshold for space charge injection at the inner interface, and well below it at the outer interface. Braun *et al* reported that 12kVmm^{-1} was only an approximate value for the threshold field and that the true value might be lower. It can be seen, however, that if charge injection has been observed in the present work then it is likely to have occurred only at the inner semicon-insulation interface and then only at the highest V_p employed. It might therefore explain the changes in the shape of the TSC characteristics above certain threshold poling voltages, which were noted at several points in chapter 5 and reported in chapter 7.

The work of Braun *et al* suggests that most of the poling voltages used in the present work are too low to encourage any significant charge injection into the samples. It is sensible therefore to attribute the TSC seen at the lower voltages to intrinsic space charge and dipolar relaxation. Caution should be maintained however when considering the effects of the high poling voltages used in the present work, which correspond closely to a macroscopic geometric field at the inner

semicon-insulation interface of similar magnitude to Braun *et al*'s critical injection field. As explained in section 3.3.2, significant field enhancement may occur at this interface as a consequence of efficient injection and the formation of double layers at the semicon-insulation interfaces. The issue of dipolar relaxation also becomes very important when considering the effect of the semicon base resin, as will be argued in section 9.4.

Thus far, only the total charge released has been discussed. However, there are some interesting differences in the main TSC peak temperature, T_{peak}, which should be commented upon here. For example, comparison of $-V_p$ measurements on a fresh samples and of the opposite $+V_p$ measurements reported in chapter 7 shows the shape of the TSC curves and the trends of T_{peak} to be different for the combinations of insulation and semicons investigated.

TSC measurements performed on 1Aa (figure 7.6) and 1Ab (figure 7.13) show peaks at $\sim$ 80°C at the lower poling voltages ($V_p \leq -15$kV). This temperature corresponds to a mechanical relaxation peak in LDPE [57] and to a TSC peak originating from charge trapped at crystalline-amorphous boundaries [6]. It can be argued then that this peak is attributable to the relaxation of space charge that had accumulated at crystalline-amorphous phase boundaries during poling and consequently relaxed when heated during TSC. It is important to note that the samples in which this 80°C peak was observed (1Aa and 1Ab) have the same semicon base resin and insulation. The 80°C peak disappeared upon repetition of the Procedure I TSC series on 1Aa and 1Ab, a fact that could be attributed to mechanical and morphological stress within the samples present since manufacture.

9.2 Thermal Gradient in Samples

As was noted briefly in chapter 7, there is a $\sim 5°C$ difference (observed primarily at the low poling voltages of $\pm 5kV$) between T_{peak} for positive V_p and those for negative V_p, which corresponds to a measured difference in temperature across a cable sample of $\sim 4°C$. The origin of this temperature difference should now be considered. The situation described below applies equally to both positive and negative charge, but only the case for negative charge will be explained here. The TSC peak polarity will depend upon the polarity of the charge.

If heat is applied to the outer electrode of the cable sample, a temperature gradient will form which depends on the rate of temperature rise and the thermal conductivities of the metal core, the semicon and the insulation materials, giving rise to the observed $4°C$ temperature difference. This temperature difference can therefore be expressed in terms of the temperature at each semicon-insulation interface, such that the the outer interface is at a temperature T °C while the inner interface is at a temperature $(T-4)°C$. As a consequence of this temperature difference, a TSC peak at the lower poling voltages ($|V_p| \leq 15kV$) may be dominated by mobile charge which has accumulated at only one electrode.

Consider negative charge which, at the elevated temperature of poling, was sufficiently mobile to migrate towards and to accumulate at the outer interface during poling under the influence of a negative V_p. Subsequently, it becomes trapped at that interface (figure 9.4a) when the temperature is reduced. As the sample is heated past the activation temperature T_a of this charge, a corresponding TSC peak will appear at T.

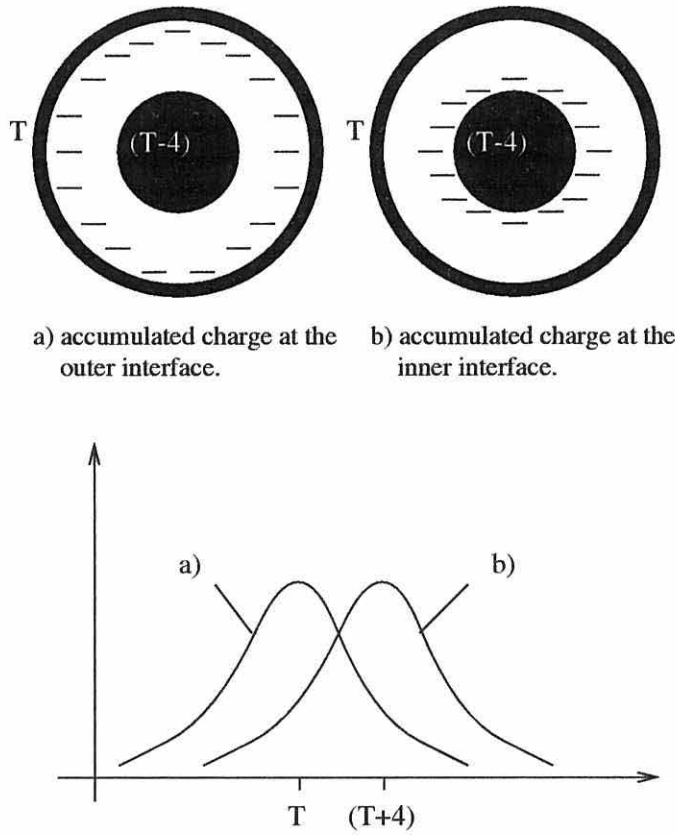

Figure 9.4. The influence of a thermal gradient on TSC peak temperature T_{peak} due to spatial location of the semicon-insulation space charge accumulation.

If the poling is then repeated but with the opposite, positive polarity V_p (figure 9.4b), the charge will now accumulate and become trapped at the inner interface. This charge will still be activated at T_a. However, the temperature at the inner interface will now be $(T - 4)$°C with regard to the *measured* temperature T_m at the outer interface. The activation temperature T_a will not be reached at the inner interface until $(T + 4)$°C, i.e., the TSC peak will now appear to be at a temperature 4°C higher after $+V_p$ poling than after $-V_p$ poling.

It can therefore be concluded that a TSC peak with this amount of temperature variation in T_{peak} under opposite polarity V_p conditions is due to mobile space charge within the cable system. A similar result could be expected for positive charge, although the peaks would be the opposite polarity. This means that, at low $|V_p|$, the relative position of the positive and negative polarity V_p peaks on the temperature scale is an indicator of the polarity of the space charge. It should also be noted that this effect was only observed in the opposite polarity measurements performed on samples of 1Aa and of 1Ab, but not on 1Ba samples. The effect was also only observed at low V_p. As V_p increased, T_{peak} became increasingly polarity independent, indicating the emergence of another charge relaxation phenomenon at higher poling voltages.

As $|V_p|$ increases above $\sim$ 25kV, the TSC changes shape (figure 7.7 for 1Aa and figure 7.13 for 1Ab). This change is most noticeable on comparison of the first and second negative V_p measurements on all the primary sample types. This effect is probably due to space charge injection. At these higher poling voltages, it is expected that some charge injection may have occurred, as will be discussed

elsewhere in this chapter.

9.3 Effect of Thermal and Voltage Cycling

Some interesting points have arisen as a consequence of repeating $-V_p$ TSC measurements performed on 1Aa, 1Ab and 1Ba.

First consider and compare the TSC of 1Aa and 1Ab. The first cycle of TSC measurements performed on 1Aa after poling from -5kV to -45kV (figure 7.6) show appreciable differences to the second cycle (figure 7.7). Close examination of the $V_p = -5$kV measurements shown in both of these figures shows that a large peak at $T \sim 80$°C in the first has become much reduced in the second. This peak, and its consequent reduction in magnitude, is also manifest in the -10 and -15kV measurements. A similar trend concerning the reduction of this peak can be observed in the first $-V_p$ measurement (figure 7.13) and second $-V_p$ measurement (figure 7.14) of 1Ab. The reduction of this peak appears to be a result of the combined thermal and voltage cycling performed during the TSC measurements. In other words, the peak reduction is a consequence of (a) morphological change, particularly in the crystalline-amorphous structure of the samples due to thermal annealing; (b) stress reduction in the cable samples; or (c) the injection of neutralising charge at the higher poling voltages where space charge injection is at least possible from one electrode. The observed TSC reductions are unlikely to be attributable to crosslinking byproducts, as the samples were taken from cables that had been stored for a period sufficient to allow them to fully degas.

If the TSC cycling of 1Ba is now considered, a very different situation is found. Recall that 1Ba differs from 1Aa and 1Ab in its semicon base resin. On repetition of the cycle (figure 7.18) the TSC of 1Ba appear very similar, but closer observation shows that the high temperature TSC (above 60°C) is greater in the second cycle than the first. This observed increase continues on further repetition, as results from sample 1Ba/1 indicate (figure 7.16). Remember that sample 1Ba/1 had more preliminary tests and thermal cycling performed on it before an organised programme of TSC measurements was established and employed. Consequently, the magnitude of the high temperature current measured in 1Ba/1 is much larger. These observations suggest that 1Ba is accumulating charge as the TSC cycles are performed. This is possible, as the higher values of V_p (and hence, electrical fields) employed will permit some space charge injection (§9.1). It may be argued therefore that the combination of insulation 1 and semicon Ba creates a system that slowly accumulates space charge with thermal cycling under the electrical stresses employed in the present work.

In summary, it can be seen therefore that 1Aa and 1Ab both exhibit a characteristic change in TSC on repetition of the TSC cycle. By comparison, the TSC of 1Ba changes in a different manner to these other two types. This shows that the type of semicon base resin used in the samples investigated has a very important role to play in: (a) the formation of crystalline-amorphous phase boundaries close to the semicon-insulation interfaces, evidenced by the change in the high temperature current of 1Aa and 1Ab from a relaxation similar to that seen in many other works (see chapter 5 for many examples); (b) injection of space charge, as seen by the increases in TSC on application of the higher V_p; and (c) neutralisation of

intrinsic charge.

9.4 Sample Composition

The composition of the cable samples has indirectly "intruded" on the discussion of the effects discussed in section 9.3. It is important, however, to state specifically the effects that arise from varying the composition of the cable materials. To enable a direct comparison of the materials to be made, two figures have been plotted using TSC data obtained from "first time" measurements described in chapter 7. Figure 9.5 shows the TSC measurements made at $V_p = -15\text{kV}$ on cable types 1Aa, 1Ab, 1Ba and 2Ba. Figure 9.6 shows similar measurements made on these cable types, but at -45kV. These figures serve to illustrate the differences from cable type to cable type, and also help to illustrate the effect of varying the semicon carbon, semicon resin, and insulation composition on the TSC measurements.

It should be emphasized that, although Braun *et al* [12] somewhat accidentally managed to compare the effect of the semicon carbon on their TSC results, no other work has been reported that comprehensively compares the consequences of alterations to the fundamental materials of such extruded cable systems.

9.4.1 Semicon Carbon

The effect of the semicon carbon can be seen by comparing 1Aa (supersmooth carbon) and 1Ab (furnace carbon). The measurements made at both -15kV (figure 9.5) and -45kV (figure 9.6) show very little difference. This observation is

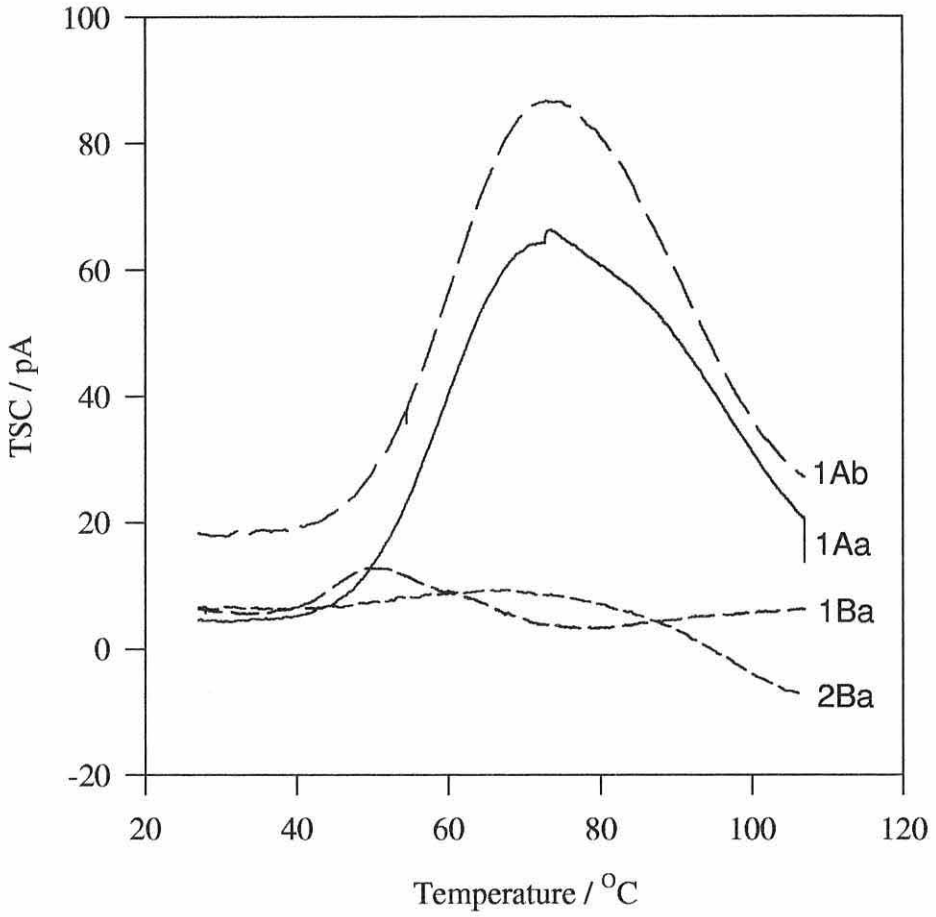

Figure 9.5. Comparison of −15kV TSC measurements made on different cable types. The TSC are taken from figures shown in chapter 7.

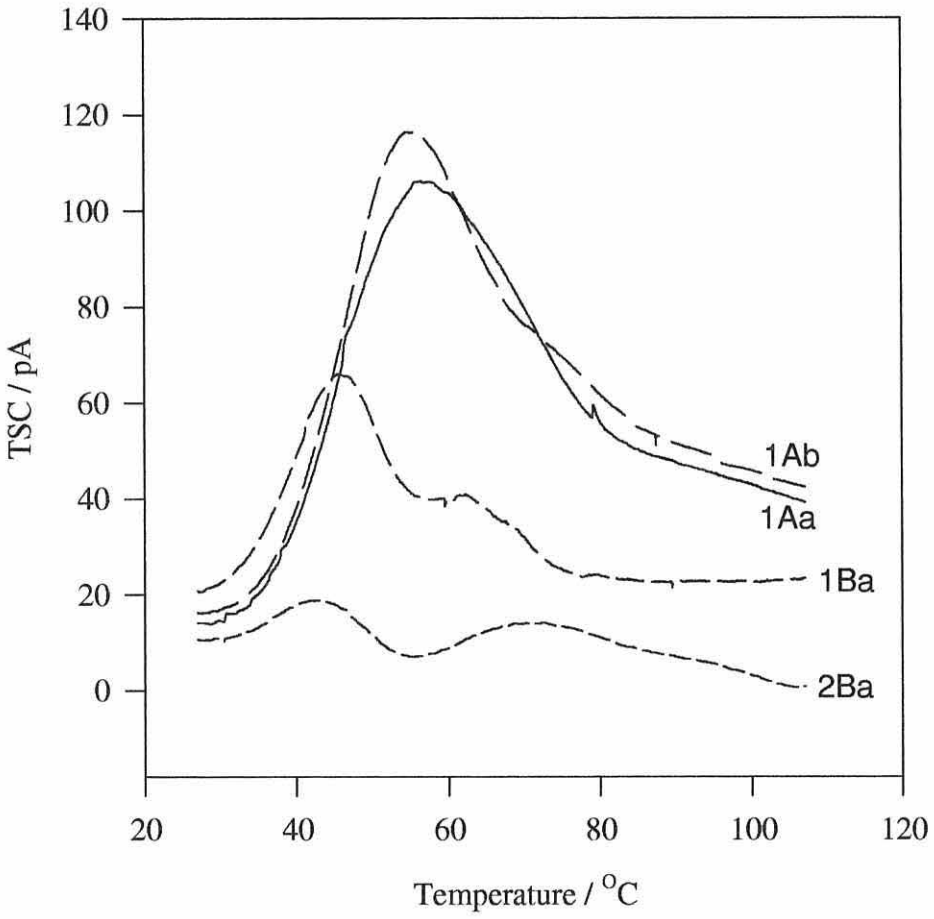

Figure 9.6. Comparison of −45kV TSC measurements made on different cable types. The TSC are taken from figures shown in chapter 7.

also echoed in the total charge measurements (figures 9.1 and 9.2) and the EK measurements (chapter 8).

The repeated TSC cycle measurements on these cable types are also very similar (figures 7.8 and 7.14). 1Ab exhibits a slightly larger total charge than 1Aa, which can be attributed to the slightly higher space charge injection at high V_p, an effect in turn due to the rougher furnace black of semicon Ab. T_{peak} in figure 7.14 for 1Ab also appears to be higher than T_{peak} for 1Aa in figure 7.8. However, this is an effect of the peak sitting on a "skewed" baseline arising as a consequence of the $\sim$ 80°C crystalline-amorphous peak underlying the main TSC peak. Cable 1Ab was expected to have significantly larger TSC peaks than 1Aa due to the field enhancement by the rougher furnace carbon particles causing local high stress regions at the interface and thus injecting more charge here (as described in section 2.4). However, this effect is small enough to conclude that space charge injection is not the main space charge process seen in the TSC measurements of samples 1Aa and 1Ab in the present work. This means that the peaks result mainly from relaxation of dipolar and intrinsic space charges within the cable samples.

9.4.2 Semicon Base Resin

The effect of the semicon base can be seen by comparing 1Aa (EBA base resin) and 1Ba (EVA base resin). The measurements shown in figures 9.5 and 9.6 show the difference in the magnitude of the TSC measurements on these samples. Corresponding differences are also seen in the EK measurements (chapter 8) and the total charge measurements (figures 9.1 and 9.3).

Other work on TSC of ethylene-based copolymers (Cited in Chapter 5 [9]) has shown that TSC peaks appear at temperatures in the region of 0°C, and a peak at $T \sim 32$°C for an BA/AA copolymer was noted as being important. The peaks that appear closest to this temperature are those at $\sim$ 50°C in the present work. The peaks in this temperature region may be attributed, therefore, to relaxation of space charges within the semicon base resins.

It is suggested that semicon base resin A produces a positive peak which results from the relaxation of accumulated space charge at the semicon-insulation interface. Similarly, semicon base resin B also produces a peak at $T_{\text{peak}} \sim 60$°C, but with a negative polarity, so that its superposition on the broad positive peak results in a net decrease in the magnitude of the TSC. This observation is reinforced by the work on 2Ba, which also shows an opposite polarity peak in the same temperature region as for 1Ba.

It is still uncertain whether the negative peak in type 1Ba simply masks the presence of the positive peak during measurement of the TSC, or whether it makes a real contribution to the reduction of space charge within a cable sample.

9.4.3 Insulation

The effect of changing the insulation can be seen best by comparing 1Ba and 2Ba shown in figures 9.5 and 9.6. Details of the difference in the additive packages of the insulation has not been forthcoming from BICC, and so only very vague speculation can be made as to the origin of the change in TSC spectra. Additionally, a very limited series of TSC measurements were made on sample 2Ba, further

restricting knowledge of the space charge in this cable type.

Comparison of the TSC shown in figures in chapter 7 and in figures 9.5 and 9.6 indicate that there is a difference between the space charge characteristics of 1Ba and 2Ba. In particular, 2Ba shows a significant fall and current inversion at the highest temperatures and highest values of V_p employed. However it is uncertain whether this is a consequence of different types of additives to the insulation, or just different quantities of the same additives.

Comparison can also be made of the Procedure II TSC measurements of 1Ab and 3Ab (figures 7.24 and 7.27 respectively). There appears to be a TSC peak at $T_{\text{peak}} \sim 65°\text{C}$ for both cable types. However, the TSC of 1Ab remains positive in polarity at all T_p, while the TSC of 3Ab exhibits a peak at $T_{\text{peak}} \sim 100°\text{C}$ which becomes more prominent as T_p increases. This 100°C, negative polarity peak appears at the same temperature as a positive peak observed previously in 1Ab (section 7.4.2). It is therefore valid to argue that the two peaks are associated with the presence (or absence) of a particular additive in the insulation.

It can be concluded that changing the insulation composition (anitoxidants, peroxides) will introduce different peaks that are related to these compounds. Changing the relative amount of these compounds from one sample to another will directly alter the magnitude of space charge peaks arising from the presence of these compounds.

Further, it can be expected that the balance of antioxidant to cross-linking peroxide is very delicate, as one will neutralise the other. This will consequently affect the amount of amorphous material in the bulk XLPE insulation, as well as

the distribution and quantity of crystalline-amorphous phase interfaces.

9.5 EK Measurements

As reported in chapter 8, it was not possible to pursue a full investigation of EK measurements due to equipment difficulties. However, those few measurements that were obtained and were reported in chapter 8 have raised some important points which will now be discussed. Correlation between the TSC and EK measurements will be discussed separately in section 9.5.2.

9.5.1 General Observations

The EK measurements reported in chapter 8 agree with the theoretical model for EK [64]. The D_{1f} measurements follow a linear dependency on v while D_{2f} measurements follow a square law dependency on v.

It is interesting to compare the EK responses of the various cable types investigated, shown in figures 8.3 to 8.6. Type 1Ab (figure 8.4) produced the largest values of D_{1f} for a given v, followed in decreasing order of magnitude by 1Aa (figure 8.3) and 1Ba (figure 8.5). However, this does not necessarily indicate that 1Ab has the most space charge in it. The measurements performed on 1Aa/1 (figure 8.6) suggest that the length of the period between poling and EK measurement has an important effect on the magnitude of D_{1f}. Further, these measurements can be argued to show that the magnitude of D_{1f} is heavily influenced by the electric field within the cable. If the electric field has not reached a steady state, then a

larger EK measurement can be expected. It has been noted during the investigation that EK measurements are very difficult to obtain immediately after poling due to instability in the lockin amplifier. It is suggested that this is due to the high mobility of space charge within the sample at this time, which in turn is associated with a change in the electric field distribution as it approaches an equilibrium. Additionally, it is suggested that the mere presence of space charge in a sample is not sufficient to produce an EK measurement. Obviously, the position of the space charge within the sample will influence the electric field. It is only as a consequence of the accumulation of space charge that such an electric field will produce a strong EK response.

The D_{2f} measurements also provide some interest. Those of 1Ab and 1Ba are both of relatively low magnitude in comparison to those of 1Aa. As reported in section 8.4.1, the D_{2f} measurements of 1Aa were significantly larger than D_{1f} at $v = 10$kV, and they were also much larger than the D_{2f} measurements of either of the other two types investigated. It is suggested that the combination of the material compounds of which 1Aa was manufactured give rise to an especially large electric field at the semicon-insulation interface. A large magnitude of D_{2f} appears to be typical for type 1Aa. The magnitude of D_{2f} at $V = 5$kV both in figure 8.3 and in the later figure 8.6 are the same, adding credibility to the argument that the D_{2f} curve is characteristic of a particular cable type. However, figure 8.6, plot 3 suggests that the characteristic D_{2f} curve of a cable will change if the temperature of the sample is raised particularly high. If this argument correctly indicates a characteristic D_{2f} measurement for a given cable type, then it would appear that concerns of variation in this parameter were unfounded. The variations

observed in the magnitude of D_{2f} during early measurements may have therefore been a result of the problems encountered, and not result from changes in D_{2f} influenced by the presence of space charge.

9.5.2 Correlation Between TSC And EK

The correlation between TSC and EK has been noted at several points. This correlation can be seen by considering the magnitudes of the D_{1f} EK measurements and TSC total charge measurements of cable types 1Aa, 1Ab and 1Ba. To aid the comparison, table 9.1 shows the mean m-coefficients (from the tables in chapter 8) and the total charge values at -15kV and -45kV for the three cable types (figures 9.1 to 9.3).

Sample	TSC total charge / nC @-15kV	-45kV	EK Coefficient m_{1f}	m_{2f}
1Aa	13.5	23.5	18.5	4.9
1Ab	19.0	25.0	22.7	0.5
1Ba	2.0	13.0	13.2	0.9

Table 9.1. Comparison of Selected TSC and EK data.

The data in this table shows excellent evidence that the TSC and EK techniques are correlated. In particular the values of the TSC total charge at -15kV and -45kV, and the shape parameter m_{1f} are directly correlated. 1Ab has the largest values of total charge and m_{1f}, followed by 1Aa and then 1Ba.

However, there is not the same correlation between the TSC total charge and m_{2f}, which suggests that m_{2f} is characteristic of the material state of the sample and not of the space charge in the sample. This has already been argued above; the

example of the overheating of 1Aa/1 to 130°C (figure 8.6) was cited as evidence.

9.6 Conclusions

The following are the main conclusions from the investigation:

- The semicon base resin has a major influence on the TSC characteristic and hence the polarisation within a cable sample. Cable samples that possess an EVA semicon have lower TSC and consequently lower space charge than those with an EBA semicon.
- Furnace semicon carbon injects more charge than supersmooth semicon carbon.
- The semicon-insulation combination also influences the TSC characteristic and hence the polarisation within a cable sample.
- A TSC peak in the region $T_{\text{peak}} \sim 50°\text{C}$ arises from the semicon-insulation interface, and is heavily influenced by the polarisation of the semicon base resin.
- TSC peaks that appear at the same T_{peak} for both positive and negative V_p are a result of either (a) the relaxation of dipolar polarisation, most probably at the semicon-insulation and morphological interfaces, or (b) the simultaneous charge injection at both interfaces.
- A temperature variation in T_{peak} between the negative and positive poling polarity TSC at the same V_p can be attributed to the relaxation of intrinsic

space charge that is mobile in the sample at a sufficiently high temperature.

- Low $-V_p$ TSC peaks that appeared in the spectra of 1Aa and 1Ab during the first TSC cycle were much reduced during the second, indicating that a morphological change has occurred in these samples as a result of the thermal and electrical cycling.

- The author is still sceptical as to whether the total charge, determined by integrating the TSC curve with respect to time, can be used as an accurate and direct indicator of the magnitude of the space charge within a cable sample. This concern would benefit by comparing results obtained using TSC to results obtained on the samples of other investigation techniques.

- The magnitude of a cable's D_{1f} EK measurement is directly correlated to its total space charge determined by integrating the TSC with respect to time.

- TSC and EK measurements give no clear independent indication to the viability of the model cables as HVDC cables. It is suggested that they are used as an indicator of suitability in conjunction with other test methods (breakdown, PEA/LIPP, etc.). Once this work is performed, however, the TSC and EK methods may be useful as diagnostic non-destructive techniques.

- It is uncertain whether 1Aa and 1Ab are better cables, due to their initially large TSC which then becomes reduced on thermal and electrical cycling, than 1Ba whose TSC increases with thermal and electrical cycling.

- Despite the previous conclusion, type 1Ba appears to be the better cable of those which were thouroughly investigated, by virtue of the lower magni-

tude of its TSC space charge and EK D_{1f} measurements. It is hoped that future work will be able to verify this conclusion.

Bibliography

[1] D. McAllister, editor. *"Electric Cables Handbook"*. Blackwell Scientific Publishing, second edition, 1990.

[2] T. J. Lewis. "Charge Transport, Charge Injection and Breakdown in Polymeric Insulators". *J. Phys. D: Appl. Phys.*, **23**, 1469–78, 1990.

[3] R. J. Fleming and D. V. Balbachas. "Charge Injection into Cross Linked Polyethylene Studied by Thermally Stimulated Depolarization". In *I.E.E.E. 1990 Annual Report, Conference on Electrical Insulation and Dielectric Phenomena* [67], pages 47–52.

[4] T. Oda, S.-N. Wang, Y. Maruyama, N. Ichiyanagi, and H. Tanaka. "Thermally Stimulated Discharge Current Observation Of Cross-Linked Polyethylene". In *Proceedings of the 3rd International Conference on Properties and Applications of Dielectric Materials* [68], pages 89–92.

[5] O. Dorlanne, S. Sapieha, M. R. Wertheimer, and A. Yelon. "Thermally Stimulated Discharge of Polyethylene Following ac Stressing". *TEI*, **17**, 199–202, 1982.

[6] G. Sawa, M. Kawade, D. Chool-Lee, and M. Ieda. "Thermally Stimulated Current from Polyethylene in High-Temperature Region". *Jap. J. Appl. Phys.*, **13**, 1547–53, 1974.

[7] H. M. Li, A. Fouracre, B. H. Crichton, and V. A. A. Banks. "The Influence of Ions on the Thermally Stimulated Discharge Current Spectra of Water-treed Additive-free Low-density Polyethylene". *TDEI*, **1**, 1084–93, 1994.

[8] S.M. Gubanski, U. Nilsson, and M.-S. E. Wang. "Thermally Stimulated Depolarization Current Measurements of different Polyolefin Compounds". In *Nordic Insulation Symp.*, pages 8.5:1–10, Västerås, Sweden, June 1992.

[9] C.S. Chern, F.Y. Lin, Y.C. Chen, and C.H. Lin. "Characterization Of Carboxylated Poly(Butyl Acrylate) Lattices Produced By A Semibatch Process". *J. Appl. Polym. Sci.*, **62**, 585–94, 1996.

[10] A. S. Ibrahim, G. Attia, M. S. Abo-Ellil, and F. H. Abd El-Kader. "Electrical Studies on PVA-PE Copolymer". *J. Appl. Polym. Sci.*, **63**, 343–8, 1997.

[11] T. Mizutani, Y. Suzuoki, and M. Ieda. "Thermally Stimulated Currents in Polyethylene and Ethylene-Vinyl-Acetate Copolymers". *J. Appl. Phys.*, **48**, 2408–13, 1977.

[12] Jean Marie Braun, R. John Densley, A. Younsi, and Howard J. Wintle. "TSDC Characteristics of Extruded Polymer Insulated Cables". In *Proceedings of the 5th International Conference on Conduction and Breakdown in Solid Dielectrics* [69], pages 33–37.

[13] K. Doughty, D. K. Das-Gupta, and D. E. Cooper. "Thermally Stimulated Discharge Current Spectra from Electrically Stressed High voltage Power Cables". In *I.E.E.E. 1986 Annual Report, Conference on Electrical Insulation and Dielectric Phenomena* [70], pages 56–62.

[14] A. Motori, G. C. Montanari, and S. M. Gubanski. "Investigation of Relaxation Processes in Thermally-Aged XLPE Cable Models". In *I.E.E.E. 1993 Annual Report, Conference on Electrical Insulation and Dielectric Phenomena* [71], pages 751–6.

[15] S. Gubanski, A. Bulinski, and S. S. Bamji. "Thermally Stimulated Current Measurements on Polymeric Cable Insulation — The Diagnostic Aspect". In *I.E.E.E. 1993 Annual Report, Conference on Electrical Insulation and Dielectric Phenomena* [71], pages 732–8.

[16] S. M. Gubanski, G. C. Montanari, and A. Motori. "TSDC Investigations Of Thermally And Electro-Thermally Aged Cables Models". In *Conference Record of the 1994 I.E.E.E. International Symposium on Electrical Insulation*, pages 54–7, Pittsburgh, PA, U.S.A., June 1994.

[17] L.A. Dissado and J.C. Fothergill. *"Electrical Degradation and Breakdown in Polymers"*, volume 9 of *I.E.E. Materials and Devices Series*. Peter Peregrinus Ltd., 1992.

[18] A. Campus, B. Lafin, and T. Sterzynski. "Structure - Morphology Modification of Cable Insulation Polymers". In *Proceedings of the 6th International Conference on Conduction and Breakdown in Solid Dielectrics* [72], pages 357–360.

[19] Tatsuki Okamoto, Masayoshi Ishida, and Naohiro Hozumi. "Effect of Agglomeration of Carbon Particles in the Semiconducting Material on the Dielectric Strength of XLPE Insulation". *I.E.E.E. Trans. Elect. Insul.*, **23**, 335, 1988.

[20] S. Betteridge, T. J. Lewis, and J.P. Llewellyn. "A Preliminary Study of the Cable Semicon-Insulator Interface using Scanning Probe Microscopy". internal report, BICC Cables Limited, 1997. Report Number WTC R/97/395.

[21] S. Nakamura, K. Saito, G. Sawa, and K. Kitagawa. "Percolation Threshold of Carbon Black-Polyethylene Composites". *Jap. J. Appl. Phys.*, **36**, 5163–8, 1997.

[22] Josef Hampl and Václav Bouda. "I–V Characteristics of the Carbon Black-Filled Polyethylene Interface with Tin Electrodes". *Synthetic Metals*, **67**, 129–132, 1994.

[23] Felix Gutmann and Lawrence E. Lyons. *"Organic Semiconductors"*. John Wiley & Sons, New York London Sydney, first edition, 1967.

[24] N. F. Mott. *Adv. Phys.*, **16**, 49–144, 1967.

[25] H. Hänsel. "The Influence of the Polymer Structure on the Electrical Properties". In *Proceedings Of The 3rd International Conference On Conduction And Breakdown In Solid Dielectrics*, pages 218–22, Trondheim, Norway, July 1989. I.E.E.E.

[26] M. Redi and J. J. Hopfield. "Theory of Thermal and Photo-Assisted Electron Tunnelling". *J. Chem. Phys.*, **72**, 6651–60, 1980.

[27] T. J. Lewis. *"Space Charge in Solid Dielectrics"*, chapter title: The Micro-Physics of Charge in Solid Dielectrics. Dielectrics Society, 1998. In press.

[28] T. J. Lewis. "Electrical Effects at Interfaces and Surfaces". *I.E.E.E. Trans. Elect. Insul.*, **21**, 289–95, 1986.

[29] E. A. Silinsh. *"Organic Molecular Crystals"*. Springer-Verlag, Berlin, Germany, 1980.

[30] C.B. Duke. "Polymers and Molecular Solids: New Frontiers in Surface Science". *Surf. Sci.*, **70**, 674–91, 1978.

[31] N.F. Mott. *"Electronic and Structural Properties of Amorphous Semiconductors"*, in Electrons in Non-Crystalline Materials. Academic Press, London, England, 1973.

[32] J. G. Simmons. "Theory Of Metallic Contacts On High Resistivity Solids — I. Shallow Traps". *J. Phys. Chem. Solids*, **32**, 1987–99, 1971.

[33] J. G. Simmons. "Theory of Metallic contacts on High Resistivity Solids (II) Deep Traps". *J. Phys. Chem. Solids*, **32**, 2581–91, 1971.

[34] R. S. Sigmond and R. Hegerberg. "Some Physical Aspects of the electrical Breakdown of Solid Dilectrics". In *CSC'3 — Proceedings of the 3rd Conference on Electric Charge in Solid Insulators*, pages 294–301, Tours, France, July 1998.

[35] R. Chen and Y. Kirsh. *"Analysis of Thermally Stimulated Processes"*. Pergamon Press, 1981.

[36] J. Vanderschueren and J. Gasiot. *"Field-Induced Thermally Stimulated Currents"*, volume 37 of *Topics in Applied Physics*, chapter 4. Springer-Verlag, Berlin, 1979.

[37] T. J. Lewis, J. P. Llewellyn, and M. J. van der Sluijs. "Report on BICC Development Programme: Electrical Endurance. 1May – 31 October 1996". pp5.5–5.17, 1996.

[38] C. Bucci and R. Fieschi. "Ionic Thermoconductivity. Method for the Investigation of Polarisation in Insulators". *Phys. Rev. Letts.*, **12**, 16–19, 1964.

[39] I. Kunze and P. Müller. "Ionic Thermocurrent Investigations of CdF_2". *Phys. Stat. Sol. (a)*, **16**, 197ff, 1972.

[40] T.A.T. Cowell and J. Woods. "The Evaluation Of Thermally Stimulated Current Curves". *Brit. J. Appl. Phys.*, **18**, 1045–51, 1967.

[41] R.A. Creswell and M.M. Perlman. "Thermal Currents from Corona-Charged Mylar". *J. Appl. Phys.*, **41**, 2365–2375, 1970.

[42] T.R. Jenkins. "On Computing the Integral of Glow Curve Theory". *J. Comput. Phys.*, **29**, 302–5, 1978.

[43] J.E. Hoogenboom, W. de Vries, J.B. Dielhof, and A.J.J. Bos. "Computerized Analysis Of Glow Curves From Thermally Activated Processes". *J. Appl. Phys.*, **64**, 3193–200, 1988.

[44] F. Henn, J. Vanderschueren, J Niezette, J. C. Giuntini, and J. V. Zanchetta. "Correlated Interaction and Dielectric Relaxation in Solids: A Discriminating Experimental Approach by Thermally Stimulated Depolarisation Current". In *Proceedings of the 6th International Conference on Conduction and Breakdown in Solid Dielectrics* [72], pages 592–5.

[45] V. Halpern. "The Interpretation of Thermally Stimulated Currents Obtained by the Thermal Slicing Technique". *J. Phys. D: Appl. Phys.*, **30**, 548–64, 1997.

[46] J.T. Randall and M.H.F. Wilkins. "Phosphorescence and Electron Traps. I. The Study of Trap Distributions". *Proc. Roy. Soc. A*, **184**, 366ff, 1945.

[47] P. Fischer and P. Röhl. "Thermally Stimulated and Isothermal Depolarization Currents in Low-Density Polyethylene". *J. Polym. Sci.: Polym. Phys. Edn.*, **14**, 531–42, 1976.

[48] G.F.J. Garlick and A.F. Gibson. "The Electron Trap Mechanism Of Luminescence In Sulphide And Silicate Phosphors". *Proc. Phys. Soc.*, **60**, 574–90, 1948.

[49] A. Halperin and A. A. Braner. "Evaluation of Thermal Activation Energies from Glow Curves". *Phys. Rev.*, **117**, 408ff, 1960.

[50] J. van Turnhout. *"Thermally Stimulated Discharge of Polymer Electrets"*. Elsevier Publishing, Amsterdam, 1975.

[51] C. Lavergne and C. Lacabanne. "A Review of Thermo-Stimulated Current". *I.E.E.E. Electrical Insulation Magazine*, **9**(2), 5–21, 1993.

[52] Kwang-Suck Suh, John Tanaka, and Dwight Damon. "What is TSC?". *I.E.E.E. Electrical Insulation Magazine*, **8**, 13–20, 1992.

[53] A.K. Vijh and J.-P. Crine. "Influence of Metallic Electrodes on Electrical Tree Initiation in Polyethylene". *J. Appl. Phys.*, **65**, 398–9, 1989.

[54] M. Kosaki, N. Shimizu, and K. Horii. "Treeing of Polyethylene at 77K". *TEI*, **12**, 40–5, 1977.

[55] Noriyuki Shimizu, Masamitsu Kosaki, and Keji Horii. "Space-Charge Effect on Local Electric Breakdown of Polyethylene at 77K". *J. Appl. Phys.*, **48**, 2191–5, 1977.

[56] I. Boustead and A. Charlesby. "Thermoluminescence in polyethylene. I. Electron traps". *Proc. Roy. Soc. London A*, **316**, 291–302, 1970.

[57] I.M. Ward. *"Mechanical Properties of Solid Polymers"*, chapter 8.4.2. Wiley-Interscience, 1971. ISBN: 0471919950.

[58] J. Brandrup and E. H. Immergut, editors. *"Polymer Handbook"*, volume 2: Polymer Properties And Characterization. Wiley Interscience, third edition, 1989.

[59] N. Amyot and S. Pélissou. "Diagnosis of Field-Aged Extruded cable Material Using the Thermally Stimulated Currents (TSC) Method". In *Proceedings of the 5th International Conference on Conduction and Breakdown in Solid Dielectrics* [69], pages 580–4.

[60] J. van Turnhout. *"Thermally Stimulated Discharge of Polymer Electrets"*. PhD thesis, University of Leiden, Netherlands, 1972.

[61] S.B. Hobdell, T.J. Lewis, J.P. Llewellyn, and S.M. Moody. "The Influence of the Semicon-Insulation Interface on the Thermally Stimulated Current Spectra of XLPE Cable Samples". In *Proceedings of the 6th International Conference on Conduction and Breakdown in Solid Dielectrics* [72], pages 581–4.

[62] T. J. Lewis, J. P. Llewellyn, and M. J. van der Sluijs. "Electrokinetic Properties of Metal-Dielectric Interfaces". *I.E.E. Proceedings - A*, **140**, 385–92, 1993.

[63] T.J. Lewis, J.P. Llewellyn, M. J. van der Sluijs, J. Freestone, and R. N. Hampton. "Electromechanical Effects in XLPE Cable Models". In *Proceedings of the 5th International Conference on Conduction and Breakdown in Solid Dielectrics* [69], pages 269–73.

[64] T.J. Lewis and J.P. Llewellyn. "The E-K Model". An updated Electrokinetic model, with special application to XLPE cable model geometries., 1998.

[65] M. Ieda. "Electrical Conduction and Carrier Traps in Polymeric Materials". *I.E.E.E. Trans. Elect. Insul.*, **19**, 162–78, 1984.

[66] J.-M. Braun, J. Densley, S/ McNabb, S. Peralta, and A. Younsi. "Optical Techniques to Evaluate Shield/Insulation Interfaces in XLPE Cables". In *Conference Record of the 1996 I.E.E.E. International Symposium on Electrical Insulation*, pages 151–4, Montreal, Quebec, Canada, June 1996. Dielectrics and Electrical Insulation Society, I.E.E.E.

[67] Dielectrics and Electrical Insulation Society. *"I.E.E.E. 1990 Annual Report, Conference on Electrical Insulation and Dielectric Phenomena"*, Pocono Manor, Pennsylvania,U.S.A., October 1990. I.E.E.E.

[68] I.E.E.E. *"Proceedings of the 3rd International Conference on Properties and Applications of Dielectric Materials"*, Tokyo, Japan, July 1991. I.E.E.E. Publications.

[69] Leicester University; I.E.E.E. Dielectrics and Electrical Insulation Society. *"Proceedings of the 5th International Conference on Conduction and Breakdown in Solid Dielectrics"*, Leicester, England, July 1995. I.E.E.E.

[70] I.E.E.E. Electrical Insulation Society. *"I.E.E.E. 1986 Annual Report, Conference on Electrical Insulation and Dielectric Phenomena"*, Claymont, Delaware, U.S.A., November 1986. I.E.E.E.

[71] I.E.E.E. Dielectrics and Electrical Insulation Society. *"I.E.E.E. 1993 Annual Report, Conference on Electrical Insulation and Dielectric Phenomena"*, Pocono Manor, PA, U.S.A., Oct 1993. I.E.E.E.

[72] ABB Corporate Research; I.E.E.E. Dielectrics and Insulation Society. *"Proceedings of the 6th International Conference on Conduction and Breakdown in Solid Dielectrics"*, Västerås, Sweden, June 1998. I.E.E.E.